Structural Organisation of the Human Kinesin-12 Kif15

by

Hamdi Hussain

Supervisors:
Prof. Andrew McAinsh
Dr. Alex Jones

Thesis

Submitted to The University of Warwick for the degree of

Doctor of Philosophy

August 2018

TABLE OF CONTENTS

List of Tables

List of Figures

ACKNOWLEDGEMENTS

I would like to thank my supervisors Prof. Andrew McAinsh and Dr. Alex Jones for providing me with this opportunity to grow as a researcher and their continued support and guidance throughout this project.
I would like to also thank MOAC DTC programme and EPSRC for the funding which allowed me to pursue this project. My deepest thanks to Dr. Hauke Drechsler, the rest of the McAinsh lab and the CMCB in general for being extremely helpful and providing me with all the support and training throughout my project. My thanks to the Proteomics facility and its members Dr. Cleidiane Zampronio, Dr. Juan Fernandez and previous member Dr Sue Slade, who have given me all their support and their invaluable expertise.

I would like to thank Dr. Nida Siddiqui and Dr. Mary Halebian for becoming more than just colleagues and their support and friendship has been an important source of support.

Last but not least, my incredible family, especially my wonderful parents and my daughter, whose continued support and love has been my source of inspiration and strength throughout this incredible journey.

DECLARATION

This thesis is submitted to the University of Warwick in support of my application for the degree of Doctor of Philosophy. It has been composed by myself and has not been submitted in any previous application for any degree.

The work presented (including data generated and data analysis) was carried out by the author except in the cases outlined below:

- XL-MS of Kif1C was a collaboration with N.Siddiqui, Straube lab.

ABSTRACT

Kinesin-12, Kif15 is a molecular motor involved in bipolar spindle assembly. Kif15 function is regulated through autoinhibition of its C-terminal tail and binding to the microtubule-associated protein Tpx2. Previous studies have reported Kif15 to function as a tetramer as well as a dimer. In this study, a cross-linking mass spectrometry (XL-MS) protocol and analysis workflow was developed to study the structural organisation of Kif15. Using XL-MS studies, it was found that Kif15 adopts a parallel tetramer conformation, which is autoinhibited by its C-terminal leucine zipper. Next, we show that this autoinhibited conformation is stabilised by the binding partner Tpx2. We also show that there is a shift in the binding interface between Kif15 and Tpx2 when microtubules are present and absent. In the presence of microtubules, Tpx2 mainly binds to the leucine-zipper of the Kif15 motor, whereas in the absence of the microtubules, this binding is exclusively localised to the fourth coiled-coil. We also reveal that Tpx2 adopts a dimeric conformation at physiological ionic strength. Finally, to understand the function of Kif15 *in-vivo*, we have developed putative Kif15 knock-out cell lines and developed a cross-linking protocol to cross-link Kif15 in cells.

List of Abbreviations

AMP-PNP – Adenylyl-imidodiphosphate

ATP – Adenosine Triphosphate

BS3 – Bis(sulfosuccinimidyl)suberate

CID – Collision induced dissociation

DSSO – Disuccinimidyl sulfoxide

EDC – 1-ethyl-3-(3-dimethylaminopropyl)carbodiimide hydrochloride

EM – Electron microscopy

ETD – Electron transfer dissociation

GTP – Guanosine Triphosphate

HCD – Higher collision induced dissociation

K-fibre – Kinetochore-fibre

Kif – Kinesin family protein

MT – Microtubule

MTOC – Microtubule organising centre

MAPs – Microtubule associated proteins

Amino acid Abbreviations

Amino acid	3-letter abbreviation	1-letter abbreviation
Alanine	Ala	A
Arginine	Arg	R
Asparagine	Asn	N
Aspartic acid	Asp	D
Cysteine	Cys	C
Glutamic acid	Glu	E
Glutamine	Gln	Q
Glycine	Gly	G
Histidine	His	H
Isoleucine	Ile	I
Leucine	Leu	L
Lysine	Lys	K
Methionine	Met	M

Phenylalanine	Phe	F
Proline	Pro	P
Serine	Ser	S
Threonine	Thr	T
Tryptophan	Trp	W
Tyrosine	Tyr	Y
Valine	Val	V

Chapter 1: Introduction

1.1 Cytoskeleton

The cytoskeleton is a dynamic cellular structure that mediates many biological phenomena, such as cell division, cell migration and extracellular matrix organisation. Specifically, the cytoskeleton is required to promote force generation to facilitate cell movement and maintain the structural integrity of intracellular compartments (Fletcher and Mullins, 2010).

To carry out these cellular functions, the cytoskeleton is composed of three elements; actin, intermediate filaments and microtubules. All components of the cytoskeleton can directly or indirectly interact with each other to mediate different cellular processes. Actin was initially discovered to be involved in promoting skeletal muscle contraction (Szent-Györgyi,1943). Actin monomers (G-actin) can polymerise to form the actin microfilament (F-actin). Both the polymerised and monomeric form of actin are present in cells and the assembly or disassembly of actin is regulated in response to biochemical stimuli (Ridley and Hall, 1992). Actin is mainly localised to the cell periphery and is predominantly involved in promoting cell movement (Carlier and Pantaloni, 2007). The polymerised actin filaments can also function as a rail for the motility of the molecular motors from the Myosin family (Sellers, 2000). The interaction between actin and the microtubule cytoskeletons is mediated through bi-functional proteins such as Tau and the microtubule-associated protein 2 (MAP2) which contain binding sites for both filament systems (Griffith and Pollard, 1982). Intermediate filaments are the most flexible cytoskeletal component as they have higher tensile strength than the other cytoskeletal elements (Herrmann et al., 2007). Also, they can interact with microtubules and the actin cytoskeleton through binding to a class of proteins called plectins (Wiche, 1998). A common class of intermediate filaments are nuclear lamins,

which are involved in many processes such as nuclear-envelope breakdown, which occurs after the nuclear lamins are phosphorylated by cyclin-dependent kinases (Tsai et al., 2006) and providing mechanical stability to the nucleus. (Dechat et al., 2008). Intermediate filaments have also been found to play a role in cellular mechanotransduction: Shear stress forces has been shown to mediate a conformational change in vimentin and keratin filaments which can, for example, increase the stiffness of the keratin fibres at the cell edges (Sivaramakrishnan et al., 2008, Helmke et al., 2000).

Microtubules are filament-like “tracks” that mediate various processes, such as intracellular transport, cell division and motility in eukaryotic cells through assembly into large-scale microtubule-based structures, such as cilia, flagella and the mitotic spindle. Microtubules are formed through the polymerisation of the heterodimeric α and β tubulin subunits (figure 1.1). In the presence of GTP, 13 tubulin polymers are assembled together in a parallel organisation to form the polarised microtubule with a hollow core and is 25 nm in diameter (Evans et al., 1985). The tubulin polymers are dynamic structures which can undergo rapid polymerisation and depolymerisation. This is mediated through the hydrolysis of GTP, which bind to the tubulin subunits. Tubulin subunits exist in a GTP or a GDP state. When the GTP-bound tubulin subunits are incorporated into the microtubules, they become hydrolysed into GDP. The growing microtubule end (plus end) has a cap of GTP-tubulin, which promotes the stability of the microtubule and protects it from disassembly. When the hydrolysis of GTP-bound tubulin reaches the growing microtubule tip, this promotes catastrophe and switches to rapid microtubule shrinkage. The shrinkage can be rescued by the binding of GTP-bound tubulin, which allows microtubule growth and restores the cap of GTP-tubulin. The stochastic switching between the states growth and shrinkage is known as dynamic instability (Mitchison and Kirschner, 1984) .

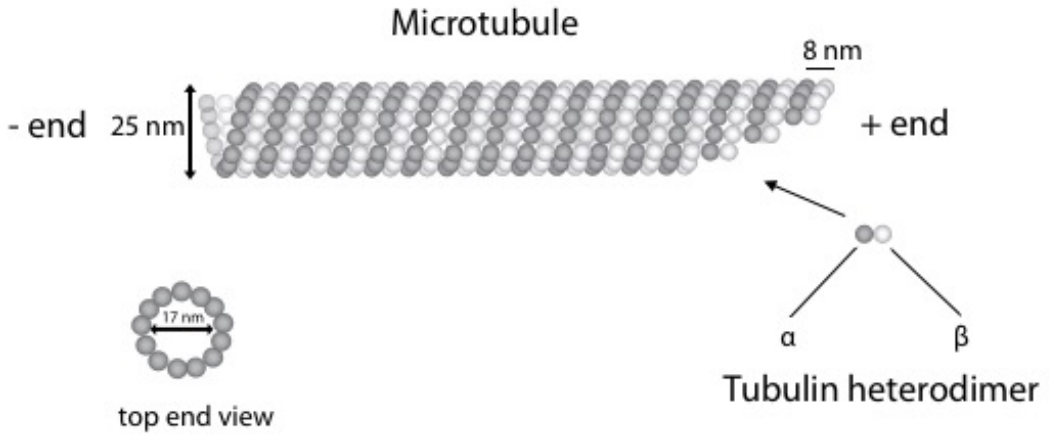

Figure 1. 1: Microtubule structure.
Depicted in this diagram is the microtubule, made up of 13 protofilaments with a hollow core and 25 nm in diameter. In dark grey is the α-tubulin subunit and light grey is the β-tubulin subunit, which forms a tubulin heterodimer that are added onto the growing microtubule plus end.

Kinesin and Dynein motors use microtubules as tracks for directional transport (Hirokawa, 1998). These motors utilise ATP hydrolysis into ADP and P_i to move along the microtubule tracks and transport cargo within the cells. The movement of these motors generates directional forces which drive complex biological processes such as bipolar spindle assembly during cell division. The motors bind to the microtubule lattice through a distinct microtubule binding site in the motor domain, with many containing a non-ATP dependent binding site in the tail to enhance their binding to the microtubules. Microtubule associated proteins (MAPs) are another class of proteins which bind and regulate microtubules and motor function (Etienne-Manneville, 2010). MAPs can be split into three classes; MT plus-end tracking proteins, MT minus-end tracking proteins and MAPs that decorate the microtubule lattice (Schuyler and Pellman, 2001, Akhmanova and Steinmetz, 2008, Hendershott and Vale, 2014, Jiang et al., 2014) . They are non-motor proteins which can affect the ability of the MTs to grow, shrink, bundle and the microtubule dynamics required for processes such as spindle assembly and stability. They are also required to localise several motors to the microtubules of the mitotic spindle (Wittmann et al., 1998, Chu et al., 2016).

1.2 Molecular Motors

1.2.1 Kinesin Motor Protein Family

Kinesins are a subgroup of molecular motors that bind microtubules and can be grouped into 14 family members based on their sequence conservation (Lawrence et al., 2004, Miki et al., 2005). Most kinesins contain three domains; a motor domain, a coiled-coil domain and a carboxy (C)-terminal tail most commonly used for cargo binding. The motor domain is where the ATP and microtubule binding sites are localised, whereas the neck linker connects the motor domain to the coiled-coiled stalk. Kinesins 1-12 are n-kinesins, whereby their motor domain is N-terminal. The Kinesin-14 family are c-kinesins and have a C-terminal ATPase motor domain, whereas the Kinesin-13s are m-kinesins, which have their motor domain in the middle region of the protein, with two coiled-coil tails at both the C- and N-terminal ends. As such, n-kinesins are generally plus-end directed, whereas c-kinesins are minus-end directed. Some motors, such as the yeast kinesin-5s, Cin8 and Cut7 can operate in a bidirectional mode (Roostalu et al., 2011, Edamatsu, 2014). M-kinesin group has an interesting microtubule depolymerisation activity that has significant implications for multiple biological processes (Ems-McClung and Walczak, 2010, Armond et al., 2015).

The conventional Kinesin, Kinesin-1 or the Kinesin heavy chain (KHC), is the most studied kinesin and work on this motor has helped to elucidate the ATPase cycle adopted by kinesins to drive their motility along microtubules (Hackney, 1994, Block et al., 1990, Cross, 2004, Carter and Cross, 2006, Carter and Cross, 2005). Each processive kinesin step on the microtubules (8-nm) hydrolyses one ATP molecule (Schnitzer and Block, 1997). As both motor heads are required to processively move along the microtubule lattice, the ATP hydrolysis must be coordinated to enable the motor to move using a hand over hand mechanism, whereby each head switches between a leading and trailing state (Howard et al., 1989, Block et al., 1990, Gennerich and Vale,

2009, Mori et al., 2007, Asbury et al., 2003, Cross, 1995). To do this, Kinesin motor domains have an ADP molecule bound in its active site, until the kinesin attaches to the microtubule. This attachment causes ATP to bind to the active site of the attached head. ATP binding then induces the neck-linker to undergo a conformational switch which moves the lagging motor head forward and allows it to come into close contact with next available binding site on the microtubule. The attached trailing head hydrolyses ATP to ADP and P_i and this allows the leading head to bind the microtubule. The trailing head releases the phosphate group and now in its ADP bound state, dissociates from the microtubules.

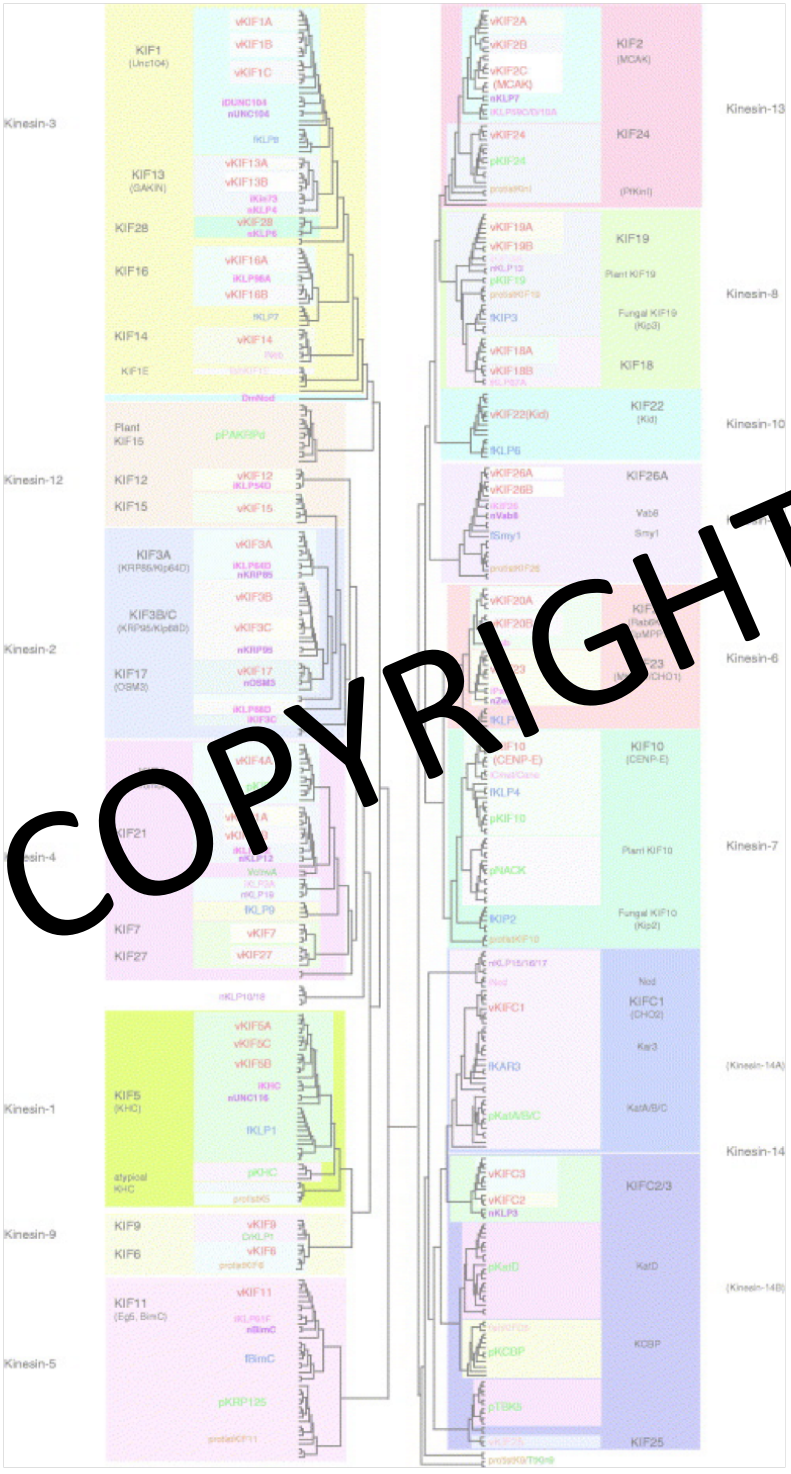

Figure 1. 2: **Kinesin family tree.**
Kinesins were grouped based on sequence alignment from 611 kinesin family proteins. The "KIF" nomenclature is exclusive for mammalian Kinesins. The kinesins were grouped into a total of 14 families. The taxonomy code used for the proteins are as follows; v, red = vertebrate; I, pink= insect; n, purple= nematode; p, green=higher plant; f, blue=fungi. Figure from Miki et al., 2005.

Kinesin superfamily is involved in mediating many cellular processes such as intracellular trafficking and ciliary functions. Henceforth, the focus here will be on the role of Kinesins in cell division. RNA-interference (RNAi) experiments in Drosophila flies has shown the crucial role kinesins play in several stages of mitosis, such as bipolar spindle assembly and chromosome segregation (Goshima and Vale, 2003). It has also been shown that specific Kinesin family members are required to carry out functions for distinct stages of cell division. In total, 9 mammalian Kinesin family members have been found to play a crucial role in the different stages of mitosis (Yen et al., 1991, Blangy et al., 1995, Mountain et al., 1999, Ganem and Compton, 2004, Zhu and Jiang, 2005, Zhu et al., 2005, Carleton et al., 2006, Tanenbaum et al., 2009).

The classic mitotic kinesin is Eg5. This Kinesin-5 (also called Kif11), was amongst the first mitotic kinesins to be characterised. RNAi experiments against Eg5 results in the formation of a monopolar spindle (Sawin et al., 1992). Eg5 is a 120 kDa plus-end directed, bipolar tetramer stabilised by a four-helix bundle (BASS domain), with two sets of motor domains at either end of the protein (Acar et al., 2013, Scholey et al., 2014). The C-terminal end of Eg5 contains an additional microtubule binding site, which given its anti-parallel conformation, is situated next to a pair of motor domain at either end of the molecule and helps the kinesin cross-link and slide overlapping, anti-parallel microtubules (Tao et al., 2006, Weinger et al., 2011). In prophase, Eg5 localises to the overlapping, antiparallel microtubule bundles situated between the centrosomes. Eg5 then moves these microtubules apart as the motor domain step towards the plus end of microtubules, thus initiating centrosome separation. After nuclear envelope breakdown, Eg5 is still involved in centrosome separation, however, once the bipolar spindle has been established, Eg5 is no longer essential as another motor, Kinesin-12 Kif15 is able to compensate for Eg5 to maintain the bipolar spindle (Vanneste et al., 2009, Tanenbaum et al., 2009) (see *4.1.2 Kif15 in Bipolar Spindle Assembly*).

Kinesins also play a crucial role in chromosome congression to the spindle equator. This includes the Kinesin-4 and Kinesin-10 family, which are known as chromokinesins, as they have a DNA binding site, which enables them to localise to the chromosomes (Funabiki and Murray, 2000). The removal of these chromokinesins results in chromosome misalignment. Another class of kinesins involved in chromosome congression is the Kinesin-13. This kinesin was first discovered as a protein concentrated in the inner centromere (Wordeman and Mitchison, 1995). Kinesin-13's are unusual as they have their motor head in the middle of the protein sequence and can function as a depolymerase at both microtubule ends (Hendershott and Vale, 2014, Goodwin and Vale, 2010, Wang et al., 2017, Benoit et al., 2018). These depolymerising kinesins regulate microtubule dynamics at the kinetochore, which is important in mediating chromosome capture, congression and alignment (Maney et al., 1998, Kline-Smith et al., 2004, Armond et al., 2015). The kinesin-8 family is also another member of the depolymerising kinesins group which modulate the assembly/disassembly dynamics of the microtubules. They are highly processive motors that are able to tip-track the microtubule plus-ends and depolymerise the microtubules in a length-dependent way (Varga et al., 2006, Mayr et al., 2007). The removal of Kinesin-8 from cells results in a lengthening of the microtubules and the spindle (Wordeman, 2010). Another Kinesin family protein involved in chromosome congression and alignment is Kinesin-7 (CENP-E). This kinesin can bind directly to the outer kinetochores as well as the microtubules. Kinesin-7 RNAi results in chromosome misalignment and incorrect segregation (Wood et al., 1997, Schaar et al., 1997).

1.2.2 Structural organisation of Kinesins

As previously described, Kinesin organisation can be divided into two main domains; a globular N-terminal ATPase motor domain, approximately 300 amino acids long, and a α-helical coiled coil, with unstructured regions distributed between the coils (Hirokawa et al., 1989, Yang et al., 1989). The motor domain is followed by a short neck-linker region, which connects the motor domain to the C-terminal coiled-coil. Based on structural data obtained for many Kinesins, it is clear that the motor domain is highly conserved amongst this class of motors, with the Myosin motor group also showing high similarity in their catalytic core (Kull et al., 1996, Sablin et al., 1996, Kull et al., 1998). The central region of the motor domain consists of β-sheets, with α-helices surrounding on both sides. The microtubule binding site and the ATP hydrolysis site are both located on the β-sheets, however they are on opposite end (Kull et al., 1996).

The highly conserved ATP hydrolysis site is not only found in the Kinesin and Myosin motor families, but also in the Ras G-protein family (Kull et al., 1998). This is due to these proteins all containing a phosphate-binding loop (p-loop) in the motor domain, and the binding of an ATP molecule to the active core causes the two adjacent regions Switch-1 (loop-9) and Switch-2 (α-helix4, loop-12 and α-helix-5) to close up and assume an active conformation, which is stabilised by a salt bridge forming between the Switch-1 and Switch-2 regions (Kikkawa et al., 2001). This closed conformation and the presence of a Mg^{+} ion in the active site induces ATP to be hydrolysed into ADP and P_i. The release of the phosphate group causes the motor domain to change its configuration back to the open conformation (Kikkawa et al., 2001). The neck-linker is a region of 12-18 amino acids, which is important in connecting the motor domain to the extended coiled-coil tail. It has also been found to be important in mediating hand-over-hand mechanism required for the processive motility of the kinesin motors (Rice et al., 1999). This is because the ATP binding to the leading head induces a structural conformation in the

neck-linker region, which allows the trailing head to shift forward 16 nm and bind to the next microtubule binding site. Of the current structures available for Kinesins, they tend to be monomeric kinesins, as the dimeric kinesins are difficult to crystallise. However, a recent study has provided insight into the motility mechanism of a microtubule-bound dimeric kinesin using an ATP analog (Liu et al., 2017). In monomeric kinesins, it has been shown that the docking of the neck region is associated with structural rearrangement of three Kinesin domains, which includes the P-loop subdomain (Cao et al., 2014, Shang et al., 2014). Whilst there is less substantial rotation than the P-loop, the switch I/II subdomains of the Kinesin head also undergo movement, which is proposed to hinder the conformational change in the neck linker and prevents docking in the leading head domain (Shang et al., 2014). Similar findings were identified for the dimeric kinesins, however, the rotations of these subdomains is smaller for the dimeric kinesin and the movements only occur in the leading head and not the trailing head (Liu et al., 2017). Interestingly, the neck region has also been revealed to be essential in determining the directional movement of the motor (Case et al., 1997, Henningsen and Schliwa, 1997). Also, the length of the kinesin neck-linker has been shown to undergo structural changes which is thought to affect the motility of these motors. For example, it has been suggested that the probability of a motor to undergo diffusion on the microtubule lattice, is dependent on the length of the neck-linker region; the longer the neck-linker region, the higher the probability of diffusion, which reduces microtubule stepping and leads to subsequent release of the motor heads from the microtubules (Andreasson et al., 2015). Studies of the neck-linker region has shown that there is a high sequence variation for the length of the neck-linker between the different Kinesin family members, although there is high sequence conservation within the same family subgroup (Hariharan and Hancock, 2009).

The Kinesin coiled-coil tails is variable in length, with the Kinesin-7 containing the longest known tail at 230 nm (Kim et al., 2008). The tail region of Kinesins displays the highest divergence amongst the Kinesin family as they contain binding sites for various binding partners and substrates, which allows the motors to mediate specific functions. The Kinesin tail is also important in folding back onto the motor domain to auto-inhibit the motor. Studies, including NMR and Bioinformatics analysis of all human 43 kinesins has also confirmed that the Kinesin tail is highly intrinsically unstructured, suggesting it can adopt several conformations, instead of a singular native configuration (Seeger et al., 2012). Cryo-EM and crystallography studies are optimal for studying static structures, and due to the inherent flexibility of Kinesins, these techniques may always not be the best method of choice. However, Cryo-EM has been used to make significant development has been made in understanding the structural basis of Kinesin assembly and function (Moores et al., 2002, Endres et al., 2006, Sindelar and Downing, 2007).

1.2.3 Regulation of Kinesins

Kinesins are important in mediating many cellular functions. As such, it is very important to fully understand the different mechanisms by which Kinesin activity can be regulated. It is crucial that Kinesins do not overcrowd the microtubules or unnecessarily undergo ATP hydrolysis, thus their activity needs to be modulated.

A common mechanism to regulate Kinesin activity is through auto-inhibition. This mechanism has best been characterised for the Kinesin-1 family, however it has been identified as a regulatory mechanism in several other kinesins as well (Hackney et al., 1992, Verhey et al., 1998, Coy et al., 1999). A crystal structure of a dimeric kinesin motor domain with its tail has provided great insight into the structural basis of the autoinhibition mechanisms of kinesins (Kaan et al., 2011). The autoinhibited conformation ensures that the

C-terminal tail of the kinesin forms direct cross-links at two distinct sites, the neck coil and the tail (Kaan et al., 2011). Unexpectedly, it has also been shown that for a dimeric kinesin, only one of the tails folds back and makes direct contact with the motor domain (Hackney et al., 2009). This autoinhibited conformation requires the kinesin to contain a hinge region in the coiled-coil tail to allow the tail to fold back on itself. This has been confirmed in several autoinhibited kinesins, as the removal of these hinge regions abrogates the ability of the kinesin to fold back on itself, thus they remain in a constitutively active conformation (Coy et al., 1999). Also, this folded conformation means that the close proximity of the tail to the motor domain, blocks the microtubule binding and the ATPase activity of the Kinesin, thus it remains in an inactive state. For Kinesin-1, a highly conserved region in the tail (the IAK domain) is essential for Kinesin-1 autoinhibition (Hackney et al., 2009). The presence of an adjacent highly charged region, further enhances the autoinhibition. Kinesin-1 autoinhibition is also achieved by the binding of the Kinesin Heavy Chain (KHC) in-between the Kinesin-1 motor heads, which prevents the processive movement of the motor (Cai et al., 2007). CENP-E, a Kinesin-7 protein is another mitotic kinesin regulated by autoinhibition. As mentioned, this protein plays a crucial role in chromosome congression. The kinesin normally adopts a folded conformation, whereby its motor domain is inaccessible to the microtubules. To activate the Kinesin, C-terminal phosphorylation by MPS1 or CDK-1 releases the autoinhibited conformation and activates the kinesin to facilitate its function for correct chromosome congression (Espeut et al., 2008). The kinesin Eg5 can also auto-regulate its activity through a slightly different mechanism. The motor uses energy-independent diffusion along a single microtubule track, but adopts processive movement when it comes into contact with a second microtubule (Kapitein et al., 2008). This ensures Eg5 only utilises ATP to undergo directed movement when it cross-links two microtubules. Lysine acetylation of residue 146 in the motor domain of Eg5 can also activate the motor (Muretta et al., 2018).

Kinesins can also be regulated through temporal and spatial protein expression. Mitotic kinesins are required for distinct function during Mitosis therefore they are only required to be expressed at certain stages of cell division. For example, there are transcription factors, such as FOXM1 that selectively activates kinesin proteins at the start of Mitosis (Alvarez-Fernandez and Medema, 2013). As well as the regulating their synthesis, other protein complexes, such as the ubiquitin ligase APC/C complex is required to degrade Kinesins containing a targeted KEN motif in their destruction domain (D-box). The kinesin-10, Kid, is a well described kinesin regulated by APC/C complex degradation. As previously described, this kinesin is an important plus-end directed motor required for chromosome congression. However, during the onset of anaphase, this kinesin is targeted for degradation, to abolish the polar ejection force which mediates chromosome congression, thus promoting the chromosomes to be pulled to opposite spindle poles (Vanneste et al., 2011, Funabiki and Murray, 2000).

Another important regulatory mechanism for Kinesins is protein-protein interactions. EB proteins have been found to act as a scaffold for the localisation of Kinesins to the microtubule plus-end. EB proteins are well characterised +TIP tracking proteins and Kinesins such as Kinesin-8 and Kinesin-13 are known to contain an SxIP motif to interact with the EB proteins and localise to the microtubule plus end (Akhmanova and Steinmetz, 2008, Honnappa et al., 2009, Stout et al., 2011). For example, it was shown that Kif18b localisation to the astral microtubules plus-ends requires EB1 and Kif18b can also form a complex with MCAK to enhance each other's affinity for the microtubule plus-end (Tanenbaum et al., 2011). Kinesin-5 and Kinesin-12 have been shown to bind and track microtubule plus-end independently of EB proteins. Proteins, such as the MAP Tpx2 can bind Kinesins and regulate their localisation. Kinesin-5 binding to Tpx2 is required to localise the motor to the spindle and inhibits the motility of the motor *in-vitro* (Ma et al., 2011, Balchand et al., 2015). Tpx2 was discovered as a spindle targeting protein for Xklp2, the Xenopus homologue of Kinesin-12 Kif15 (Wittmann et al.,

1998).Tpx2 is important in acentrosomal-independent microtubule nucleation (Chen et al., 2017) and is able to promote microtubule nucleation *in-vitro* using purified tubulin (Roostalu et al., 2015). Tpx2 also plays a crucial role throughout the different stages of Mitosis, through the recruitment of proteins to the bipolar spindle or direct activation of mitotic regulators. Amongst these regulators is the serine/threonine mitotic kinase Aurora A. Residues 1-43 of Tpx2 is required for binding to Aurora A, which stabilises the autophosphorylation of Thr288 in the kinase loop through a conformational shift which makes the Thr288 residue inaccessible for dephosphorylation by protein phosphatase 1 (PP1) (Bayliss et al., 2003). Tpx2 is also required for the localisation of the kinase to the mitotic spindle (Kufer et al., 2002).

Phosphorylation by mitotic kinases is an essential mechanism utilised to regulate mitotic kinesin localisation during mitosis. Eg5 has been shown to localise to the spindle microtubules through the phosphorylation of its C-terminal tail by CDK1 (Sawin and Mitchison, 1995, Blangy et al., 1995). Another example is the multi-phosphorylation of the Kinesin-13, MCAK by Aurora A, which regulates its localisation to the kinetochores, spindle poles and chromosome arms (reviewed in (Ems-McClung and Walczak, 2010). The activities of the kinase CDK1 and protein phosphatase 1 (PP1) are required for Kif18A-dependent regulation of pre-anaphase chromosome oscillations (Hafner et al., 2014).

1.3 Kinesin-12

1.3.1 Kinesin-12 Kif15

The naming of the Kinesin families, including the Kinesin-12 family, was initially based on sequence conservation and function (Hirokawa, 1998). However, based on substantial genome sequencing since the original paper, there has been a suggestion that some of the Kinesin families were incorrectly grouped. Amongst these is the Kinesin-12 family, which was suggested to be split into Kinesin-16 (containing *Hs*Kif12) and Kinesin-15 (HsKif15 and AtPAKRP1) (Wickstead and Gull, 2006). The Kinesin-12 family has been shown to be involved in bipolar spindle assembly in both animal and plant cells. PAKRP1/Kinesin-12A and PAKRP1L/Kinesin-12B were identified as playing a critical role in cytokinesis of male gametogenesis in *Arabidopsis* (Lee et al., 2007).

The kinesin-12 Kif15, was first discovered in *Xenopus laevis* (Xklp2), where it was shown to be localised to the centrosomes instead of the chromosomes and is required for maintenance of the bipolar spindle (Boleti et al., 1996). Xklp2 was initially characterised as a homodimeric Kinesin, which requires the microtubule-associated protein Tpx2 (targeting protein for Xklp2) to localise to the mitotic spindle and microtubule minus-ends (Wittmann et al., 1998). Also, a single point mutation in the C-terminal leucine zipper of Xklp2 was shown to abrogate spindle targeting of the motor. The *Caenorhabditis elegans (* C. *elegans)* and sea urchin homologues for Xklp2 have also shown that this Kinesin plays a role in bipolar spindle assembly (Rogers et al., 2000, Segbert et al., 2003). The human Kif15 (Hklp2) is a kinesin which mainly functions in mitosis and has some overlapping functions with Eg5, however it is structurally and mechanistically different from Eg5 (Vanneste et al., 2009). The small molecule inhibitor of Eg5 (Monastrol) is known to recognise and bind to Loop-5 of Eg5, which stabilises the inactive conformation of the motor and puts it in a weakly bound state (Cochran et al., 2005, Crevel et al., 2004). The structure of the L5 region is specific for Eg5, thus explaining why this inhibitor is

ineffective for Kif15. Human Kif15 has been reported as a homotetramer based on biochemical examination of the full length Kif15 expressed and purified from insect cells (Drechsler et al., 2014, Drechsler and McAinsh, 2016) and from Kif15 protein purified from mammalian cell extracts (Mann et al., 2017). However, the Ohi lab report Kif15 to function as a dimer and propose based on truncation experiments that Kif15 has an additional microtubule binding site in the region containing the first coiled-coil domain and the adjacent unstructured region (Kif15 1-700) (Sturgill et al., 2014).

The N-terminal motor domain of Kif15 is the main microtubule binding site (Figure 1.4B, 1.4C). A crystal structure for Kif15 motor domain (residues 19-375), show the motor adopts the conserved kinesin fold (Klejnot et al., 2014). Single molecule assays have shown that Kif15 is a plus-end directed motor with short minus-end directed movement on microtubules and that it is able to processively walk for over 1 μm and undergo diffusion on the microtubule lattice (Drechser et al., 2014). However, the run-length of Kif15 motors is significantly lower under load, with a stall force of ~6 pN (McHugh et al., 2018). The motor is also able to effectively switch microtubule tracks and is able to recognise and bind to the plus-ends, independently of EB proteins (Drechsler et al., 2014, Kapitein et al., 2005). Kif15 is also able to cross-link microtubules however, no clear evidence to indicate extensile sliding of anti-parallel microtubules was identified. In fact, fully anti-parallel microtubules tend to recruit multiple motors with no movement of microtubules observed. It was also shown that in the presence of Tpx2, Kif15 binding to microtubules was enhanced. Tpx2 significantly reduces the proportion of motile motors and optical trapping experiments further confirmed this, but also showed that Tpx2 increased the load-bearing capability of Kif15 (Drechsler et al., 2014, Mann et al., 2017). Kif15 motility can also be regulated by autoinhibition, mediated by the C-terminal tail (residues 701-1388) (Sturgill et al., 2014). Specifically, the C-terminal leucine-zipper (residues 1294-1388) has been identified as essential in stabilising this autoinhibited conformation that tightly locks onto the microtubules, which is further stabilised by the presence of Tpx2 (McHugh

et al., 2017).On dynamic microtubules, the motor has also been shown to track microtubule plus-ends, cross-link and transport one microtubule relative to the other, resulting in the formation of parallel microtubule bundles (Drechsler and McAinsh, 2016, Drechsler et al., 2014). The role of Kif15 in driving parallel bundles is also consistent with studies with C. *elegans* Kinesin-12 (KLP-18), showing this motor is required for promoting the formation of parallel microtubules around meiotic chromosomes (Segbert et al., 2003). It has also been suggested that a second microtubule binding site is required for Kif15-dependent microtubule sliding (Sturgill et al., 2014).

In recent years, several studies have attempted to characterize the mechanochemical properties of Kif15 (Drechsler et al., 2014, Reinemann et al., 2017, McHugh et al., 2018, Milic et al., 2018). It has been reported that the Kif15 motor is processive under assisting and hindering loads, and the run-length of Kif15 motors significantly lower under load, with a stall force of ~6 pN (McHugh et al., 2018, Milic et al., 2018). Further work has also been done to characterize the mechanochemical cycle of Kif15, which can be simplified into 4 steps as seen in figure 1.3 (Milic et al., 2018). The first step involves the binding of ATP to the nucleotide-free, microtubule-bound (apo) leading head in the ATP-waiting state. This step is followed by the partial docking of the neck-linker (NL) to the leading head. Full docking of the NL occurs after ATP hydrolysis which enables the tethered head to bind to the microtubules on the next available binding site and release ADP. The final step is the release of the phosphate group, which detaches the trailing head from the microtubule and converts the kinesin to its original one-head-bound state. Modelling the mechanochemical cycle between Kif15 and Eg5 has produced interesting results; the rates of transitions for the Kif15 steps were up to 4-fold faster than those rates reported for Eg5. For Kif15, the phosphate-release step which promotes the release of the rear-head, is 10 times faster than the hydrolysis step. This indicates that unlike Eg5, Kif15 spends most of its time in a single-head-bound state (Milic et al., 2018, McHugh et al., 2018).

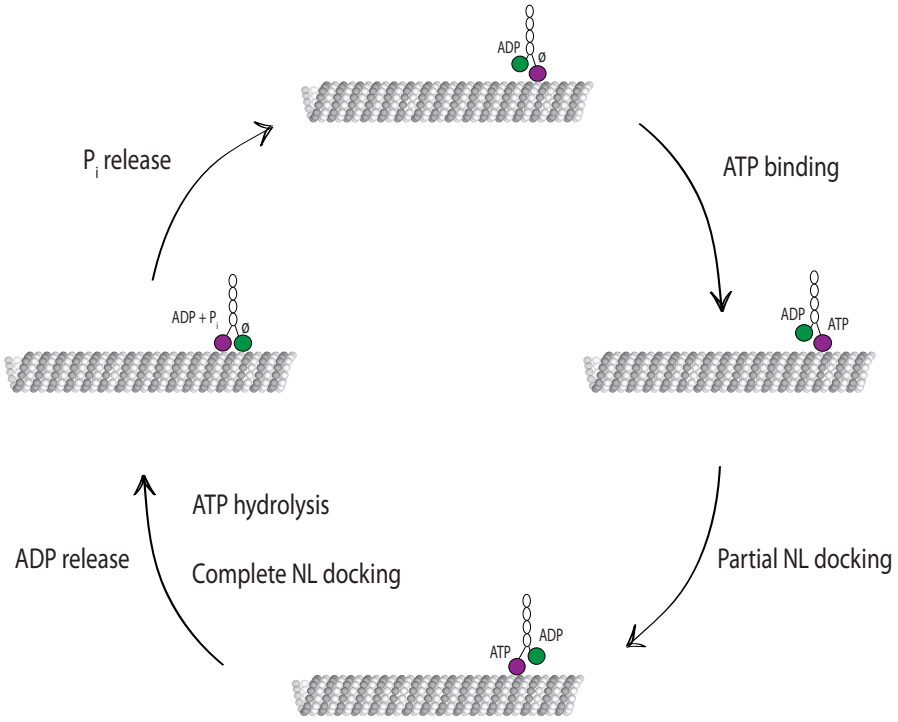

Figure 1.3: Mechanochemical cycle of Kif15.
This cycle can be simplified into 4 steps. Firstly, ATP molecule binds to the microtubule-bound, nucleotide-free (∅) leading head. This is followed by a mechanical step, which involves the partial docking of the neck-linker to the microtubule-bound head. ATP hydrolysis then promotes the complete docking of the NL and ADP release from the tethered head promotes binding to the microtubules. Finally, the release of the phosphate group detaches the trailing head and returns the motor to its single-head-bound state.

The N-terminal motor domain of Kif15 is also the proposed binding site for the novel binding partner KBP (Brouwers et al., 2017, Kevenaar et al., 2016). It was shown that KBP does not have a significant effect on Kif15 localisation to the spindle poles, but KBP depletion reduces Kif15 localisation to the spindle equator and the chromosomes (Brouwers et al., 2017). Kif15's localisation to the chromosomes is mainly mediated by the chromosome marker Ki67. Depletion of Ki67 results in significance decrease of Kif15 levels from the chromosomes but localisation to the spindle is retained (Vanneste et al., 2011).

In interphase, Kif15 forms evenly dispersed puncta in the cytoplasm and co-localise with the microtubules, however Tpx2 is required to localise the motor to the spindle microtubules and k-fibres in prometaphase. Kif15 can also co-localise to the outer-kinetochore protein Hec1 in HeLa cells (Sturgill and Ohi, 2013). The C-terminal region (residues 710-747) of Tpx2 has been confirmed as essential in localising Kif15 to the mitotic spindle (Mann et al., 2017). It has also been recently shown that phosphorylation of Kif15 by Aurora A at S1169 is important in localising the motor the spindle poles, as it has been shown that spindle localisation of Kif15 is decreased upon Aurora A inhibition (van Heesbeen et al., 2017). Both Aurora A and Kif15 activity is regulated by Tpx2 so it is possible that the phosphorylation by Aurora A promotes Kif15 to fold into a conformation that makes the leucine-zipper accessible for Tpx2 binding.

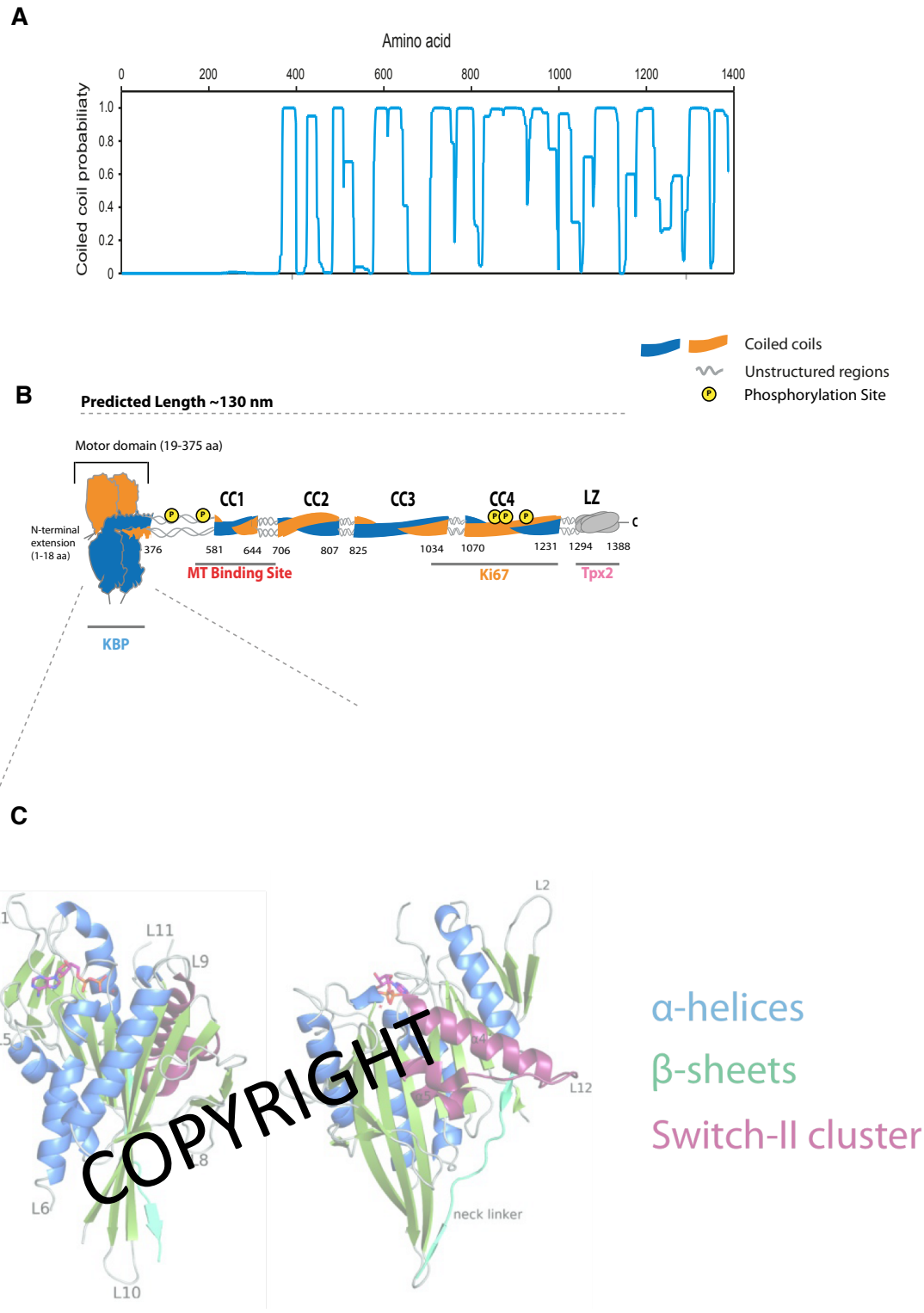

Figure 1. 4: Domain organisation of Kif15.
A; Coiled-coils prediction plot from Uniprot. **B;** Domain organisation of Kif15 based on ELM (Eukaryotic Linear Motif) coiled coil prediction software. A minimum of 20 amino acids (or about 3 heptad repeats) were used for the coiled-coil predictions. N-terminal motor domain is where the kinesin binding protein (KBP) has been shown to bind. The first coiled coil domain harbours a proposed second ATP-independent microtubule binding site. The C-terminal

tail contains the Ki67 and Tpx2 binding sites. The phosphorylation sites are localised to unstructured region adjacent to the motor domain and the fourth coiled-coil (CC4) domain. **C;** Crystal structure of Kif15 motor domain (from Klejnot et al., 2014).

1.3.2 Kif15 in Bipolar Spindle Assembly

The mitotic spindle has a bipolar configuration with approximate dimensions of 10 x 10 x 10 μm, and is composed of a microtubule super structure and additional protein components. At the spindle poles the microtubules are anchored at the microtubule organizing centre (MTOC), which is the centrosome for eukaroytic cells. The bipolar spindle contains three microtubule elements; astral microtubules, inter-polar microtubules and kinetochore fibres (figure 1.4). The astral microtubules are microtubules emanating from the centrosomes to the cell cortex, thus help spindle positioning and control the cell division plane orientation (Grill et al., 2001, Grill et al., 2003). Despite their role in centrosome separation during prophase (Rosenblatt, 2005), astral microtubules are not essential for cell division (Khodjakov et al., 2000).

The interpolar microtubules are microtubules that extend from the centrosome and interdigitate with each other in an anti-parallel manner at the equator of the bipolar spindle to provide structure and support. These non-kinetochore microtubules are the most abundant subset of microtubules found within the spindle and are very dynamic, with a half-life of ~50 seconds (Zhai et al., 1995). The kinetochore fibers (k-fibres) are the third class of microtubules found in the mitotic spindle. They are composed of ~20-25 bundled parallel microtubules that attach the chromosomes to the spindle poles, thus allowing the sister chromatids to be separated into new daughter cells (Rieder, 1981, McEwen et al., 1997). These K-fibers are more stable than the interpolar microtubules, with an average half-life of ~6 minutes (Bakhoum et al., 2009, Zhai et al., 1995).

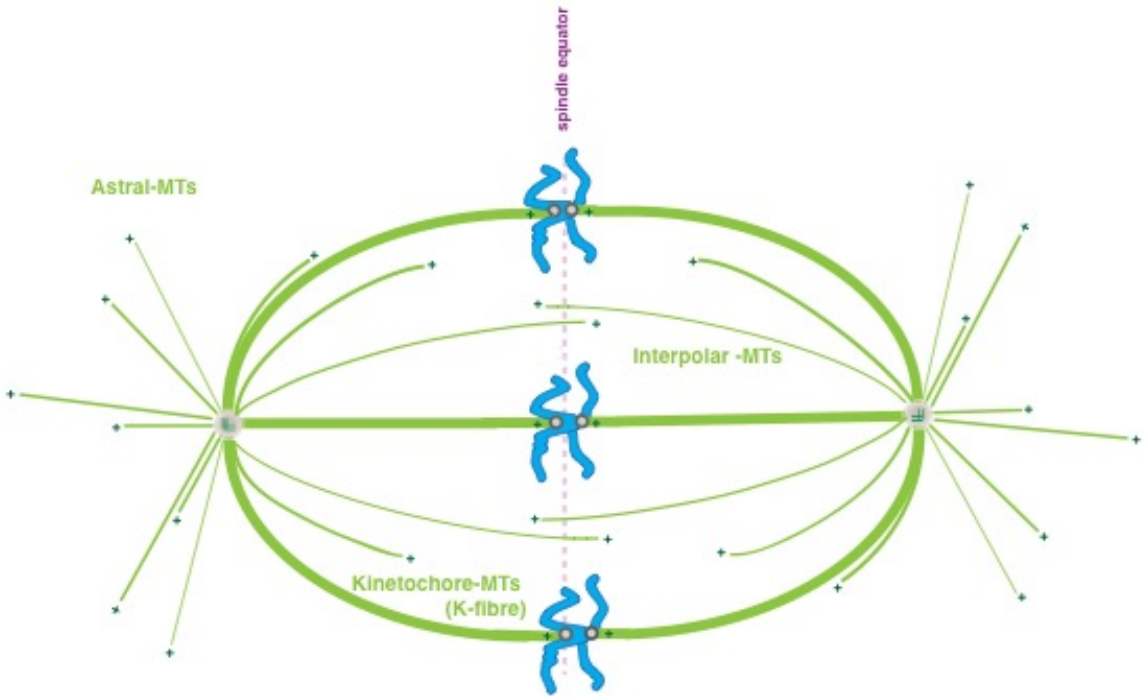

Figure 1. 5: Microtubule components of the bipolar spindle.
The Astral MTs extent out towards the cell cortex and do not play a crucial role in cell division, but important for spindle positioning. The interpolar MTs provide structure and stability to the bipolar spindle. The kinetochore MTs are essential for mediating attachment to the chromosomes. Adapted from Auckland & McAinsh, 2015.

In order for cell division to occur, the bipolar spindle needs to be established and then maintained throughout Mitosis. To establish the bipolar spindle, balanced forces exerted on the microtubules by molecular motors are needed. As previously described, the Kinesin-5, Eg5 is crucial for establishing the bipolar spindle by separating the duplicated centrosomes. In the absence of Eg5, Kif15 overexpression can compensate and establish the bipolar spindle, as both these motors exert the outward pulling forces required for the establishment of the bipolar spindle (Vanneste et al., 2011, Vanneste et al., 2009, Tanenbaum et al., 2009). However, Kif15 overexpression-dependent bipolar spindle assembly requires Tpx2 (Mann et al., 2017). Centrosome separation also requires the presence of minus-end directed motors such as

dynein and the Kinesin-14 HSET, which provide the inward pulling forces to balance the forces exerted (Sharp et al., 2000, Tanenbaum et al., 2008). This has been confirmed by depletion experiments in cells, whereby removal of Eg5 resulted in the formation of a monopolar spindle and the subsequent depletion of dynein restored the bipolar spindle (Tanenbaum et al., 2008)

In HeLa cells, Eg5 inhibition using Monastrol does not affect the maintenance of the bipolar spindle as Kif15 is able to compensate and provide the outward pulling forces required to maintain the bipolar spindle (Vanneste et al., 2009). However, when the cells where depleted of both plus-end directed motors, the spindle collapsed into a monopolar state. If Dynein was then removed in a Eg5 and Kif15 depleted background, the bipolar spindle was re-established however there was an increase in chromosome misalignments (van Heesbeen et al., 2014). This suggests that force balance is also important in mediating correct kinetochore-microtubule attachments.

Despite the requirement of overexpression of Kif15 to assemble the bipolar spindle in the absence of Eg5, basal levels of Kif15 are enough to maintain the established bipolar spindle. Also, due to the localisation of Kif15 to the k-fibres which it also stabilises (Sturgill and Ohi, 2013) it may be that these microtubules are crucial in mediating Kif15-dependent bipolar spindle assembly. The Ohi lab investigated this and established that not all human cells respond the same to Eg5 depletion. In fact, the ability of the cells to use the Kif15-dependent bipolar spindle assembly is largely dependent on the stability of the k-fibres in the cells. In HeLa cells, the k-fibres are very stable and in the absence of Eg5, Kif15 is able to maintain the bipolar spindle. However, in cells such as RPE cells, the k-fibres are less stable and in the absence of Eg5, Kif15 is not able to re-establish the bipolar spindle (Gayek and Ohi, 2014).

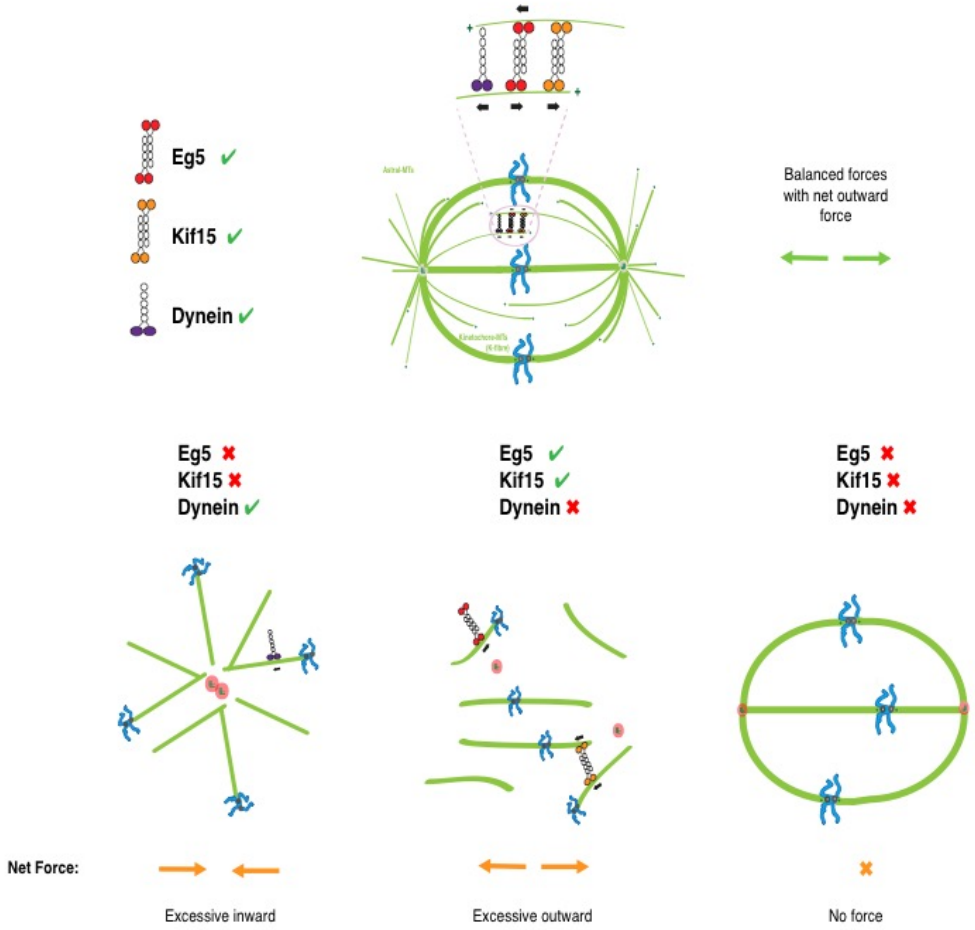

Figure 1. 6: Force balance model for bipolar spindle assembly. Eg5, Kif15 and Dynein localise to over-lapping microtubules to generate balanced forces required. In the absence of Eg5 and Kif15, the excessive inward force generated by Dynein results in the formation of a monopolar spindle. In the absence of Dynein, Eg5 and Kif15 produce excessive outward force. In the absence of all three motors, the bipolar spindle is able maintain its configuration, however, there is an increase in chromosome misalignments.

1.3.3 Non-mitotic function for Kinesin-12 motors

Despite the crucial role of Kif15 in mitosis, the is some evidence that the motor can perform several non-mitotic functions. Kif15 has recently been shown to play a role integrin trafficking. Specifically, it was found that α2 integrin trafficking is inhibited by Kif15 (Eskova et al., 2014). This is promoted through Kif15-dependent localisation of the clathrin adaptor, Dab2 to the plasma membrane. This suggests that Kif15 may function as a transport Kinesin in interphase.

Kif15 plays an important role in mediating cell migration in post-mitotic neurons and axonal growth. Depletion of Kif15 also causes uncontrolled axonal growth, decrease in axonal branching and growth cone size (Liu et al., 2010). Kif15 phosphorylation of T1142 mediates its interaction with myosin-IIB, which has been shown to promote astrocyte migration (Feng et al., 2016). One possibility is that these effects of cell migration are a consequence of the reported interaction between Kif15 and actin (Liu et al., 2010). Further work will be needed to determine the interaction between Kif15 and actin, and how this contributes to cell migration.

Interestingly, Kif15 has also been revealed to be involved in remodelling the actin cytoskeleton during infection. This idea came from yeast two-hybrid experiments that found an interaction between C-terminal end of Kif5 (residues 1092-1347) and EspW, an effector of the type III secretion system of bacterial cells (Sandu et al., 2017). EspW has been found to mediate actin dynamics of infection sites using a RAC1-dependent mechanism. EspW interacts with Kif15, which in turns activates Rac1 that is required to remodel the actin cytoskeleton to respond to an infection.

1.4 Project Outline

There are conflicting views in the field regarding the structural organisation of Kif15, as it has been found that Kif15 functions as a tetramer (Drechsler et al., 2014, Mann et al., 2017) as well as a dimer (Sturgill et al., 2014). Also, the exact structural assembly of Kif15 remains unknown and whether the tetramer is bipolar or parallel is also yet to be elucidated. To fully understand the role of Kif15 and its functional redundancy with Eg5, a clear understanding of its structural assembly is required (Hancock, 2014). Also, the mechanism by which Kif15 autoinhibits at a structural level remains uncovered.

In this project, we have successfully been able to provide a detailed understanding of the structural assembly of Kif15 into a tetramer. Also, presented here is an understanding of the effect on the structure of Kif15 when the C-terminal leucine zipper is absent. Finally, we have also uncovered the molecular mechanism by which Tpx2 inhibits Kif15.

Chapter 2: Materials and Methods

2.1 Molecular Biology

2.1.1 CRISPR genome-editing

CRISPR genome editing was used to generate RPE1-mCherry-Tubulin cells depleted of Kif15. The protocol was followed as described in Ran *et al.,* (2013). A 20 small guide RNA nucleotide sequence, 5' GGTGAGGGCGCTATGGCACC 3' was used to target the Cas9 to the Kif15 genome sequence. The Cas9 enzyme cuts between the 17th and 18th base of the guide sequence, which corresponds to the 5th and the 6th nucleotide of Kif15 exon 1. This nucleotide sequence is only found once within the human genome, thus minimizing off-target effects.

The sgRNA sequence was cloned into pSpCas9-2A-GFP plasmid (Addgene plasmid ID:48138) using primers 5' CACCGGGTGAGGGCGCTATGGCACC 3' and 5' AAACGGTGCCATAGCGCCCTCACCC 3'. This plasmid was then transfected into RPE1-mCherry-Tubulin cells as described in *2.2 Plasmid DNA Transfection*. After 48-hour transfection, the cells were prepared for cell sorting. The transfected cells were trypsinised, spun at 200 g for 5 mins and replaced with starving media (Sigma dulbecco's modified Eagle's medium F-12 Ham 1 % FBS (Sigma), 1 % Penstrep (Sigma) and 2 mM L-Glutamine (Sigma)) and sorted using a BD influx FACS cell sorter (Bioscience) to enrich for transfected cells. The cells were then seeded for single clones using 1000 cells in a 20 cm dish. The sorted cells were replaced with standard RPE1 media (Sigma dulbecco's modified Eagle's medium F-12 Ham 10 % FBS (Sigma), 1 % Penstrep (Sigma) and 2 mM L-Glutamine (Sigma)). The cells were allowed to expand for 2-3 weeks and single clones were selected using cloning discs (Sigma). The cells were then grown in a 24-well plate and passaged for immunofluorescence screening (see section *2.5.3 immunofluorescence* for more details)

2.2 Cell Biology

2.2.1 Mammalian Cell Maintenance

RPE1-mCherry Tubulin cells (Gift from Straube Lab), were cultured in Sigma dulbecco's modified Eagle's medium F-12 Ham 10%FBS (Sigma), 1%Penstrep (Sigma) and 2mM L-Glutamine (Sigma) and grown in a 37% humidified incubator with 5% CO_2. To maintain the cells, they were grown until 80% confluency, washed with PBS then split using 1:1000 Trypsin. To check the cells have become detached, an inverted microscope was used, followed by a 1:10 dilution of the cells into pre-warmed RPE media.

2.2.2 Plasmid DNA Transfection

For plasmid DNA transfection, 750 μl Optimem (Gibco) and 10 ug DNA were separately mixed and incubated for 5 minutes, and 750 μl Optimem and 30 μl Fugene (Promega) were also mixed and left for 5 minutes. After this incubation period, both tubes were mixed together and left to homogenise for 30 minutes before adding to the cells. During this incubation period, the media in cells seeded in the 10 cm plate were replaced with fresh pre-warmed medium.

2.2.3 Insect Cell Maintenance and transfection

SF9 cells (Invitrogen) were grown in SF900 serum free media, containing 100 U/ml Penicillin (Sigma), 100μg/ml Streptomycin (Sigma). The cells were grown at 28^0C and 105 rpm shaking incubator. The cells were allowed to reach a density of $1.5x10^6$ cells/ml, before they were split 1:3 into fresh SF900 media.

SF9 cells were re-suspended to a final density of $1x10^6$ in 24 well-plate. Transfection of SF9 cells with DNA was carried out using the BacMagic DNA Kit (Novagen) as described in the user manual; 12 μl Escort IV (Sigma), 5 μl vector DNA, 5 μl BacMagic DNA and 1 ml SF900 media were mixed well and incubated for 30 minutes before adding to the cells. After 5-7 days, the cells were spun at 400 g for 5 minutes, and the virus-containing supernatant is

filtered through a 0.45μm filter to collect the passage 1 (P1) virus stock. SF9 cells at a density of $0.5x10^6$ were infected with 50 μl of P1 virus. After 36 hours, the cells were spun down and re-suspended with SF900 media, 20% FBS and 10% DMSO. The cells were then collected as 500 μl aliquots and stored in -80^0C.These cells are henceforth referred to as Baculovirus Infected Insect Cells (BIICs).

2.3 Biochemistry

2.3.1 Protein Expression

Protein expression was carried out by infecting SF9 cells with BIICs cells and 1 ml aliquots of the cells were taken every 24 hours for 96 hours then ran on a hand-cast 10% SDS-PAGE gel followed by western blotting to determine optimal protein expression. For the western blotting, the Penta-His monoclonal antibody (Thermo Scientific) was used at a concentration of 0.1 *μ*g/mL. The protein was transferred onto a PVDF membrane (pre-activated using 100% methanol for 1 minute) for one hour using 20V. The membrane was then blocked for one hour, using 5% milk in BSA, followed by incubation with primary Penta-His monoclonal antibody (in 1.5% milk and TBST). The membrane was washed three times with TBST for 10 minutes each, followed by incubation with secondary anti-mouse Horseradish-Peroxidase (HRP) Antibody (Thermo Scientific). The signal was detected using the Chemiluminescent ECL Western Blot Kit (Biorad), following the manufacturers protocol.

For large scale protein expression, 500 ml SF9 cells at $1x10^6$ were infected with 500 μl of the BIICs stocks then left for 96 hours as done in Wasilko *et al.,* 2009). The cells were then harvested at 96 hours by spinning at 1200 rpm for 20 minutes using an ss-34 rotor. The wet weight of the cell pellet was determined on a standard analytical balance and the pellet was resuspended in 4 ml per gram of cell pellet using SF9 lysis buffer (see table 2.1), containing

0.1 mM ATP, EDTA-free protease inhibitor (Roche), 1 mM DTT. The lysate was snap-frozen in liquid nitrogen and stored in -80^{0}C.

SF9 Lysis Buffer
50 mM HEPES, pH 7.55
150 mM NaCl
1.5 mM MgCl2
3mM EGTA
5% Glycerol
0.1% Tween

Table 2.1: SF9 Lysis Buffer.

2.3.2 Protein Purification

For Kif15 purification, a two-step method was used as described in Drechsler *et al.,* 2014. The lysate was spun at 20 0000 rpm for 30 minutes in an ss-34 rotor, followed by 1:3 dilution of the supernatant in 50 mM Sodium Phosphate buffer. 10 ml SP sepharose beads (Sigma) were loaded onto gravity columns and pre-equilibrated using 3 bed-volume of SP equilibration buffer. The beads were then incubated with the supernatant and placed on a mixer roller for 2 hours. Next, the supernatant was eluted using gravity flow. 1.5 bed-volume SP wash buffer 1 was used to elute protein of the column. At the same time 1 ml Talon beads were pre-incubated in 3 bed-volume talon beads equilibration buffer. The sample was then mixed with the talon beads and 10 mM imidazole was added and allowed to incubate for 2 hours. The talon beads were washed using Talon wash buffer 1 (20 bed-volume) and 2 (30 bed-volume), and the protein was eluted as 300 μl fractions from the beads using Talon elution buffer.

SP Equilibration Buffer	**SP Elution Buffer**
50 mM Sodium Phosphate (pH 7.0) 50 mM Sodium Chloride 1 mM $MgCl_2$ 0.05% Tween20 5% Glycerol 0.1 mM ATP	50 mM Sodium Phosphate (pH 7.5) 50 mM Sodium Chloride 1 mM $MgCl_2$ 0.05% Tween20 5% Glycerol 0.1 mM ATP
Talon Equilibration Buffer	**Talon Wash Buffer 1**
50 mM Sodium Phosphate (pH 7.5) 100 mM Sodium Chloride 1 mM $MgCl_2$ 5% Glycerol 0.05% Tween20 0.1 mM ATP	50 mM Sodium Phosphate (pH 7.5) 300 mM Sodium Chloride 1 mM $MgCl_2$ 0.05% Tween20 5% glycerol 0.1 mM ATP
Talon Wash Buffer 2	**Talon Elution Buffer**
50 mM Sodium Phosphate (pH 7.5) 100 mM Sodium Chloride 1 mM $MgCl_2$ 0.05% Tween20 5% glycerol 0.1 mM ATP 10 mM imidazole	50 mM Sodium Phosphate (pH 7.5) 150 mM Sodium Chloride 1 mM $MgCl_2$ 10% Glycerol 0.1 mM ATP 50 mM imidazole

Table 2.2: Kif15 purification buffers.

For the Tpx2 purification, again, the protocol was followed as described in Drechsler et al., 2014. The lysate was spun at 20000 rpm for 30 minutes using an ss-34 rotor. The supernatant was diluted 1:3 using 50 mM Sodium Phosphate buffer. 10 ml SP beads were equilibrated using 3 bed-volume of SP equilibration buffer, followed by being mixed with the supernatant and incubated for 2 hours. Next, the SP beads were washed using SP wash buffer

1 (5 bed-volume) and eluted using SP wash buffer 2 (3 bed-volume). 1 ml talon beads were equilibrated using 3 bed-volume talon equilibration buffer, mixed with the sample and 10 mM Imidazole and incubated for 2 hours. The beads were washed using Talon wash buffer (50 bed-volume) and eluted as 300 μl using the Talon elution buffer. All proteins were quantified using image J with a BSA standard curve and Bradford assay.

SP Equilibration Buffer	**SP Wash Buffer**
50 mM Sodium Phosphate (pH 7.5) 50 mM Sodium Chloride 1 mM $MgCl_2$ 0.05% Tween20 5% Glycerol	50 mM Sodium Phosphate (pH 7.5) 100 mM Sodium Chloride 1 mM $MgCl_2$ 0.05% Tween20 5% Glycerol
SP Elution Buffer	**Talon Equilibration Buffer**
50 mM Sodium Phosphate (pH 7.5) 300 mM Sodium Chloride 1 mM $MgCl_2$ 0.05% Tween20 5% Glycerol	50 mM Sodium Phosphate (pH 7.5) 100 mM Sodium Chloride 1 mM $MgCl_2$ 5% Glycerol 0.05% Tween20
Talon Wash Buffer	**Talon Elution Buffer**
50 mM Sodium Phosphate (pH 7.5) 150 mM Sodium Chloride 1 mM $MgCl_2$ 10% Glycerol 10 mM imidazole 0.05% Tween20	50 mM Sodium Phosphate (pH 7.5) 75 mM Sodium Chloride 1 mM $MgCl_2$ 10% Glycerol 150 mM imidazole

Table 2.3: Tpx2 purification buffers.

2.3.4 In-vitro tubulin polymerisation

Tubulin prep from previous members of the McAinsh lab was used. 8 μl of 72 μM Tubulin were mixed with 2 μl of 100 mM GMP-CPP, 10 mM DTT and 8 μl BRB80 buffer (table 2.4). The sample was then incubated on ice for 30 minutes, followed by a 1 hour 37°C incubation. To remove free tubulin, microtubules were spun in an airfuge for 5 mins and washed with pre-warmed BRB80 to 20 μl final volume. Taxol was added at a final concentration of 10 μM.

BRB80 Buffer
80 mM PIPES pH 6.8 1 mM $MgCl_2$, 1 mM EGTA

Table 2.4: Composition of BRB80 buffer.

2.4 Cross-linking Mass Spectrometry

2.4.1. BS3 Cross-linking

Bis(sulfosuccinimidyl)suberate (BS3) (Thermo Scientific – catalog number: 21580) was freshly prepared each time by dissolving 1.43 mg of BS3 in 100 μl conjugation buffer (see table 2.4) to obtain a BS3 stock concentration of 25 mM. For monomeric cross-linking 200 μM of BS3 for 2 μM for the protein of interest was used. For dimeric cross-linking 3 mM of BS3 for 2 μM protein was used. Tetrameric cross-linking was achieved using 5 mM BS3 for 2 μM protein. The reaction was Incubated at 23°C for 1 hour in a thermomixer using 500 RPM and quenched with 1 M TRIS pH 7.5 to a final concentration of 50 mM.

The protein complexes were then separated on either SDS-PAGE or Native-PAGE gels, or taken directly to the tryptic digestion.

BS3 Conjugation Buffer
20 mM Sodium Phosphate buffer pH 7.5 50 mM NaCl 1 mM EGTA 1 mM $MgCl_2$

Table 2.5: BS3 conjugation buffer used.

For isotopic BS3, the BS3-d0 and BS3-d12 come in pre-weighed 1:1 mixed 1 mg aliquots. The powder was dissolved in conjugation buffer to obtain 25 mM BS3 d0/d12 stock concentration. For BS3 d0/d4 cross-linking, 1 mg BS3-d4 powder was dissolved in conjugation buffer to obtain 25 mM stock concentration. The BS3-d0 and BS3-d4 are mixed 1:1 to obtain a 25 mM stock of BS3 d0/d4.

2.4.2 EDC Cross-linking

1-ethyl-3-(3-dimethylaminopropyl) carbodiimide hydrochloride (EDC) (Thermo Scientific - catalog number: 22980) was dissolved in deionized water to obtain a stock concentration of 25 mM. For the EDC cross-linking experiments, the addition of Sulfo-NHS (Thermo Scientific) dissolved in deionized water was added to optimise cross-linking conditions by further stabilising the amine-reactive intermediates.

For the EDC cross-linking experiments for Tpx2 and Kif15 in the absence of microtubules, 2.5 μM dimeric Tpx2 and 80 nM tetrameric Kif15 stored in their purification buffer was found as the optimal protein concentrations to be used after titration experiments. The proteins were incubated with 6 mM EDC/Sulfo-NHS which was found as the optimal cross-linking concentration and quenched for 30 minutes using 1 M TRIS pH 7.5 at a final concentration of 50 mM. A standard in-solution digest protocol was then followed.

For the EDC cross-linking experiments in the presence of microtubules, 33 nM dimeric hTpx2 and 16.5 nM tetrameric hKif15 were first incubated for 10 minutes with 5 μM microtubules stabilized using GMP-CPP (Jena Bioscience) and in the presence of 2 mM AMP-PNP (Sigma) to enable the kinesin to lock onto the microtubules. The sample was then spun at 13000 r.p.m on a microcentrifuge, to remove unbound Kif15, Tpx2 and free tubulin subunits. The sample was then cross-linked with 3 mM EDC/Sulfo-NHS for 1 hour and quenched for 30 minutes using 1 M TRIS pH 7.5 at a final concentration of 50 mM.

2.4.3 DSSO cross-linking

For disuccinimidyl sulfoxide (DSSO) (Thermo Scientific – catalog number: A33545) cross-linking, DSSO was dissolved with DMSO to 50mM stock. Before cross-linking the protein, the sample was buffer exchanged 3 times to 50 mM sodium phosphate buffer using Amicon Ultra Filter (Merck Millipore). 2 μM Kif15 was cross-linked using 1 mM DSSO, followed by quenching using 1 M TRIS pH 7.5 at a final concentration of 50 mM. The sample was then desalted using Amicon Ultra filters (30 Kda cut-off), followed by a standard in-solution digest.

2.3.4 Sample Digestion and LC-MS Method

For an in-gel digestion, the protein sample band was excised from the gel and washed with 50% ethanol in 50 mM ammonium bicarbonate for 20 minutes, followed by gel dehydration using 100% ethanol for 5 minutes. The disulfide bonds were reduced by adding 10 mM DTT in 50 mM ammonium bicarbonate for 60 minutes at 57ºC and cysteine residues were alkylated using 55 mM iodoacetamide (or chloroacetimide) in 50 mM ammonium bicarbonate for 20 minutes in the dark. 2.5 ng/µL Trypsin (Sequencing grade; Promega) per protein band was used overnight at 37 ºC. To extract the peptides from the gel pieces, 5% formic acid in 25% acetonitrile was added followed by 5 -10 min sonication. This step was repeated three times. The peptide supernatant was dried overnight at 40 °C using a Speed-Vac. The sample was then re-suspended in 2.5% acetonitrile containing 0.05% trifluoroacetic acid and sonicated for 30 minutes. Finally, the sample was centrifuged at 17,000 *g* for 5 mins.

For an in-solution digestion, the sample was diluted using in 50 mM ammonium bicarbonate. This was followed by cysteine reduction using 1mM DTT for 60 minutes and alkylation using 5.5mM iodoacetamide in the dark for 20 minutes. Lys-C digestion (1µg per 100 µg protein) was done for 3 hours at room temperature, followed by Trypsin digestion (1µg per 100 µg protein) overnight at 37 ºC. The sample was then de-salted using C18 stage tips (Rappsilber et al., 2007).

For analysis by mass spectrometry, an UltiMate® 3000 HPLC series was used for peptide concentration and separation. Samples were separated in Nano Series™ Standard Columns. The gradient used was from 3% to 35% solvent B (0.1% formic acid in acetonitrile) for 30 min, followed by 35% to 70% solvent B for 20 min and finally 70% to 90% solvent B for 30 min. Peptides were eluted directly (~ 300 nL min^{-1}) via a Triversa Nanomate nanospray source into a Thermo Orbitrap Fusion mass spectrometer. Survey scans of peptide precursors from 350 to 1500 *m/z* were performed at 120 K resolution (at 200 *m/z*) with automatic gain control. (AGC) $4x10^5$. Precursor ions with charge

state 2–7 were isolated and subjected to HCD fragmentation in the Orbitrap at 15 K resolution and recorded in centroid mode. MS/MS analysis was performed using collision energies 25, 30 and 37, AGC $1x10^4$ and max injection time 200 ms. The dynamic exclusion duration was set to 45 s with a 10 ppm tolerance for the selected precursor and its isotopes. Monoisotopic precursor selection was turned on. The instrument was run in top speed mode with 2 s cycles.

2.3.5 Mass Spectrometry analysis parameters

MS2 spectra peak lists in a Mascot Generic Format (mgf) files were generated using the Xcalibur raw files, which are used for the subsequent analysis steps.

To analyse the data, MASCOT search engine was used to confirm the presence of the proteins in the sample. Table 2.6 summarises the search parameters used. To search the data, mascot generic format (mgf) files are required.

Enzyme	Trypsin
Missed cleavages	3
Fixed modifications	Carbamidomethylation
Variable modifications	Methionine oxidation
Peptide tolerance (+/-)	20 ppm
MS/MS tolerance (+/-)	20 ppm
Peak type	Monoisotopic

Table 2.6: Search parameters used for MASCOT.

To analyse the cross-linked peptide, the software Stavrox (version 3.5.1) was used (Gotze et al., 2012). Presented in table 2.7 are the search parameters used. An mgf file of the MS2 spectra peak list and the fasta file for the protein sequence of interest were used as the input files.

Protease	Trypsin
Missed cleavages	3 for Lysine and 1 for Arginine
Minimum peptide length	4
Fixed modification	Carbamidmethylation
Variable modification	Methionine oxidation BS3-OH (Lys), BS3-NH2 (Lys)
Cross-linker	BS3 or EDC
Precursor precision (+/-)	20 ppm
Fragment ion precision (+/-)	20 ppm
Ion Type	b and y ions
Deisotoping	yes
Losses	Neutral loss of all fragments

Table 2.7: Stavrox software search parameters used.

To quantitatively analyse the cross-linked peptides, the label-free quantitation (LFQ) of MaxQuant was used. Most of the parameters were left as default, alterations are presented in table 2.8 for the specific search parameters for the LFQ module.

LFQ minimum ratio count	2
LFQ minimum number of neighbours	3
LFQ average number of neighbours	6
Match type	Match to and from file
Mass tolerance	+/- 10 ppm
Time tolerance	+/- 1 min
Time tolerance for label	+/- 1 min

Table 2.8: MaxQuant LFQ search parameters used.

To normalise the LFQ values, a standard MaxQuant search was done to obtain the three most abundant linear peptides for each of the samples. An average intensity for these peptides were used to normalise the intensity of cross-linked peptides.

The DSSO cross-linked peptides were analysed using the DSSO module of Proteome Discoverer (version 2.2).

2.5 Microscopy

2.5.1 TIRF Microscopy

For the single molecule experiments, the flow chamber was created using double-sided scotch tape placed on top of a glass slide. The Sialylated coverslips were prepared as stated in (Bechstedt et al., 2011). The experiments were carried out using GMP-CPP (Jena Bioscience) stabilized Alexa-488 microtubules (Cytoskeleton). The flow chamber was blocked with 1% Pluronic F-127 (Sigma-Aldrich) and 1 mg/ml kappa casein, followed by anti-beta tubulin antibodies (TUB 2.1, Sigma-Aldrich) used to adsorb the microtubules to the surface. The sample mix as stated in table 2.9 was flown into the chamber, which was sealed with VALAP (vaseline, lanolin, paraffin mixed 1:1:1).

Sample Mix
10 nM mKate2-Tpx2 0.1 mg/ml kappa casein 80 μg/ml glucose, 40 μg/ml glucose-oxidase 16 μg/ml catalase 1 mM DTT 50 mM KCl

Table 2.9: Sample mix used for single molecule assays.

The sample was imaged at 25°C on an Olympus CELL$^{R/TIRF}$ microscope (Olympus) using a 100x NA 1.49 objective with 1.6x additional magnification and 488 nm, and 640 nm lasers. An ImagEM emCCD camera (Hamamatsu Photonics), with an environmental chamber and a stage-top-incubator (Okolab). 3-min time-lapse videos were recorded at 2 frames per second (fps) with a 100 ms exposure.

2.5.2 Negative stain electron microscopy

Formvar and carbon coated grids (300 mesh) were glow-discharged using an ELMO glow-discharge system (Cordouan) at 10 mA for 30 seconds. 5 μl of Kif15 was added at 1-2 μM concentration. The sample was incubated on the grid for 60 seconds before any excess was blotted off the grid using filter paper. The sample was stained using 5 μl of 0.7-2% uranyl acetate. The excess stain was blotted using filter paper. The sample was visualised using the JEOL 2011 microscope with Gatan Ultrascan 4000 CCD camera used for data imaging and collection.

2.5.3 Immunofluorescence and fixed cell imaging

For immunofluorescence, the AKIN-13, Anti-Hkpl2 polyclonal antibody (Cytoskeleton), was used and the method was followed as described in the manufacturers protocol; the cells were fixed with 100% Methanol at -20^{0}C for 3 minutes. The cells, were washed once with PBS at room temperature for 30 seconds, followed by a blocking step using 3 % Bovine serum albumin (BSA) for one hour, and another PBS wash step. 200 μl of 1 μg/ml (1:250) dilution of the Hklp2 antibody in blocking solution was added to the coverslips and incubated for one hour. The coverslips were then washed three times using 1 % Triton X-100 for 5 minutes per wash. 200 μl of 1:500 dilution of the secondary rhodamine-conjugated anti-rabbit antibody was added and incubated for 30 minutes. The fixed cells were then washed three times with PBS and counterstained with DAPI (Invitrogen) for 5 minutes with 200 μl of 100 nM DAPI in PBS and mounted using Vectashield antifade mounting medium (Vector laboratories).

Fixed cells were imaged using a 1000x oil NA 1.4 objective on an Olympus Deltavision microscope (Applied Precision, LLC), connected to the imaging software SoftWorx (Applied Precision). Samples were imaged using the GFP channel (32%), mCherry channel (32%) and DAPI channel (10%). Approximately 64 z-slices were taken separated by 200 nm (covering a total z-distance of 12.8 µm). All images acquired were deconvolved and projected using SoftWorx.

2.6. General analysis and figure preparation

All graphs were generated using OriginPro, Excel or outputted using the mass spectrometry software used (Stavrox, MaxQuant and Proteome Discoverer). All figures were prepared using Adobe Illustrator.

Chapter 3: Development of a Cross-Linking Mass Spectrometry Workflow

3.1. Introduction

In the last decade, a new technique combining chemical cross-linking and mass spectrometry (XL-MS) has emerged as a very powerful technique to study protein topologies and protein-protein interaction networks (Sinz, 2006). XL-MS works by chemically cross-linking amino acids using a bifunctional reagent that captures protein interactions in their native state. The reagent usually cross-links lysine residues and has a functional distance that can be used to inform about the space between the cross-linked residues (Rappsilber, 2011, Merkley et al., 2013). After cross-linking, the protein is subjected to proteolysis, typically using trypsin that cleaves at lysine and arginine residues, to generate a set of non-overlapping peptides. Resultant peptides are identified using liquid chromatography and mass spectrometry to determine the exact amino acids involved in the cross-linking. XL-MS is a very useful technique for providing detailed understanding of the precise interactions sites of proteins, and it is often used in combination with techniques such as Cryo-EM to obtain a high resolution 3D structure of proteins and protein complexes (Schmidt and Urlaub, 2017). XL-MS is less time consuming than other techniques such as Cryo-EM and also is better in providing structural information of flexible regions that is not easily obtained with higher resolution techniques. Also, XL-MS can be used to study the conformational changes induced upon protein binding using quantitative cross-linking techniques (Schmidt and Robinson, 2014).

Mass spectrometry analysis for the identification of peptides is usually done using tandem mass spectrometry (MS/MS). During MS/MS, molecules are analysed in consecutive steps. Firstly, the intact protein is digested using a protease such as Trypsin. The digested peptides, which contain linear peptides and cross-linked peptides are separated using a reverse phase C18 chromatography column followed by electrospray ionisation to generate

positively charged peptide ions which are injected into the mass spectrometer. The first mass spectrometer analyser step (MS1) is used to generate intact precursor ion masses of a specific m/z range and these ions are selected for subsequent peptide fragmentation. These fragmented ions are selected and analysed in a second mass spectrometer analyser step (MS2).

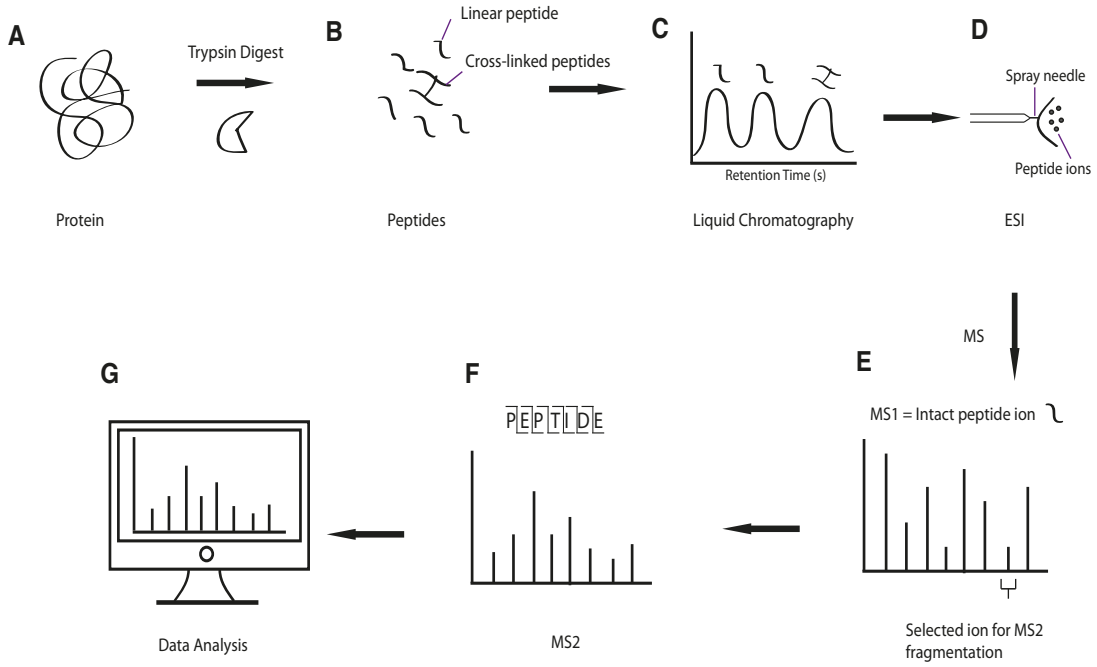

Figure 3.1: Schematic overview of tandem mass spectrometry.
A; First, a protein is digested to generate peptides. **B;** Digested peptides consist of linear peptides and cross-linked peptides. **C;** The digested peptides are separated on a reverse-phase C18 column, **D;** The peptides are ionised to generate positively charged precursor molecules and injected into the mass spectrometer. **E;** In MS1, the precursor ions are analysed and selected for peptide fragmentation. **F;** In MS2, the fragmented ions are selected and analysed. **G;** Mass spectra data is analysed to reveal the cross-linked peptides.

The mass spectrometer instrument used was an Orbitrap Tribrid Fusion (Thermo Scientific). The Orbitrap fusion instrument has two separate detectors, the Orbitrap detector and the ion trap's electron multiplier detector, which can be used at either MS1 or MS2 level. Also, the Orbitrap fusion instrument has three fragmentation modes; collision-induced dissociation (CID), high-collision dissociation (HCD) and electron-transfer dissociation (ETD). The Orbitrap detector works by inducing oscillations which are guided

by polarised detector plates. The oscillation regularity and spin varies depending on the mass/charge ratio of the ions (Makarov, 2000), with the signal transformed using Fourier transform to give a mass spectrum signal (Makarov, 2000). The components of the Orbitrap instrument are presented in figure 3.2. The s-lens is the first component, which focuses and enables the ions to be transmitted into a coherent ion beam. The curve in the ion beam improves signal/noise ratio by preventing uncharged molecules from travelling through to the quadrupole mass filter. The Quadrupole can allow all ions through or can select the precursor ions depending on the mass range set. Ions can be directed between different areas for fragmentation, to the Orbitrap detector, or to the linear ion trap's electron multiplier detector. The selected precursor ions are then transported to the ion-routing multipole or the pressure cell of the ion trap for HCD or CID/ETD fragmentation, respectively.

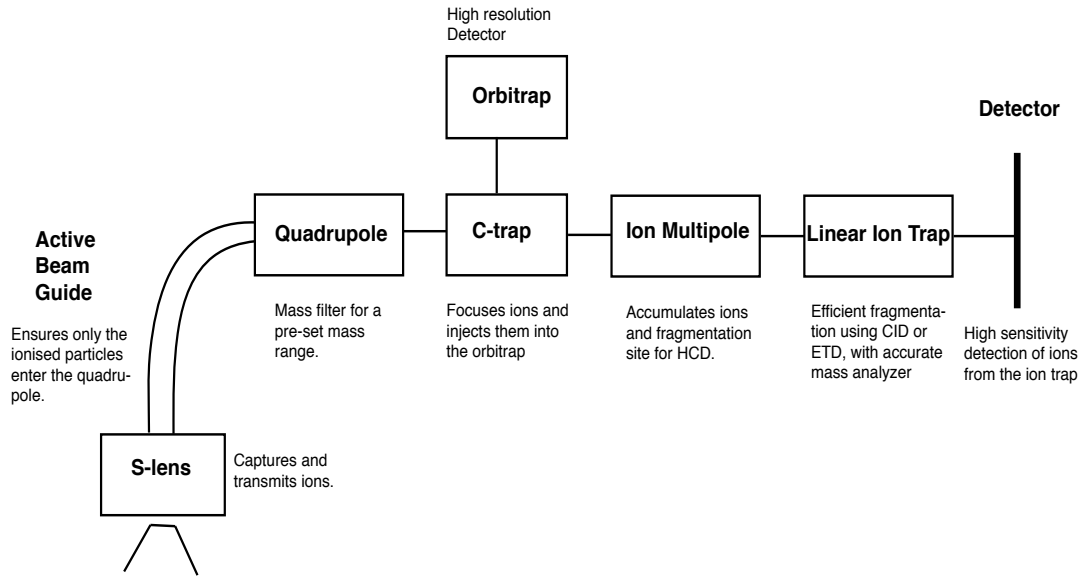

Figure 3.2: Overview of the Orbitrap Tribrid Fusion instrument.
The first component, the s-lens is required to focus and transmit the ions into the ion beam. The curve of the ion beam reduces background signal by ensuring only the charged particles enter the quadrupole. The quadrupole selects precursor ions based on a pre-set mass range. MS1 analysis can be done using the Orbitrap detector or the linear ion trap's electron multiplier detector. Selected precursor ions are fragmented using the ion-routing multipole or the pressure cell in the ion trap for HCD or CID/ETD fragmentation, respectively.

The Orbitrap Fusion mass spectrometer has been an excellent instrument to work with as it provides three types of fragmentation methods and two types of detector. The Fusion instrument is able to switch between high resolution and mass accuracy detection using the Orbitrap detector or faster speed and sensitivity, which is offered by the ion trap. The three different fragmentation modes offered are CID, HCD, and ETD. Depending on the fragmentation mode, the ions are fragmented in the Ion trap (CID, ETD) or the Ion-Routing Multipole (HCD) and generate different ion types (figure 3.3).

Which type of fragmentation is best can depend on charge state, intensity and m/z value. The most commonly used fragmentation technique in proteomics is collision-induced dissociation (CID), whereby the precursor ions enter a collision cell and neutral gas molecules such as helium are introduced which collide with the precursor ions and generate vibrational energy. This vibrational energy induces amide bond fragmentation, which generates characteristic b and y ions, whereby the peptide charge is retained on the N-terminal or c-terminal, respectively (figure 3.3). There are also neutral loss fragmentations that generate molecules such as water and ammonia associated with CID. CID fragmentation is ideal for short peptides with small charge states. Also, fragmentation of modified peptides, such as phospho-peptides, is not suitable using CID.

Another technique that produces the same ion types as CID, is higher-collision dissociation (HCD). This technique is a very attractive technique for high resolution analysis, as the fragmentation ions are normally analysed using the Orbitrap detector instead of the ion trap. The ion trap is unable to detect the lowest 1/3 of m/z fragment ions, thus invaluable fragmentation data is lost. This is not the case for HCD fragmentation. Whilst HCD fragmentation produces b and y ions as well, there is a bias towards y ions than b ions and producing fragment ions of a lower charge state (Shao et al., 2014).

ETD fragmentation has more often been used to study post-translational modifications as it can acquire good sequence coverage whilst keeping the modification intact (Mikesh et al., 2006). This is because ETD does not use collision based fragmentation, but instead uses a radical anion to transfer an electrode to the positively charged precursor ion, which causes a cleavage in the N-Cα bond to produce c and z ions (figure 3.3). It has also been shown that ETD fragmentation works better for precursor ions of a higher charge state (Chalkley et al., 2010)

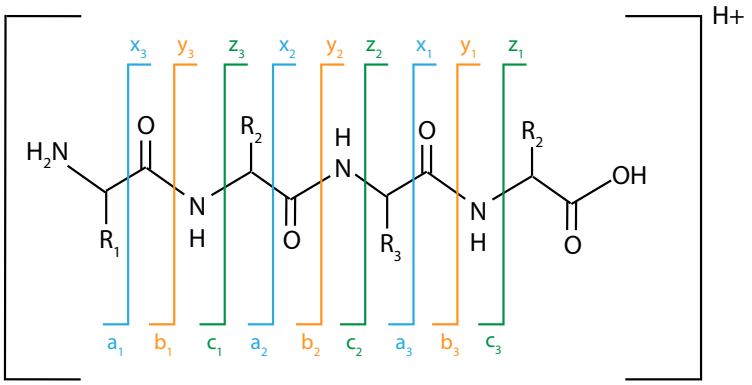

Figure 3. 3: Peptide fragmentation ions.
CID and HCD generates b and y ions, whereas ETD fragmentation generates c and z ions.

The first stage of cross-linking mass spectrometry is selecting the cross-linker of choice. The most common cross-linker used is bis(sulfosuccinimidyl) suberate (BS3). This is a bifunctional cross-linker that can cross-link primary amines including lysine, serine, tyrosine and threonine residues (Kalkhof and Sinz, 2008). The cross-linker functions at physiological pH conditions between 7-9 (Madler et al., 2009) and has a functional distance of 11.4 Å (figure 3.4). Using lysine residues as the reactive group for cross-linking is an attractive choice as lysine is one of the most abundant amino acids in protein sequences. Also, lysine residues are generally solvent accessible and exposed on the surface of protein structures. Isotope labelled BS3 cross-linker can also be used for cross-linking.

1-ethyl-3-(3-dimethylaminopropyl) carbodiimide hydrochloride (EDC) cross-linker that cross-links carboxyl group of amino acids such as aspartic and glutamic acid, to primary amines. Since this cross-linker has a spacer arm length of 0 Å (figure 3.4), it provides a more accurate idea of direct contact sites as the cross-links identified with EDC must all be within a salt-bridge distance (Rivera-Santiago et al., 2015). This is due to the EDC cross-linker's generation of an unstable ester intermediate, which directly cross-links the carboxyl group to a primary amine. The specificity of a cross-linker molecule, whilst desirable a lot of the times, can also be a disadvantage. Due to EDC only interacting with N-terminal end of proteins, lysine, aspartic and glutamic acid, protein regions not enriched with these residues would be unable to generate cross-links. Also, proteins folded in such a way that these reactive groups are buried will also not be able to generate significant cross-links (Rivera-Santiago et al., 2015). EDC cross-linker is also not amenable to modifications such as isotope labels, thus this cannot be used a confidence filtering strategy.

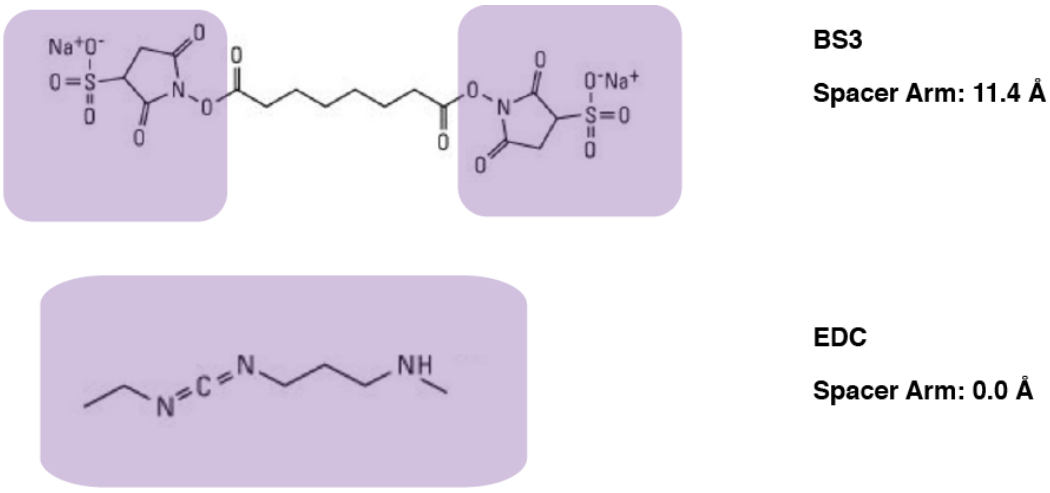

Figure 3. 4:Structures of different chemical cross-linkers used.
BS3 is the most common cross-linker used in the literature. It is water soluble and has a spacer arm length of 11.4 Å. EDC is also water soluble however the spacer arm length is 0.0 Å. Shaded in purple are the regions of the reagent which disappear in the case of a successful cross-link. As is clear from this figure, the whole EDC reagent is not present in the final cross-linked product. Figure is adapted from Thermo Fisher Scientific.

Chemical cross-linking leads to the formation of three product types (figure 3.5). The first type is the mono-linked peptide. This is when one reactive group side of the cross-linker cross-links to a peptide, but the second reactive group undergoes hydrolysis and the peptide becomes modified with an OH and NH2 group, thus unable to form a second cross-link site. Particularly with BS3 cross-linking, the generation of these mono-linked peptides are common as they undergo fast hydrolysis rates. However, due to the cross-linking chemistry of EDC cross-linkers, they are less likely to produce mono-linked peptides as in the absence of a primary amine group to cross-link to, the intermediate ester group reverts back to the stable carboxyl form (Rivera-Santiago et al., 2015). This makes any downstream analysis easier to handle as the dead-end products can make up a significant portion of the data to be analysed. The second type is the loop-linked peptide, (intra-peptide bonds). This is when the cross-linker loops and cross-links residues within the same peptide. The third type and the most structurally informative product type associated with cross-linking is when two individual peptides are cross-linked by forming covalent bonds to either side of the bifunctional reagent (inter-peptide bond).

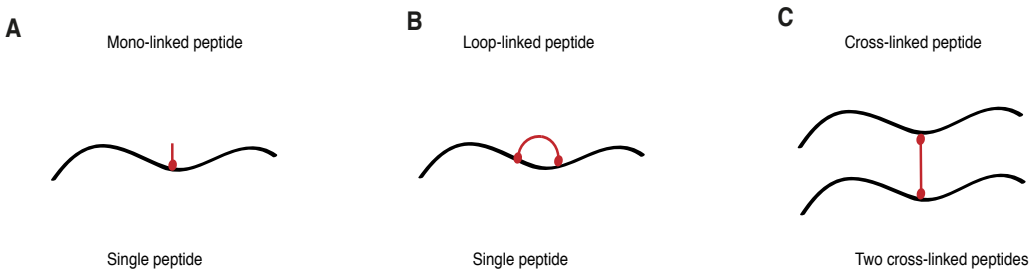

Figure 3.5: Product types associated with cross-linking mass spectrometry. A; When the cross-linker attaches to the peptide on one reactive site and undergoes hydrolysis at its second reactive group, this results in the formation of a mono-linked peptide. **B;** When a cross-linker cross-links two residues within the same peptide, this results in a loop-linked peptide. **C;** For the cross-linked peptide, two peptides are tethered together using the cross-linker.

Depending on the chemical cross-linker and the product type formed, a different mass modification is produced, which is summarised in Table 3.1.

Cross-linker	Bifunctional cross-linked amide bond	Mono-linked hydrolysis
BS3-d0	138.067 amu	156.078 amu
BS3-d4	142.092 amu	160.013 amu
BS3-d12	150.143 amu	167.883 amu
EDC	-18.011 amu	

Table 3.1: Mass modifications associated with cross-linking with BS3, stable isotope labelled BS3 and EDC cross-linkers.

There are several types of mass spectrometry software used by the XL-MS community. Mascot software is a general peptide identification software used to analyse mass spectrometry data. The mascot search engine takes an input protein database in a fasta file format and tries to match peptide ions data gathered from the mass spectrometer. Specifically, the experimental ion masses are compared to a list of expected digested peptide and fragment ion masses calculated from the protein sequences provided in the fasta files. These masses are then scored according to how well they match. Mascot can also calculate the expected peptide and fragment ion masses associated with a digested peptide ion modified with a chemical group, such as phosphorylation or a mono-linked peptide. However, it cannot be used to calculate and identify the fragmentation of two digested cross-linked peptides.

Stavrox is a leading software for the analysis of cross-linked peptides (Gotze et al., 2012). Based on an *in-silico* digest of your protein sequence, the software calculates all possible theoretical cross-linked peptide candidates, and then calculates all possible b and y ion series for a given cross-link site, with the reactive groups associated with a particular cross-linker set as the default cross-link site. Both EDC and BS3 target lysine residues and since

trypsin is sensitive to steric hindrance, the analysis must permit an increase in the number of missed lysine- trypsin cleavage sites. The Stavrox scoring algorithm is based on how well the expected and observed fragmentation ions match up. This scoring algorithm also takes into account the intensity of the fragment ions identified and how many high intensity peaks are unidentified, the S/N ratio of the spectra and how well each of the cross-linked peptides are fragmented and how long the fragment ion series are. In summary, in order to achieve a good Stavrox identification with a score ~100 the following criteria should be met:

- Observed fragmentation ions within ~20 ppm of expected fragment ions
- Fragmentation ion series observed for both peptides, specifically, those fragment ions that include the cross-linker and the attached second peptide
- Fragmentation ions account for most of the high intensity peaks present in the spectra
- Only a few high intensity signals unidentified in spectra
- There is little noise in spectra

The development of cross-linking mass spectrometry has become a very useful tool to probe the structural organisation of proteins and protein complexes. However, a major bottle-neck has become how to optimise the experimental design and the analysis pipeline. Although this technique is increasingly popular, there are only a handful of research groups such as Professor Albert Heck (Utrecht University, Netherlands), Professor Juri Rappsilber (University of Edinburgh, UK) and Professor Andrea Sinz (Martin Luther University Halle-Wittenberg, Germany) who routinely apply this method study protein topology.

The aim of this chapter was to produce an optimised cross-linking mass spectrometry protocol and analysis workflow. At the start of my project, the Orbitrap Fusion was a new state-of-the-art mass spectrometer, just purchased for the Proteomics facility, thus this required a lot of time to optimize cross-linking conditions. Also, given that there is not a standard cross-linking analysis pipeline, a lot of time was spent on establishing an integrated software analysis workflow. Presented in figure 3.6 is an overview of a standard cross-linking mass spectrometry workflow. Highlighted with a star are the sections discussed in-depth in this chapter. Adjacent to the workflow are the optimisation experiments that were tested for the individual protocol steps to create a coherent cross-linking mass spectrometry analysis pipeline.

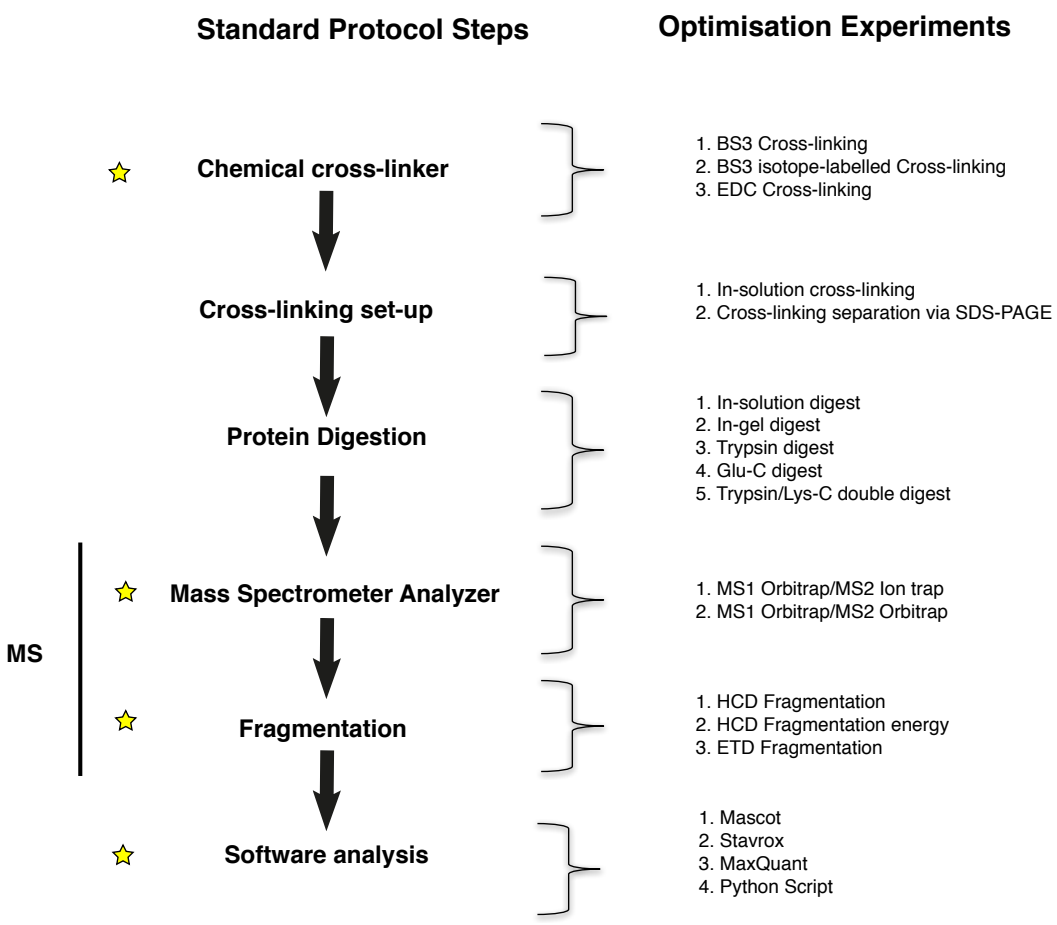

Figure 3. 6: Cross-linking mass spectrometry workflow.
On the left hand side is a typical workflow for cross-linking mass spectrometry. The stars indicate the steps discussed in this chapter. On the right hand side are the optimization experiments that were tested in order to obtain a standardized cross-linking mass spectrometry workflow.

3.2. Chemical cross-linking

3.2.1 Chemical cross-linking

The monomeric Kif15 cross-linked data will be presented in this chapter to provide examples of the method development workflow. Presented in table 3.3 (p80) is the list of monomeric Kif15 cross-linked peptides identified.

The two steps of the cross-linking mass spectrometry workflow that will not be discussed in depth in this chapter is the cross-linking set-up and the protein digestion steps which go hand in hand. As for the cross-linking setup, this has to be tailored for the experiment and the molecular weight of the complex expected, which will be further discussed in chapter 4. With regards to the protein digestion, depending on whether the cross-linking was separated on a gel or done in-solution, the digest was done accordingly.

The cross-linked peptides analysis was started by doing a basic database search to identify the tryptic peptides of Kif15. The search engine of choice was Mascot. This software can search the identification of linear peptides through matching the expected peptide fragmentation masses to the observed masses acquired from the mass spectrometer. As only a portion of our protein will be cross-linked in any circumstance (Holding et al., 2015) we still expect to see a good sequence coverage for the protein, thus a good protein coverage is essential before any subsequent cross-linked peptides analysis. The protein coverage for the untreated and treated samples averaged at 75%. Also, as previously mentioned, Mascot is able to analyse and identify linear peptides and any modification associated with these peptides. However, it is not able analyse the fragmentation ions expected for two peptides cross-linked together.

To prove that the cross-linking chemistry has occurred, we used the Mascot search engine to search against linear peptides of Kif15 which have been modified with a reactive group from the BS3 cross-linker. This occurs when

the cross-linker attaches to a peptide on one end, however, the second reactive group undergoes hydrolysis, thus unable to form a second cross-link to another peptide. As this results in the formation of a linear peptide with a known mass modification of +156 Da, indicative of hydroxyl group modified mono-link (Schilling et al., 2003), which can easily be included in our Mascot search. For an average cross-linked sample, there were ~50 BS3 modified monolinked peptides identified. EDC does not generally produce mono-linked peptides, as the intermediate ester returns to its original carboxyl state when it is unable to cross-link to a primary amine (Rivera-Santiago et al., 2015).

Presented in figure 3.7 is an example of a peptide ($_{40}$SGSADGEQNLCLSVLSSTSLR$_{60}$), modified at the Ser-52 with the BS3 mono-link. Another modification seen is a mass of 57 Da added to the Cys-50 residue. This is a common modification, as the cysteine residues are alkylated during the digestion protocol to prevent any cysteine cross-reactivity, and this added mass is indicative of the alkylation process.

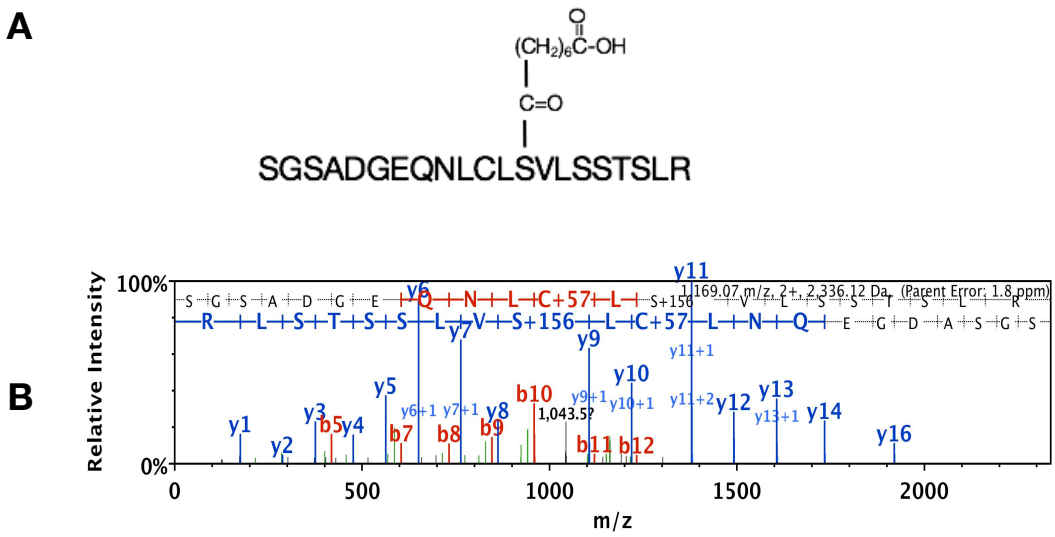

Figure 3.7:Mono-linked peptide $_{40}$SGSADGEQNLCLSVLSSTSLR$_{60}$.
A; schematic showing the modified peptide with hydrolysed BS3. **B;** Annotated MS2 spectrum for the monolinked peptide $_{40}$SGSADGEQNLCLSVLSSTSLR$_{60}$, whereby the blue peaks indicate the y-ions and the red peaks indicate the b-ions. The "S+156" indicates the addition

of the hydrolysed BS3 molecule to Ser-52. The “C+57” shows the modified mass associated with the cysteine alkylation of Cys-50.

3.2.2 Different chemical cross-linkers for cross-linked peptides analysis

As BS3 and EDC have difference spacer lengths (11.4 Å and 0 Å, respectively), they provide different information on residue proximity. Specifically, BS3 cross-links indicate residues which are within a 11.4 Å distance whereas, EDC cross-links infer information about direct contact sites. Also, the reactive groups are not exactly the same. BS3 is a homo-bifunctional reagent, which reacts with primary amines, including lysine, serine, threonine and tyrosine residues. EDC is a heterobifunctional cross-linker that cross-links carboxylic acid containing residues such as aspartic acid and glutamic acid, to primary amines.

With cross-linked peptides, you have two peptides bridged by a chemical cross-linker with a known mass. As such, the fragmentation of the cross-linked peptides can be calculated as being the mass of the first peptide with additional mass of the cross-linker and the second peptide that forms the cross-link. For simplicity, the longer peptide chain is called the “alpha peptide” whereas the shorter peptide is called the “beta peptide”. In order to confidently identify a cross-link, it is best to have as many fragments arising from both peptides. In particular, the fragments ions containing the additional mass of the cross-linker and the second peptide are crucial as they are the only way of confirming that the two peptides have indeed been cross-linked. Also, neutral losses from the fragments, such as water or ammonia molecules is often seen as well.

Presented below in figure 3.8 is an example of the peptide $_{407}$DKK$_{409}$ cross-linked to $_{1035}$KQEVDILDLK$_{1044}$ (K15$_1$), identified with both EDC and BS3. The BS3 precursor ion exists as a 3+ ion and the EDC ion is a 2+ ion. As the reactive groups are not exactly the same for these two cross-linkers, only the

cross-link identified in the alpha peptide is the same. For the beta peptide, the BS3 cross-links to the lysine residue whereas for the EDC example, the cross-link is matched to the adjacent aspartic acid residue. As such, the modified mass associated with the cross-linker is not the same and since the cross-linked residues are not the same, the masses of the fragment ions cannot be compared. However, there is a general pattern seen, whereby there is a continuous y ion series seen for the alpha peptide in both spectra. The BS3 spectra also produced a continuous b ion series. Since the precursor ion for the BS3 cross-linked peptide was found at a higher charge state, there are more fragments identified for this spectra.

A

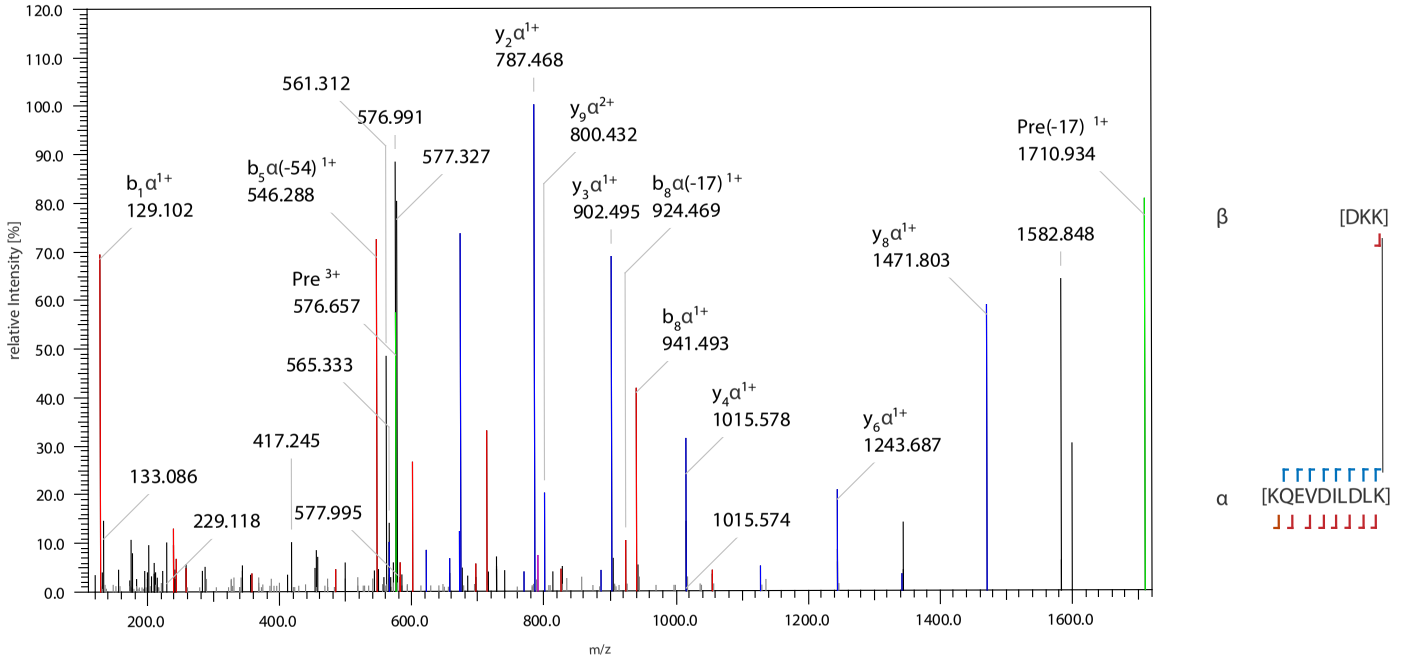

Figure 3.8A: Fragmentation spectra of K15$_1$ cross-linked using BS3. On the left hand side is the mass spectrum showing the fragment ions associated with this cross-link. On the right is a fragmentation schematic of the cross-linked peptides, whereby the b and y ions are coloured in red and blue, respectively. The alpha peptide is the longer peptide with more fragment ions, and the beta peptide represents the shorter fragment ion with less fragments identified.

B

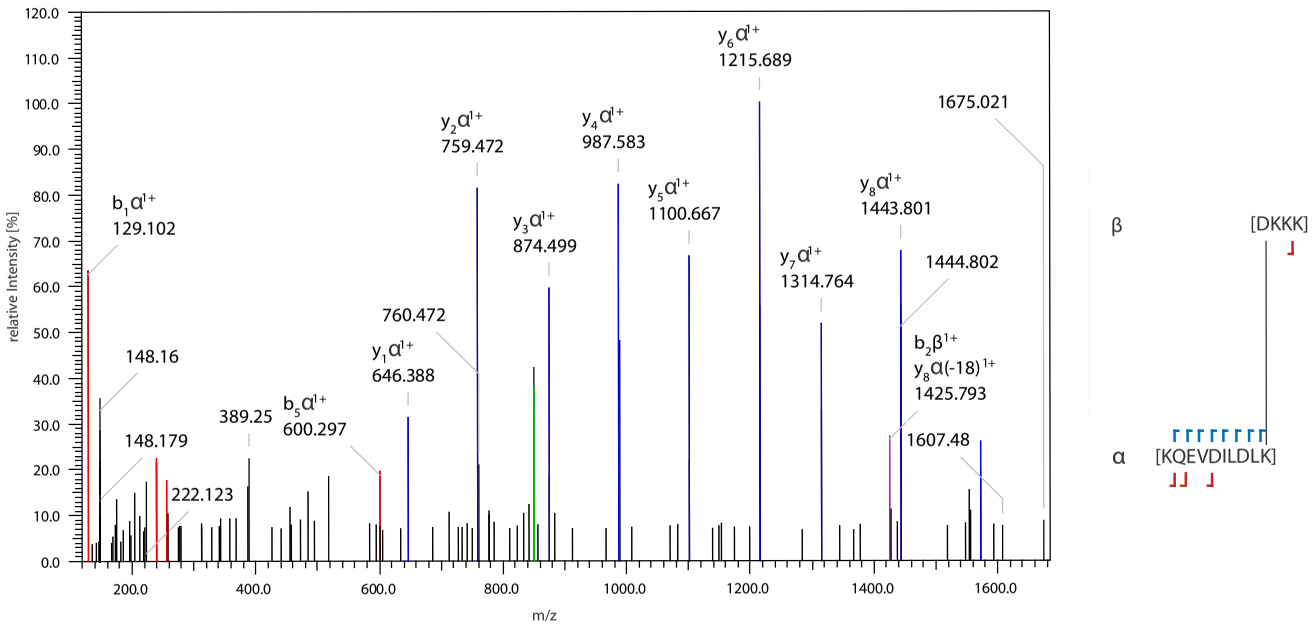

Figure 3.8B: Fragmentation spectra of K15$_1$ cross-linked using EDC. On the left hand side is the mass spectrum showing the fragment ions associated with this cross-link. On the right is a fragmentation schematic of the cross-linked peptides, whereby the b and y ions are coloured in red and blue, respectively. The alpha peptide is the longer peptide with more fragment ions, and the beta peptide represents the shorter fragment ion with less fragments identified.

3.3 Mass Spectrometry Analysis – Impact of mass resolution on XL-MS Analysis

The Orbitrap offers two detectors, the Orbitrap and the electron multiplier (located by the ion trap). These detectors have difference advantages/disadvantages in sensitivity, speed and resolution. Because cross-linked peptides are expected to occur at low overall abundance, we compared the performance of the low mass accuracy (but fast and sensitive) ion trap to the higher resolution (but slower and less sensitive) Orbitrap detector. MS1 level detection was done using the Orbitrap, however, the fragment ions at MS2 level was analysed using the Orbitrap and the electron multiplier detector.

The use of the Orbitrap for the detection of MS2 fragment ions has significantly affected the accuracy and reliability for the detection of cross-linked peptides. Firstly, the fragment ions are detected with an accuracy of 20 ppm or less, thus increasing the reliability of the fragment ions identified (Leitner et al., 2010). Also, the Orbitrap detector has an increased mass accuracy and resolving power, thus the isotope clusters for the fragment ions can be resolved more easily, thus these ions can be assigned a correct charge state and mass (Leitner et al., 2010).This increases the accuracy of the fragment ion annotation, thus increasing the reliability of the cross-linked peptides identified. A full width half maximum (FWHM) resolution of 120,000 was selected for the MS1 level, whereas a resolution of 15,000 was selected at the MS2 level. HCD fragmentation was used instead of CID, as HCD, is a method whereby fragmentation of the lower 1/3 of ions that are lost from the ion trap are retained. As such, fragments detected with HCD do not have a low *m/z* cut-off, much better resolution and increase in the number of detected ion fragments (Jedrychowski et al., 2011). Also cross-linked peptide identification using HCD instead of CID has been shown to improve peptide spectrum identification and the percentage of cross-linked peptides identified (Giese et al., 2016).

However, the use of high resolution detection using the Orbitrap does come with its disadvantages. The scanning rate per mass spectrum and detection time is much slower than the Ion trap, thus less fragments are detected (scan rate of 15 Hz and 20 Hz for the Orbitrap and Ion trap detectors, respectively). As such, it may affect the number of fragments that can be assigned for the cross-linked peptides. In figure 3.9, the same cross-linked peptide detected using the Orbitrap and the Ion trap is compared. In figure 3.9A and 3.9B are the fragmentation spectra of cross-linked peptides $_{884}$NLQNFKK$_{890}$ and $_{916}$LSLQFEEDK$_{924}$ (K15$_{13)}$ identified using the Orbitrap and ion trap detectors, respectively. Adjacent to the fragmentation spectra is a visual representation of the fragments found for the cross-linked peptides. As is clear from the spectra for the ion trap detector, many more fragments ions are assigned to the cross-linked peptides. However, due to the higher error rate associated with these detected fragment ions, they are much less accurate than the Orbitrap detected fragments.

As can be seen from figure 3.9C, irrespective of the m/z value of the detected fragments from the Orbitrap, the error of fragments detected is close to zero, when compared to the fragment ion error associated with the ion trap. This makes it more difficult to trust the data obtained from the ion trap as the complexity of assigning fragments ions to two different peptides with different charge states increases the number of false positive matches.

Overall, utilising a high/high strategy whereby the Orbitrap detector was used at both MS1/MS2 level, yielded the best results. In total, the average number of MS2 spectra acquired using the Orbitrap detector for a general digest (both treated and untreated samples) were ~600, with 50% of them successfully identified as Kif15 peptides. For a BS3 cross-linked sample, ~4% of MS2 spectra were assigned to a cross-linked peptide and ~12% were assigned to a monolinked peptide. As for the Ion trap, an average of ~900 MS2 spectra were identified with 0.6% of these identified as cross-linked peptides.

A

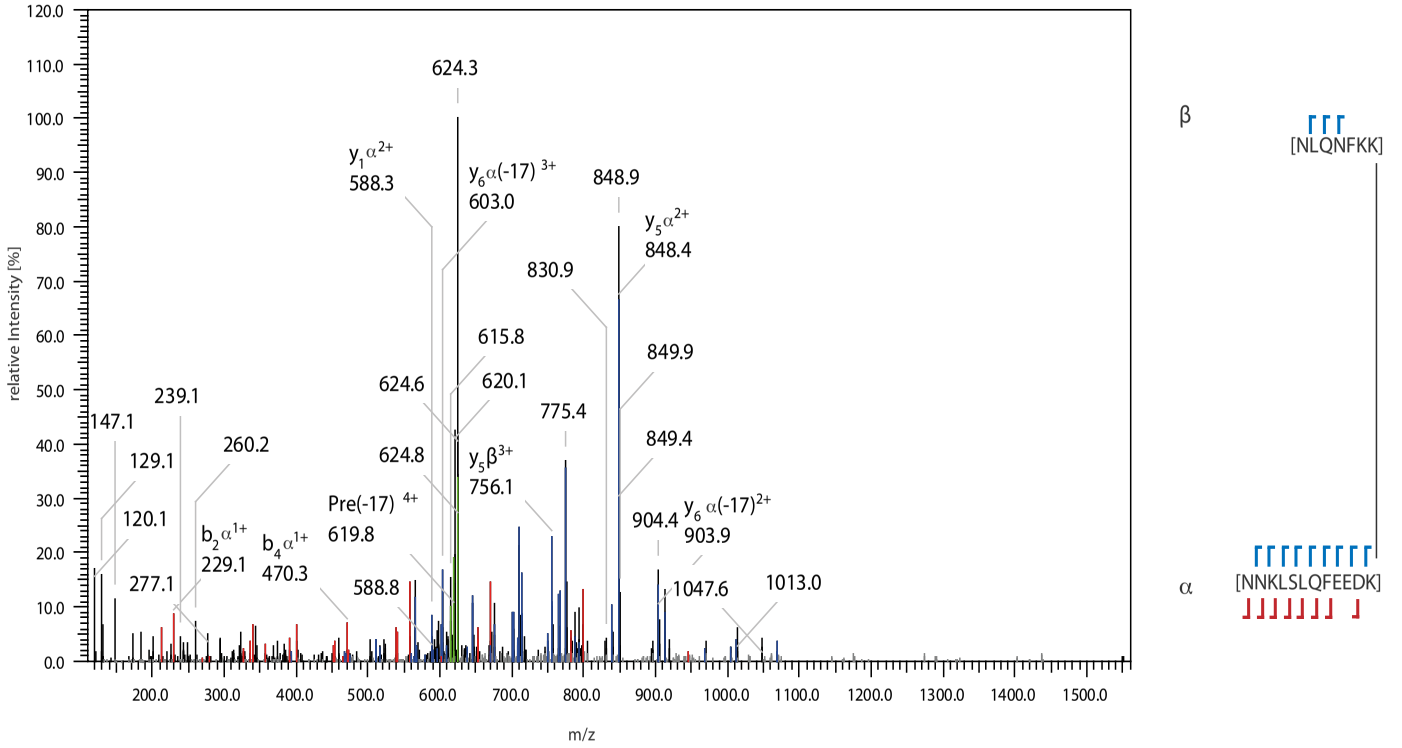

Figure 3.9A: Detection of K1513 cross-linked peptide fragments using Orbitrap for MS2 analysis. The cross-linked peptide is NLQNFKK and NNKSLSLQFEEDK. A schematic of the fragmentation of the cross-linked peptides is also presented, whereby the b ions are coloured in red and the y ions in blue.

B

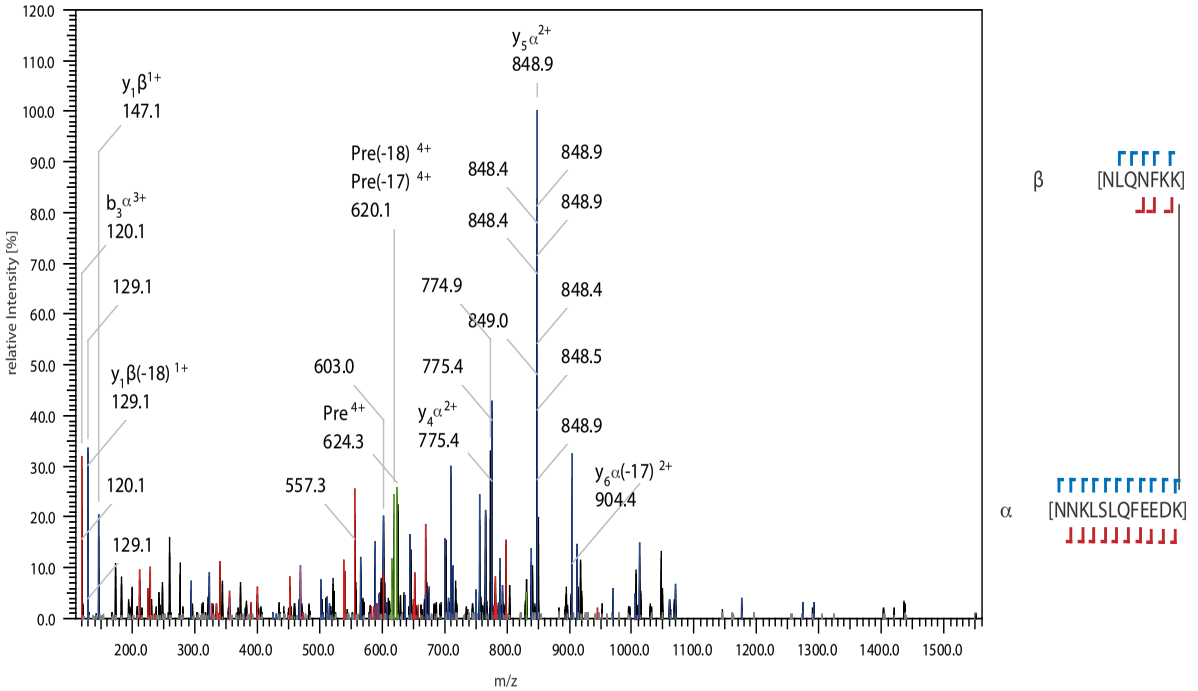

Figure 3.9B: Detection of K1513 cross-linked peptide fragments using Ion trap for MS2 analysis. The cross-linked peptide is NLQNFKK and NNKSLSLQFEEDK. A schematic of the fragmentation of the cross-linked peptides is also presented, whereby the b ions are coloured in red and the y ions in blue.

C

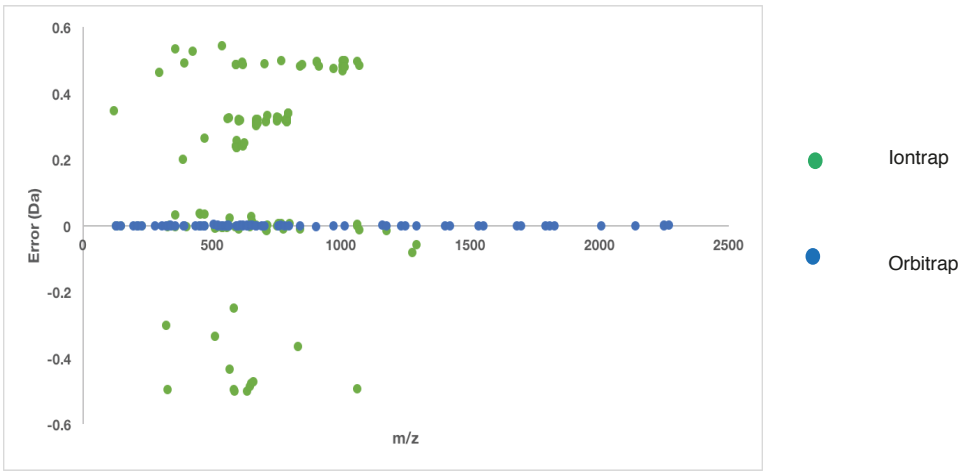

Figure 3.9C: Calculated error window for the fragment ions detected using the Obritrap and Ion trap.

3.4 Differential Fragmentation modes for cross-linked peptides

3.4.1 Effect of HCD and ETD on fragmentation of cross-linked peptides

The Orbitrap Tribrid Fusion has the ability to perform three modes of fragmentation; CID, HCD and ETD fragmentation. For XL-MS, HCD fragmentation is often the most used fragmentation technique, as it allows the detection of the lowest 1/3 m/z masses which is absent from the data collected with the ion trap. This additional fragmentation data is important in allowing unambiguous identification of cross-linked peptide. To systematically assess and compare the different fragmentation modes of the Orbitrap Fusion, HCD and ETD were tested on the sample cross-linked and digested sample, with 3 individual replicates. HCD is a beam-type CID fragmentation mode, essentially using a higher collision-induced dissociation to produce b and y ions. ETD fragmentation is more often been used to study post-translational modifications (Mikesh et al., 2006) as it can acquire good sequence coverage whilst keeping the modification intact. It has also been shown that ETD fragmentation works better for precursor ions of a higher charge state (Kim et al., 2012). As we expect to see more highly charged precursor ions for cross-linked peptides (Chen et al., 2010), it seemed like a good choice to test this fragmentation mode along with HCD. Also, HCD and ETD generated different ion types; b and y-ions for HCD and c and z-ions for ETD.

Presented below in figure 3.10A and 3.10b are the spectra for the cross-linked peptides $_{884}$NLQNFKK$_{890}$ and $_{916}$LSLQFEEDK$_{924}$ (K15$_{13)}$ fragmented with HCD and ETD, respectively. As expected, we see a continuous y ion series for the alpha peptide in the HCD spectra. Since the cross-link site is located at the c-terminus of the alpha peptide, each of these y ions, confirms the presence of the cross-linker and the second peptide attached. We also see a nice b ion series for the alpha peptide to reaffirm the identification of this peptide is correct. As for the beta peptide, we see fragmentation to help identify the peptide, although not as nice an ion series as seen in the alpha peptide. This

is not as surprising as the shorter peptide tends to fragment less than the longer peptide in the cross-link. For the ETD spectra, again we see a nice fragmentation ion series for the alpha peptide, with continuous z ions detected. We also see the presence of c ions to increase confidence in the assignment of the alpha peptide. The beta peptide also has less ETD fragments than the alpha peptide.

Although presented here is a nice example of the same cross-linked peptide identified with both ETD and HCD, it is worth noting that ETD did not work very well for all the cross-links. We have only been able to identify 2/22 cross-links using ETD fragmentation. The reason ETD did not work very well is not clear, however given that the cross-links are mainly a charge state of 3+, this may be the reason for the lack of successful identification using ETD as this fragmentation mode prefers precursor ions of a higher charge state (4+ or higher).

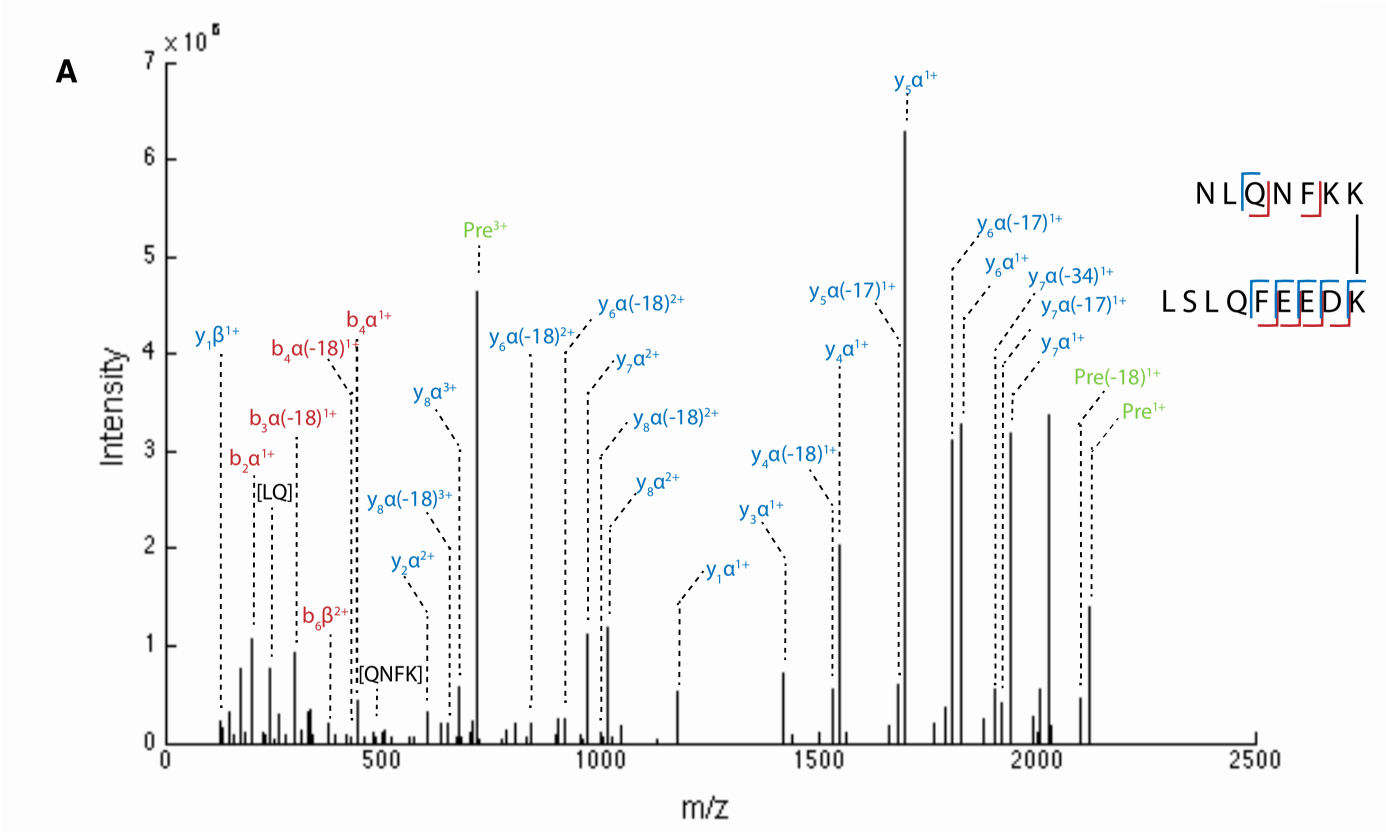

Figure 3.10A: Fragmentation spectra of cross-link K15$_{13}$ undergoing HCD fragmentation. In green is the precursor ion, with b and y ions in red and blue, respectively.

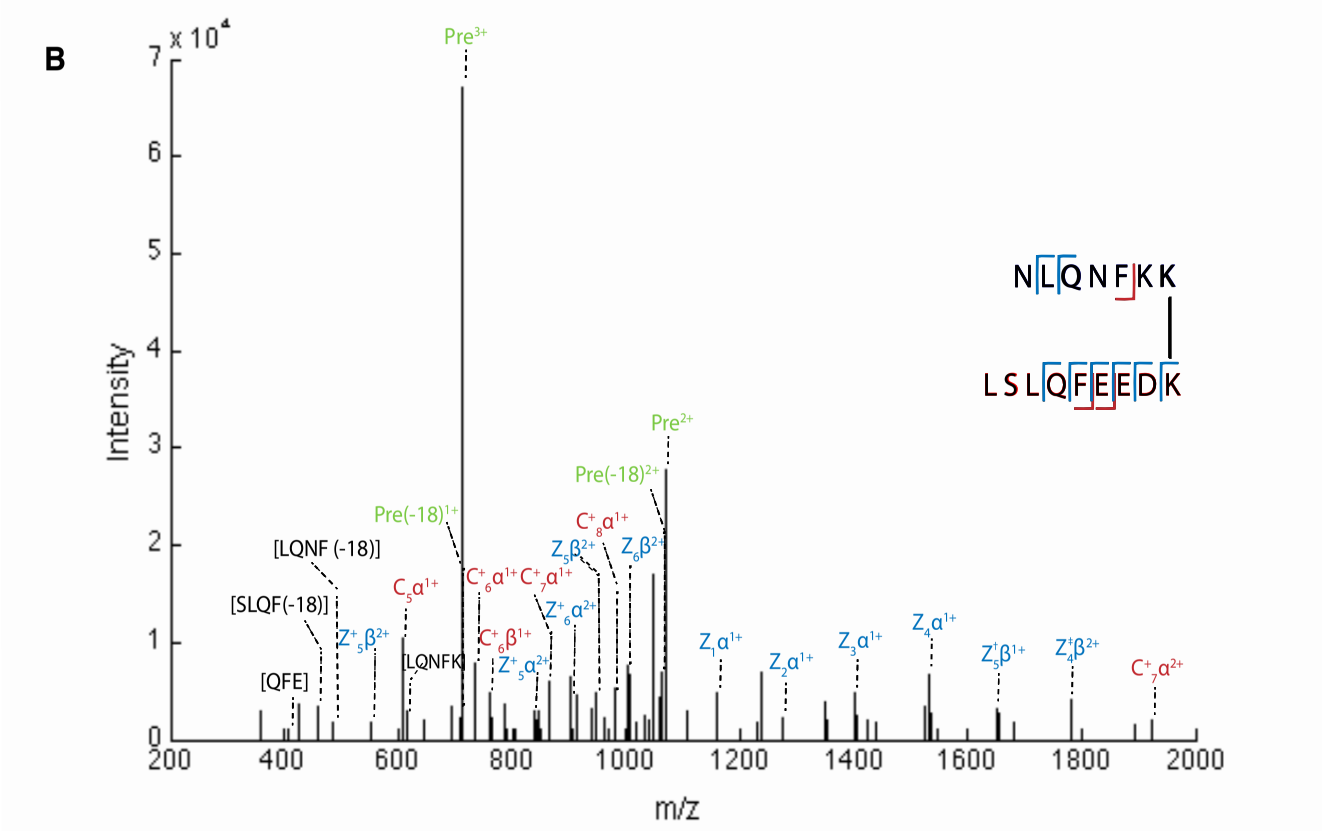

Figure 3.10B: Fragmentation spectra of cross-link K15$_{13}$ undergoing ETD fragmentation. In green is the precursor ion, with c and z ions in red and blue, respectively.

3.4.2 Optimisation of collision energy for HCD fragmented cross-linked peptides

In order to have a good identification of cross-linked peptides, good fragmentation must be achieved for both of the peptides involved in the cross-linking. Cross-linked peptides identification can also be affected by the collision energy employed. There should be enough collision energy applied to allow for identification of b and y ion series. However, too much fragmentation energy can often result in over-fragmentation, thus rendering the spectra unhelpful in identifying cross-linked peptides.

For the HCD fragmentation, collision energy ranging from 25-37% was tested. It was noted that there is not a single collision energy that works for all cross-linked peptides, however, using a lower-range collision energy from 25-30% worked much better for the identification of cross-linked peptides. It also gave more reliable scoring value from the Stavrox software. Presented in table 3.2 is a summary of out of 22 cross-links, the number of cross-linked peptides identified in Stavrox using different HCD fragmentation collision energies.

Collision Energy	**Number of cross-links identified**
25%	21
30%	22
37%	13

Table 3.2: Cross-linked peptides identified in Stavrox using different collision energies.

As an example, presented below in figure 3.11 is the fragmentation spectra for the cross-linked peptides $_{884}$NLQNFKK$_{890}$ and $_{916}$LSLQFEEDK$_{924}$ (K15$_{13)}$ fragmented using 3 collision energies; 25%, 30%, 37%. From the spectra it is very clear that the 37% collision energy is not a good choice of fragmentation energy as it over-fragments all the higher m/z fragments that could be used to identify the cross-linked peptides. As a result, the spectra is now dominated

by smaller m/z fragments, which may be useful in confirming the presence of a smaller portion of a single peptide, but not enough to confirm the presence of the second cross-linked peptide. In fact, Stavrox software was unable to assign this spectrum to any cross-linked peptide candidate, as the over-fragmentation renders it useless in identifying what peptides are involved in the cross-link.

Fragmentation using 25% and 30% gave reliable spectra that could be used to identify the cross-linked peptides. Both spectra also gave good Stavrox scores of 194 and 177, respectively.

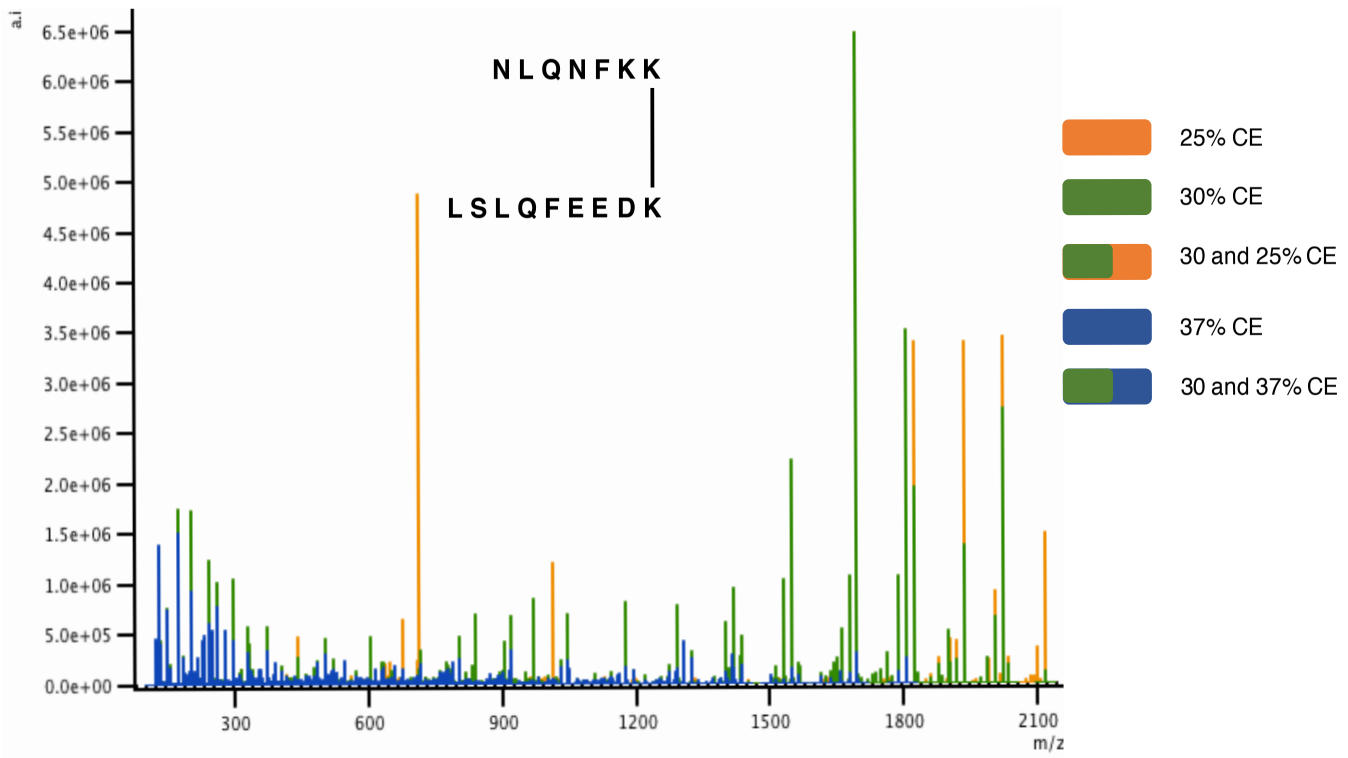

Figure 3.11: Cross-link K15$_{13}$ subject to different HCD collision energies (CE). In blue are the fragment ions produced using 37% collision energy. In orange and green are the fragment ions produced using 25% and 30%, respectively. Fragment ions produced by two collision energies are also indicated by two colours. As can be seen, fragmentation using 37% CE over-fragments the peptide, prducing a disproportionate number of fragments with a low m/z. Fragmentation using 25-30% produces much better distribution of the fragment ions, especially those fragments ions of a higher m/z which are crucial in identifying the cross-linker and the attached peptide.

3.5 Software analysis and confidence filtering of cross-links

3.5.1 Stable isotope-labelling for cross-linking

Isotope labelling is another way in which cross-linking can be validated. This method can serve as an internal control to validate whether the presence of a cross-linked peptide is a true cross-link or not. With the isotope labelling, the standard BS3 cross-linker is mixed in a 1:1 ratio with a deuterated form of the BS3 cross-linker. Both the undeuterated and deuterated form of BS3 theoretically have an equal chance of forming a cross-link, thus the presence of both cross-links can unambiguously confirm the presence of the cross-link.

As previously been reported, the deuterated BS3 molecule, in particular the BS3 d12 molecule, can have an effect on the retention time of the cross-linked peptide (Fischer et al., 2013). To test the stable isotopes, the Kif15 protein was cross-linked with both BS3 d0/d4 and BS3 d0/d12 mixed in a 1:1 ratio. To look at the effect of the deuterated molecules on the retention time of the precursor ion, the data was analysed for the BS3 d0/d12 dataset as the d12 deuteration will have the biggest effect on retention time.

Presented below in figure 3.12 shows the retention time difference of BS3 d0 and d12 for 10 cross-linked peptides. It is clear that the BS3 d12 molecule does not significantly cause a shift in the elution profile of the cross-linked peptides. This suggests that both the BS3 d12 and the BS3 d4 molecules can be mixed in a 1:1 ratio with the lighter BS3 molecule without a significant effect on the retention time of the cross-linked peptides.

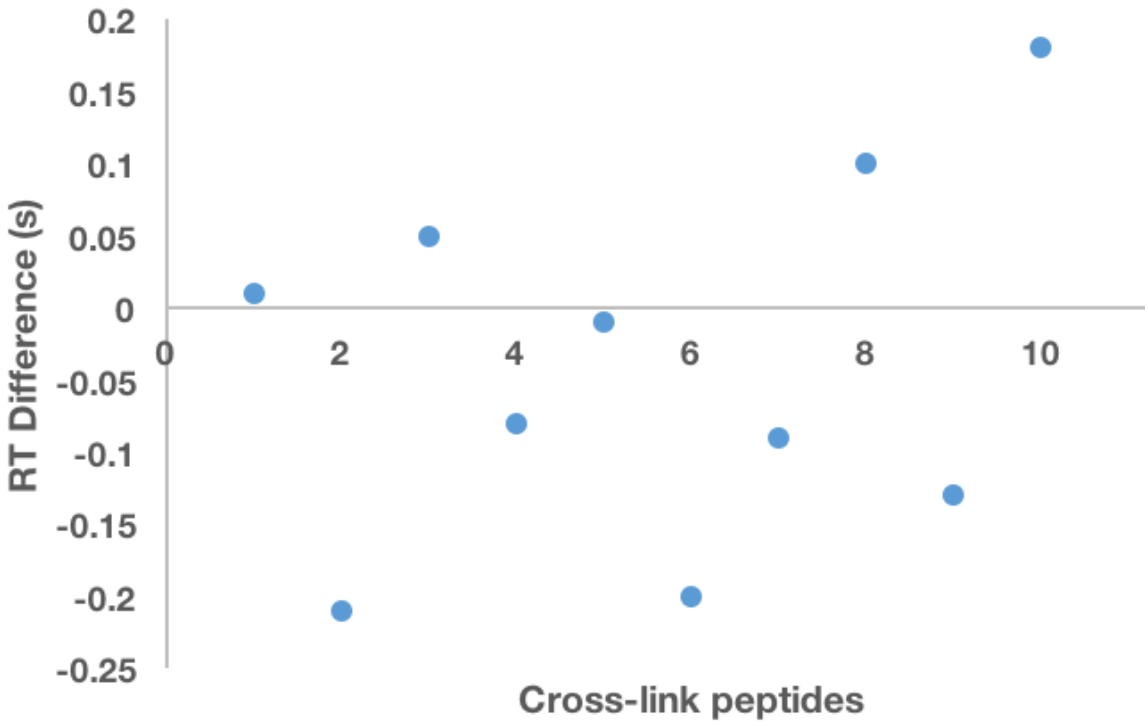

Figure 3.12: The effect of BS3 d12 labelling on the retention time difference between BS3 d0 labelling and d12 labelling.

Presented in figure 3.13 is an example of a cross-linked peptide identified with BS3 undeuterated molecule (red spectra on top) and BS3 d12 molecule (green spectra on bottom). From the two spectra below we should see some fragment ion peaks that are the same mass (orange fragments) and some shifting mass peaks (blue fragments). Of particular interest is the y ion series seen for the alpha peptide. These fragments should shift according to the m/z of the peaks. Since these fragments are mainly 1+ ions, the corresponding fragments on the heavy spectra should be shifting by 12 da.

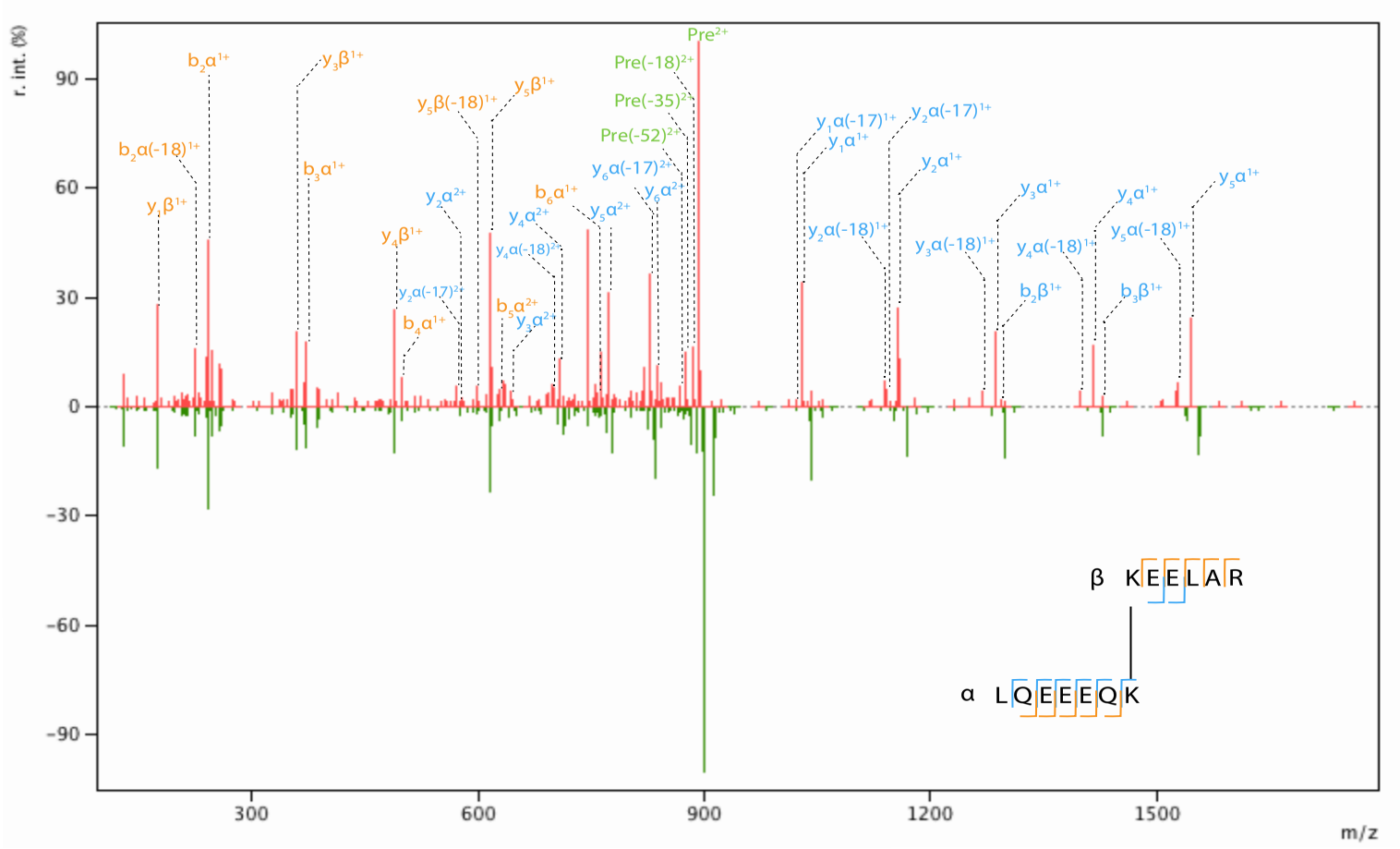

Figure 3.13: Example of stable isotope labelled Tpx2 cross-link between peptides KEELAR and LQEEEQK. The top red spectra is the BS3-d0 (undeuterated) cross-linker and the bottom green spectra is the BS3 d-12 labelled spectra. The fragmentation schematic for the cross-linked peptides is also presented. However, the blue colour is used to indicate the fragments containing the cross-linker and the second peptide. As such, these fragment ions should be shifting between the top and bottom spectra. In orange is the fragment ions spefici to a single peptide and therefore should be identical between the two spectra.

However, isotope labelling is not error-proof as it does not consistently produce the mass shifted cross-linked peptides. It was found that isotope labelling only worked for a small number of the validated cross-linked peptides. Of the 22 monomeric cross-linked peptides identified, only 2 were also identified using stable isotope labelled BS3 cross-linker. Even some of the cross-linked peptides validated through HCD and ETD fragmentation ions, were not matched to an isotope labelled precursor ion. We were concerned about these 'missing' isotope pairs and wondered if the identification by Stavrox was confounding the analysis, especially as the numbers of MS2 spectra were very high (~600). Therefore, we developed a python script to help reduce the numbers of MS2 presented to Stavrox and to determine if isotope pairs could be identified.

To help maximise the number of cross-linked peptide pairs recovered, an in-house developed python script was used, which is an extension of a previously developed software by the Jones lab (Wilhelm and Jones, 2014) and similar to another software called Modificomb, which is used to study mass shifts associated with post-translational modifications (Savitski et al., 2006). The python script looks for precursor mass ion pairs related by a specific mass shift (such as 12) and then tests the fragment ions to see if the fragment ions are related by looking for masses that stay the same (like the orange ions annotated in figure 3.13) and masses that move by 12 Da (like the blue ions annotated in figure 3.13) enabled to search a large dataset to match heavy and light precursor ions relative to their charge state. A threshold window can also be adjusted for the ppm and retention time difference. The output file is a much smaller file and can be used to input into Stavrox to identify the cross-linked peptides. The python script yielded much better results as seen in figure 3.14. The number of cross-linked peptide pairs identified with the python script are greater than those seen with the Stavrox software alone.

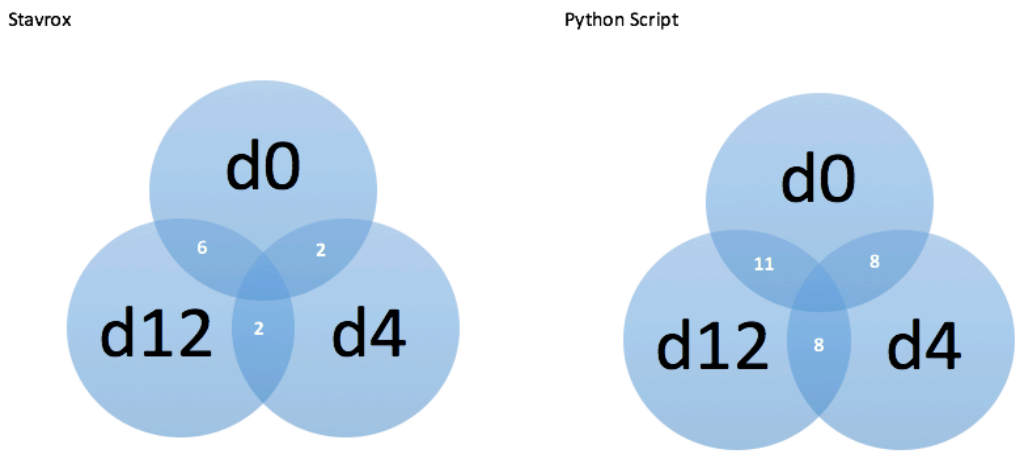

Figure 3.14: Venn diagram representing the isotope-labelled cross-linked pairs found using the standard Stavrox software and the in-house python script. The venn diagrams show how many BS3-d4 and BS3-d12 pairs can be found for a list of 22 cross-linked peptides.

3.5.2 Missed cleavages and differential charge states for cross-linked peptides

Trypsin cleavage occurs after lysine and arginine residues. Due to lysine residues being a candidate for cross-linking, and that trypsin is very sensitive to steric change, the number of missed cleavages is expected to increase for when database searching is done for cross-linked peptides. Missed cleavages in tryptic peptides is not uncommon. In fact, if a cross-linked peptide can be found in different forms, with a missed cleavage and without missed cleavages, these give rise to two independent fragmentation spectra with ions that can be used to verify the same cross-link.

Presented below in figure 3.15 is an example of a cross-link peptide found with a missed cleavage in the alpha peptide (top red spectra) and one without the missed cleavage in the alpha peptide (bottom green spectra). Annotated in orange are the fragmentation ions that should be present in both spectra, whereas those fragments in light blue are those that differ between the two spectra. A nice y ion series is identified in both spectra to confirm the identity of the presence of the alpha peptide and the corresponding beta peptide cross-linked.

Another useful indicator of a true cross-link is to find the same cross-linked peptide in different charge states. If the precursor ion for a cross-linked peptide can be identified at different charge state, this will produce different MS2 fragmentation spectra that can be used to independently verify the presence of the cross-linked peptide.

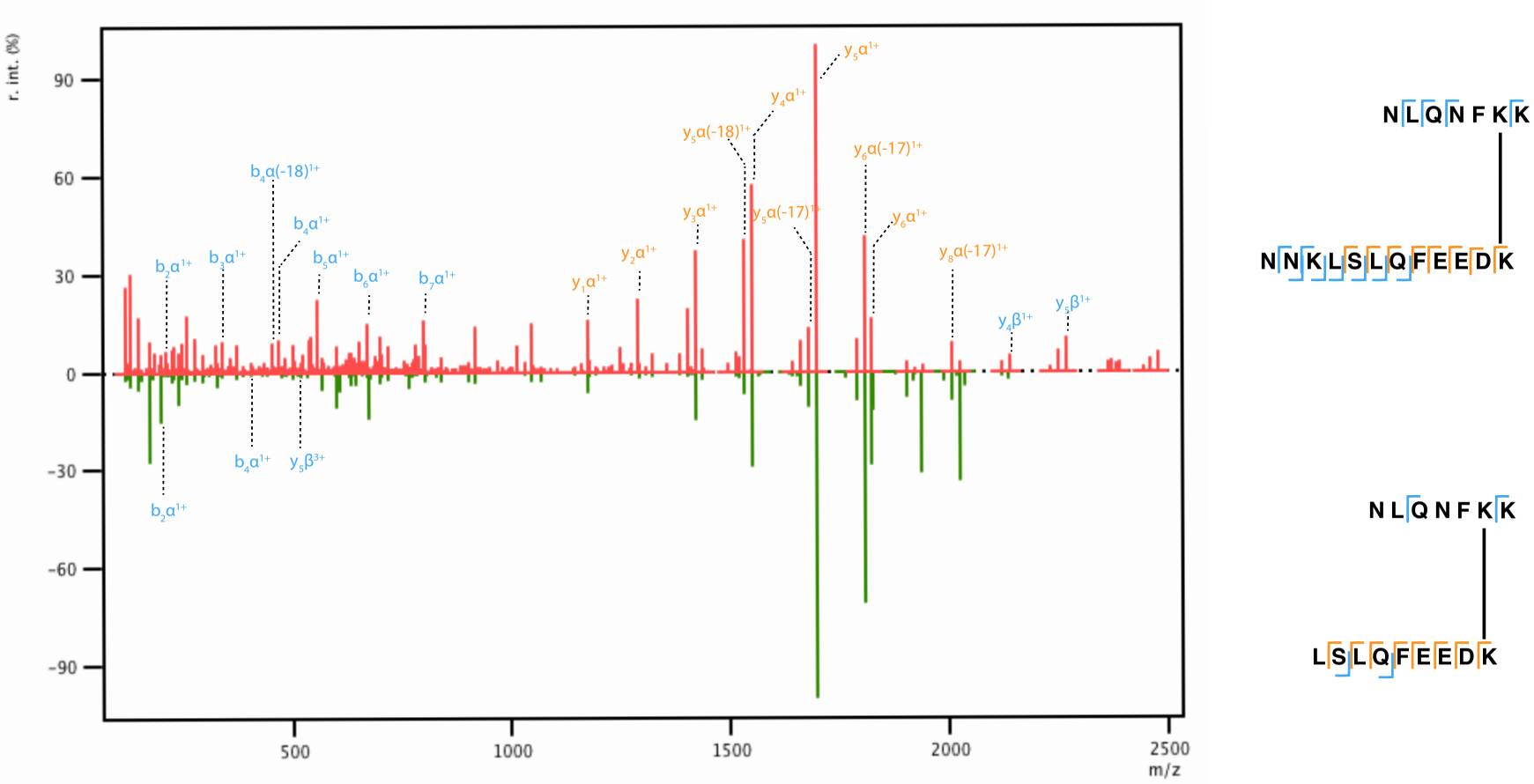

Figure 3.15: Cross-linked peptide K15$_{13}$ identified with and without missed cleavage. The top right spectrum is the cross-linked peptide identified with the uncleaved alpha peptide containing the "NNK" sequence at the n-terminal. The bottom spectrum is the cross-linked peptide identified with the cleaved alpha peptide. The schematics show the peptides fragmentation. The orange ions are those fragments that should be the same between the miscleaved and uncleaved cross-linked peptides. The blue ions indicate those fragments that are different between the two cross-linked peptides as they are fragments containing ions towards the n-terminal of the alpha peptide, where the miscleavage occurs.

A

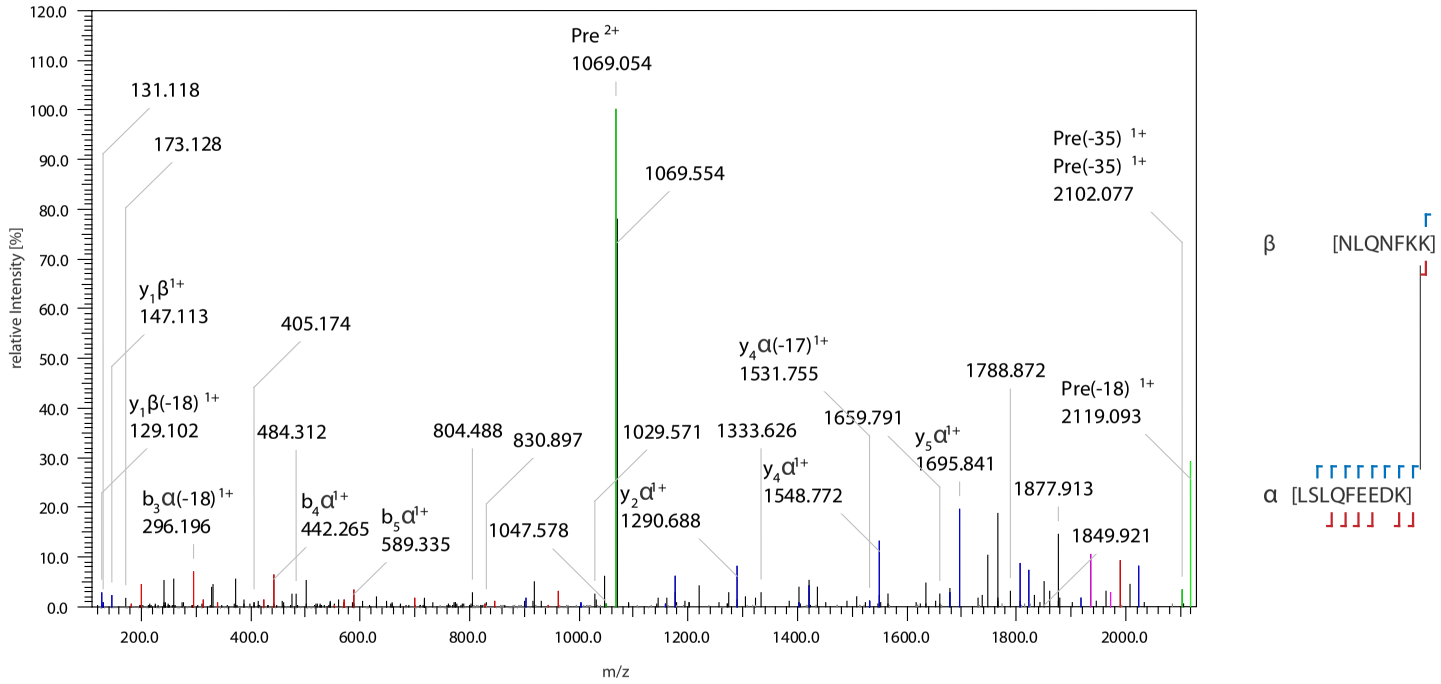

Figure 3.16A: Cross-linked peptide K15$_{13}$ identified as a 2+ precursor ion. On the right hand side is the mass spectrum showing the fragmentation ions associated with this cross-link in its 2+ charge state. On the right hand side is a schematic illustration of the b and y ions identified, shown in red and blue, respectively.

B

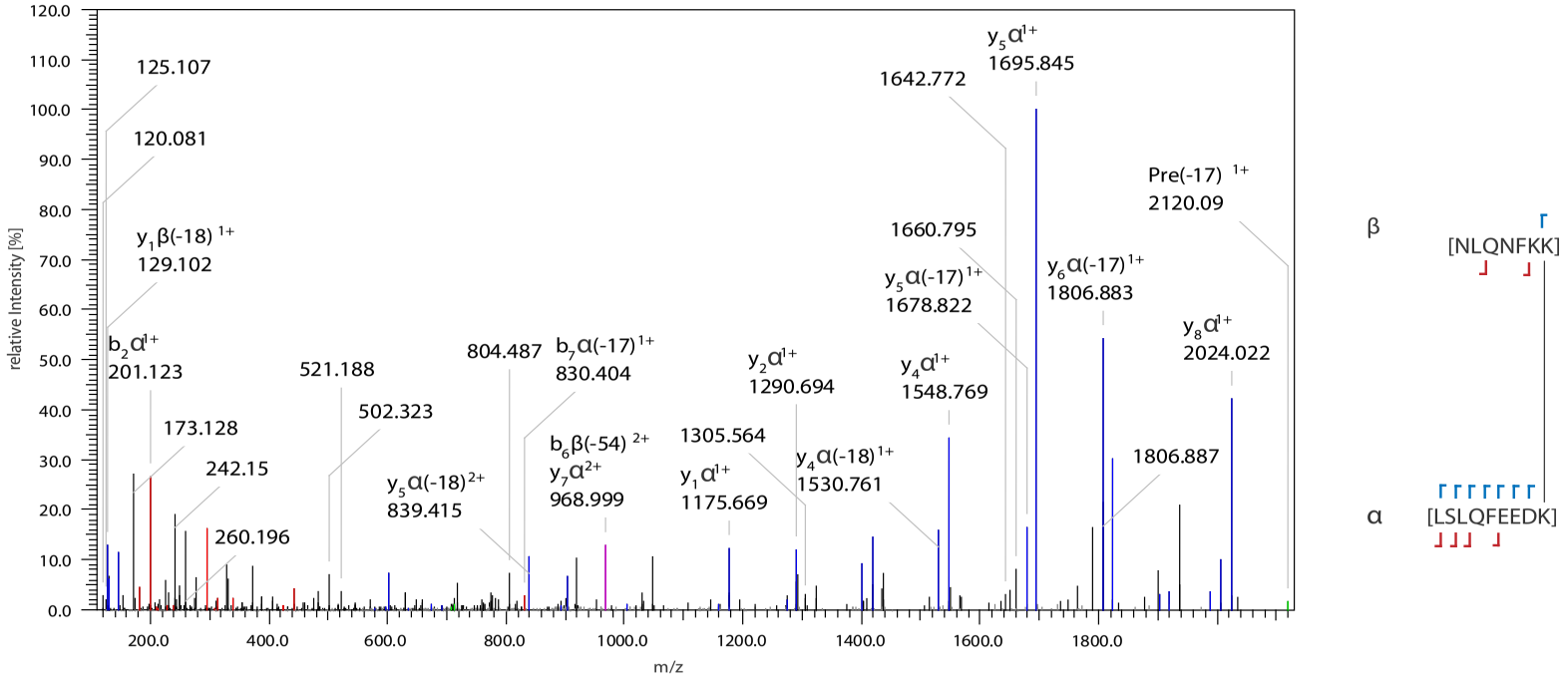

Figure 3.16B: Cross-linked peptide K15$_{13}$ identified as a 3+ precursor ion. On the left hand side is the mass spectrum showing the fragmentation ions associated with this cross-link in its 3+ charge state. On the right hand side is a schematic illustration of the b and y ions identified, shown in red and blue, respectively.

C

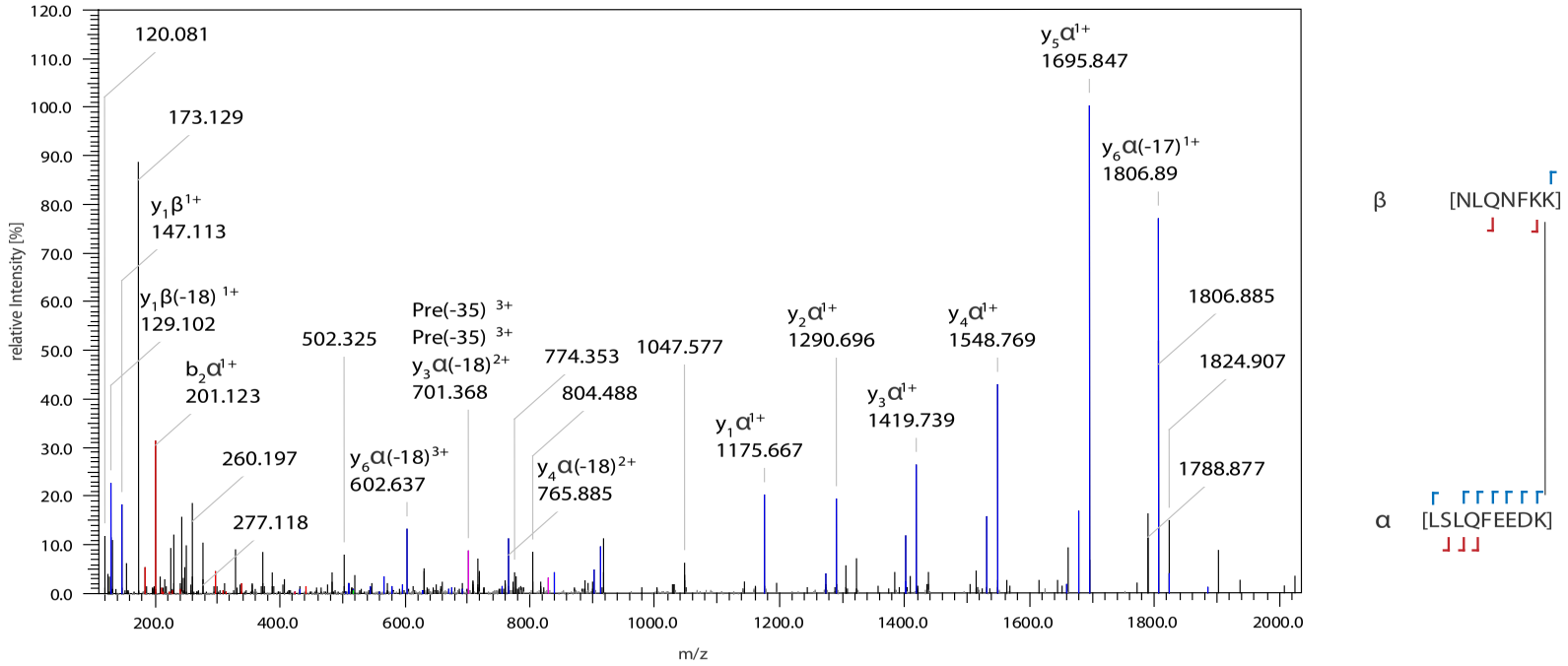

Figure 3.16C: Cross-linked peptide K15$_{13}$ identified as a 4+ precursor ion. On the left hand side is the mass spectrum showing the fragmentation ions associated with this cross-link in its 3+ charge state. On the right hand side is a schematic illustration of the b and y ions identified, shown in red and blue, respectively.

3.5.3 Quantification using MaxQuant

Maxquant is one of the leading proteomics tools for quantitation (Cox and Mann, 2008). Although mostly used for SILAC experiments, the software has been expanded to include label-free quantitation (Cox et al., 2014). For any given cross-link, the linear peptides of a cross-link should be in a higher abundance in the control sample and lower in the cross-linked sample (Figure 3.17). As such, this can be used as a simplified method to account for a change in the abundance of linear peptides between untreated and treated samples. In chapter 4, we will also use this quantitation method to help assign cross-linked peptides to be dimeric or tetrameric.

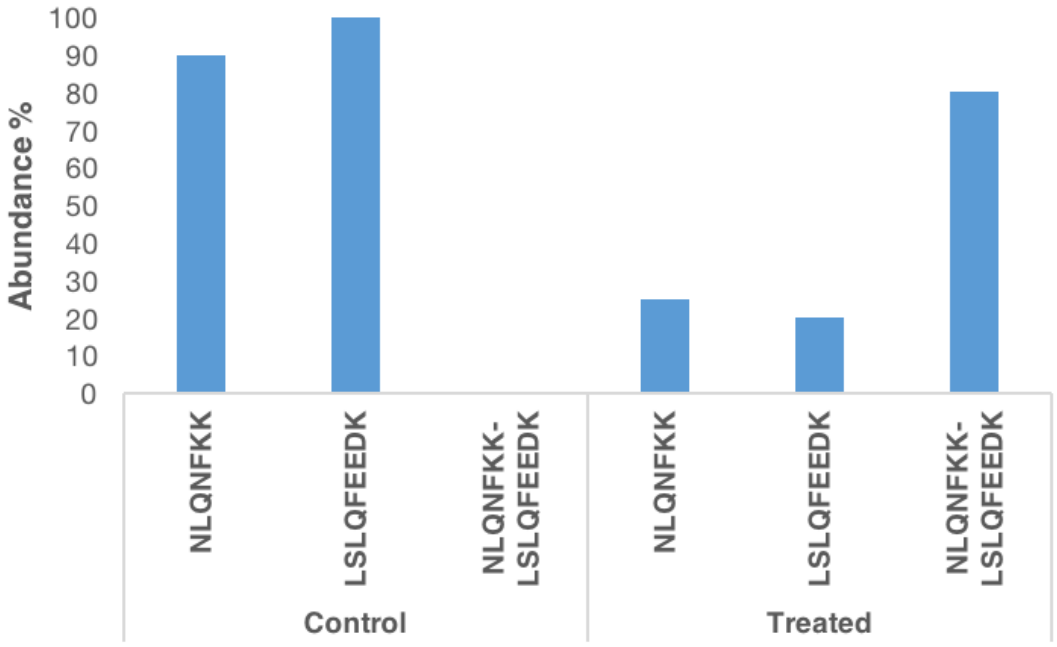

Figure 3.17: Quantitation of cross-linked peptide $K15_{13}$.

3.6 Kif15 monomeric cross-links summary

To standardize the cross-linking workflow, Kif15 monomeric cross-links have been used as an example to demonstrate the different optimization steps involved. Presented in figure 3.18 is the schematic organization of Kif15 monomer. The N-terminal motor domain is followed by several coiled-coil domains and a final leucine zipper domain. The numbers presented correspond to the list of cross-links presented in table 3.3. Given that Kif15 does not physiologically function as a monomer, most of these cross-links may not be relevant for the understanding of the function of this motor in cells. Presented in table 3.3 is also other evidence to increase confidence in the presence of the cross-links, such as the presence of the cross-linker in several charge states and different cleavage states.

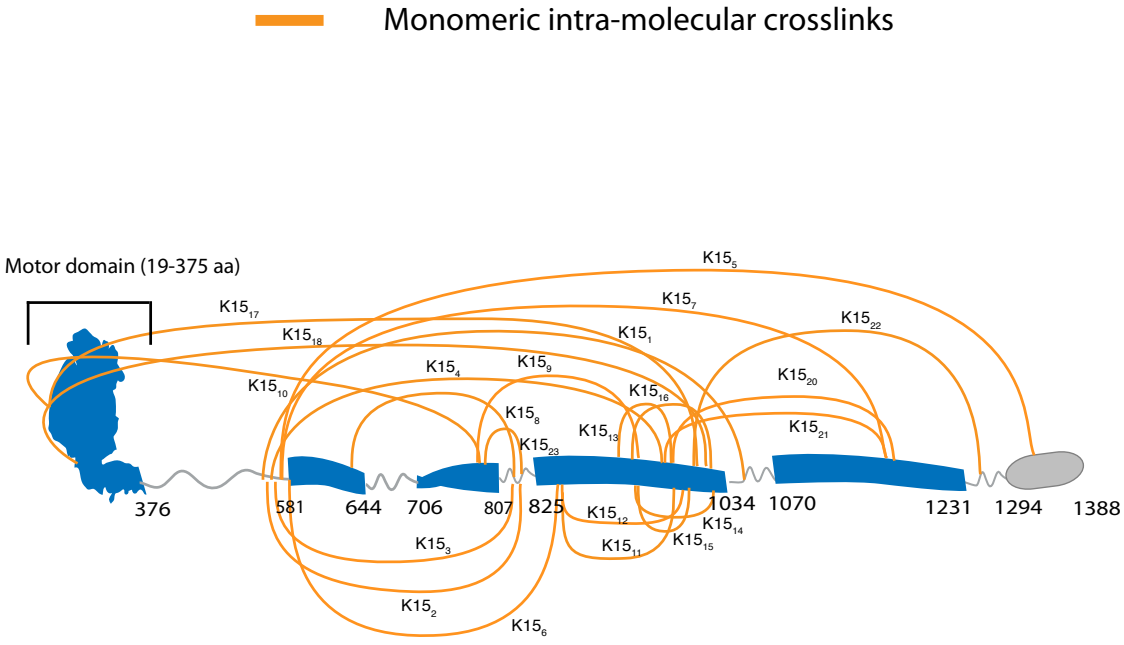

Figure 3.18: Schematic of the kif15 monomeric cross-links identified. The N-terminal motor domain is followed by 4 coiled-coil domains and a final leucine-zipper domain. The numbers on the cross-links correspond to the cross-links numbers presented in table 3.3.

Cross-link Name	Peptide 1	Residue Number 1	Peptide 2	Residue Number2	BS3	Triplicates	EDC	BS3 isotope	Different Charge states	Different Cleavage States	Met Oxidation
K15 1	DK($)K	409	KQEVDILDLK($)	1044	✔	✔	✔	✗	✔	✔	N/A
K15 2	KS($)LIEK	438	VVLHSADKELSSVK($)	818	✔	✔	✗	✗	✔	✔	N/A
K15 3	MIVK($)	461	VVLHSADK($)	812	✔	✔	✗	✗	✔	N/A	✔
K15 4	NEIQT($)LR	499	LSLQFEEDK($)	924	✔	✔	✗	✗	✔	✔	N/A
K15 5	LEK($)	549	AFQEK($)	1305	✔	✔	✗	✗	✔	N/A	N/A
K15 6	SDK($)	562	TNQEKEFNK($)	834	✔	✔	✗	✗	✔	✗	N/A
K15 7	AQK($)	573	EALIQELQHK($)	1106	✔	✔	✗	✗	✗	N/A	N/A
K15 8	ACK($)R	641	VVLHSADK ($)	812	✔	✔	✗	✗	✔	N/A	N/A
K15 9	LQQHVDK($)	749	ACLQDSYDNLQEIMK($)	875	✔	✔	✗	✗	✔	N/A	✔
K15 10	IDWTK($)	770	T($)AIIANVHPGSR	334	✔	✔	✗	✗	✗	N/A	N/A
K15 11	TNQEK($)	830	LEESLLATEK($)	968	✔	✔	✗	✗	✔	N/A	N/A
K15 12	TNQEK($)	830	DSDK($)KVVADLMNQIQELR	981	✔	✔	✗	✗	✗	✔	✔
K15 13	NLQNFKK($)	890	LSLQFEEDK($)	924	✔	✔	✗	✗	✔	✔	N/A
K15 14	LSLQFEEDK($)	924	VLIKK($)QEVDILDLKETLR	1034	✔	✔	✗	✗	✔	✔	N/A
K15 15	ENSS($)K	929	TETIDTLKQELK($)	1009	✔	✔	✗	✗	✔	✔	N/A
K15 16	SRDS($)DKK	979	ACLQDSYDNLQEIMK($)	875	✔	✔	✗	✗	✔	✔	✗
K15 17	QELK($)	1013	T($)AIIANVHPGSR	334	✔	✔	✗	✗	✔	N/A	N/A
K15 18	DINCK($)	1017	S($)GSADGEQNLBLSVLSTSLR	40	✔	✔	✗	✗	✔	N/A	N/A
K15 19	LNQK($)K	1110	ENET($)LK	894	✔	✔	✗	✗	✗	✗	N/A
K15 20	NEYNFK($)	1121	KENETLK($)	896	✔	✔	✗	✔	✔	N/A	N/A
K15 21	MT($)DEVER	1288	ACLQDSYDNLQEIMK($)	875	✔	✔	✗	✗	✔	N/A	✔
K15 22	NDFLK($)	797	SEVHDLR($)	810	✔	✔	✔	✔	✔	N/A	N/A

Table 3.3: Summary of the identified monomeric Kif15 cross-links.

3.6 Conclusion

The aim of this chapter was to develop a standardized cross-linking mass spectrometry workflow. This involved optimization of the individual steps involved in cross-linking mass spectrometry (see figure 3.6) as well as developing a software analysis pipeline.

We have successfully been able to optimize the individual steps involved in cross-linking mass spectrometry (figure 3.19). Cross-linking using BS3 is a good option as the fragmentation chemistry of this cross-linker is well understood and the reactive residues of this cross-linker (lysine, serine, threonine and tyrosine) are abundant amino acids in proteins. To build a constraint map and understand the topology of a protein/protein complex of interest, we repeated the cross-linking experiments using a cross-linker with a shorter functional distance such as EDC. It was found that cross-linking using isotope-labelled BS3 did not produce consistent results, thus this step was omitted from the final cross-linking protocol. Depending on the molecular mass of the protein of interest the cross-linked sample is separated on a gel (less than ~400 kDa) and digested or just cross-linked in solution (any molecular weight) and digested in-solution. For a standard gel digest, Trypsin is the protease of choice. For an in-solution digest, a combination of Trypsin/Lys-C works best as the Lys-C is also able to cleave c-terminal of lysine residues, but works better at getting inside tightly folded proteins and digesting less accessible areas, which are often missed by the Trypsin. Analysing the precursor ions and fragmentation ions using the Orbitrap provides the resolution desirable to unambiguously identify the cross-linked peptide. With regards to the fragmentation mode, HCD is the best option, and the use of a lower collision energy (25-30%) gives the best fragmentation distribution required for successful identification of cross-linked peptide. To analyse the cross-linked peptides, a combination of Stavrox and MaxQuant seems to yield the best results. Stavrox can be used to identify the cross-links, and the

MaxQuant software can be used to provide some quantitative data to inform the confidence of the cross-linked peptide identified.

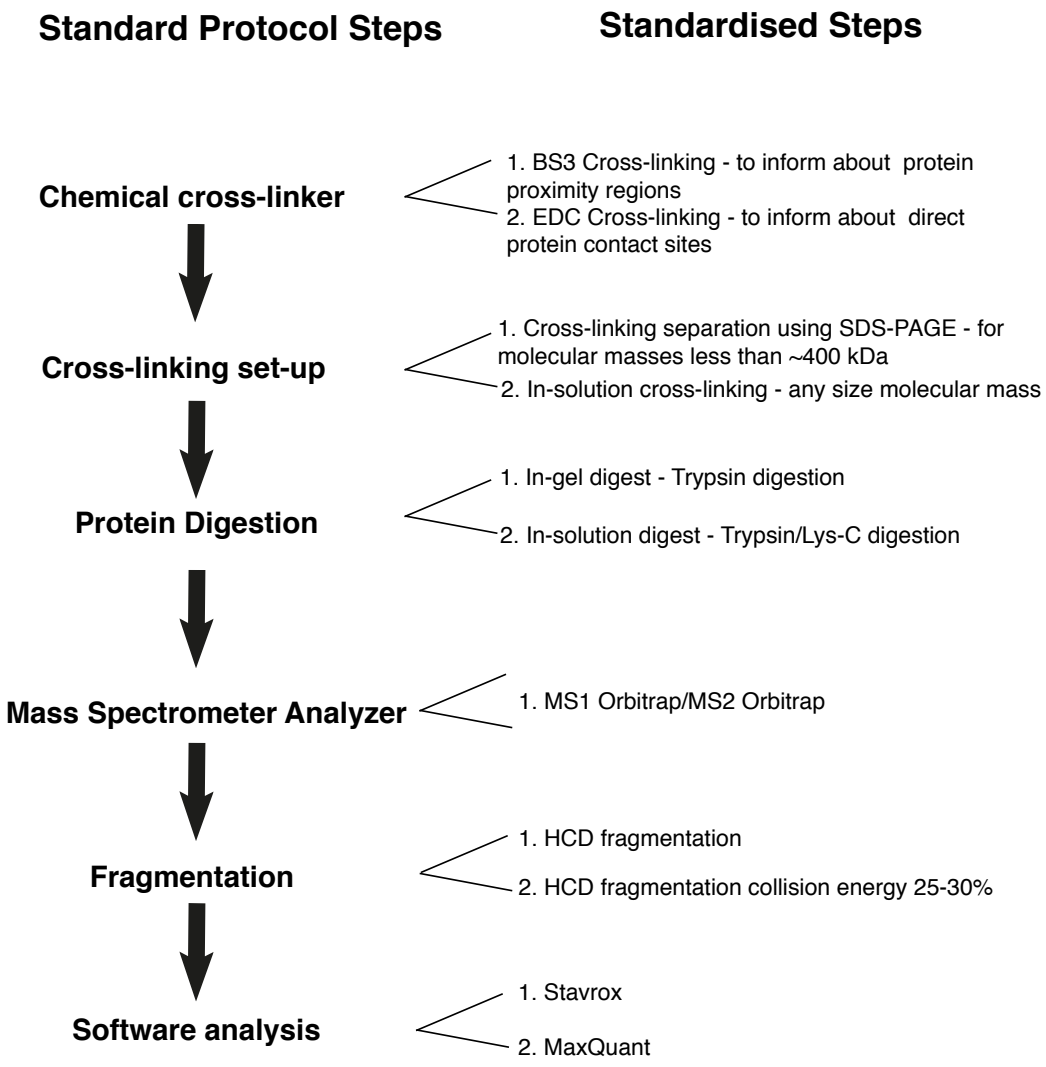

Figure 3.19: Optimised Cross-linking mass spectrometry workflow.

Chapter 4: Structural Assembly of Tetrameric Kif15 and its Interaction with Tpx2 Revealed by Cross-linking Mass Spectrometry

4.1. Introduction

Kinesin 12, Kif15 is a Kinesin that plays an important role in bipolar spindle assembly and maintenance (Tanenbaum et al., 2009, Vanneste et al., 2009). It consists of 1388 amino acids, with the protein organizing into a tetramer at physiological conditions but dissociates into a dimer at higher ionic conditions (Drechsler et al., 2014, Mann et al., 2017). However, another group reports Kif15 functions as a dimer (Sturgill et al., 2014). Like many kinesins, Kif15 is thought to be auto-inhibited by the back-folding of the carboxy-terminal tail interacting with the motor head, thus prohibiting the accessibility of the motor domain from binding to the microtubules. Along with Eg5, Kif15 is a second tetrameric kinesin which mediates bipolar spindle assembly and maintenance, however, unlike Eg5, the structural organization of Kif15 is not well studied. Also, the mechanism by which Kif15 auto-inhibits is relatively unknown.

The localisation of Kif15 to the spindle is mediated through the binding of the MAP Tpx2. Localisation of kif15 to the spindle requires the C-terminal leucine zipper of the motor (Wittmann et al., 2000). Tpx2 C-terminal domain is required to localise Kif15 to the spindle (Mann et al., 2017) and the full-length protein also inhibits Kif15 motility in vitro (Drechsler et al., 2014; Mann et al., 2017). The molecular mechanism by which Tpx2 inhibits Kif15 motility remains unclear. It has been shown that Kif15 cannot bind directly to Tpx2 in the absence of microtubules (Wittmann et al., 2000). However, more recent work has shown that using ~30-fold excess of Tpx2 dimers (2.5 μM Tpx2 and 80 nM Kif15) enables complex formation with Kif15 in the absence of microtubules, with an enhanced affinity in the presence of microtubules (Drechsler et al., 2014).

Targeting motor proteins involved in cell division, such as Eg5 and CENP-E, have become attractive options for cancer therapies. However, cancer cells are developing drug resistance to current Eg-5 inhibitors due to the compensatory role of Kif15 in bipolar spindle assembly (Ma et al., 2014). This suggests the best way forward for cancer drugs inhibiting bipolar spindle assembly would be to simultaneously target both Eg5 and Kif15. In order for this to be achieved, further understanding of the structural organisation and the functional role of Kif15 is needed. The aim of this project was to understand the structural organization of Kif15 from a monomer, to dimer and into a tetramer. Also, we wanted to study the auto-inhibited conformation of Kif15 and which regions of the protein is involved in stabilizing this conformation. After understanding the structural assembly of Kif15, this was extended to understand the binding interface between Kif15 and Tpx2 and how the presence of microtubules may affect this interaction.

4.2. Cross-linking/MS analysis of full-length Kif15

4.2.1 Cross-linking/MS analysis for Monomeric and Dimeric Kif15

Human Kif15 full length protein containing an amino-terminal polyhistidine tag was expressed in SF9 insect cells and purified using a two-step method consisting of anion exchange chromatography using a sepharose column, and metal affinity chromatography column using a TALON column as reported in Drechsler et al., 2014 (Figure 4.1A). Overall, this method enabled the purification of 6His-Kif15 to homogeneity, with the protein concentration calculated at 2 μM (Figure 4.1B). The protein migrated with expected molecular mass of ~165 kDa. The binding to the SP column enables the removal of impurities in the sample, as seen in the SP flow-through. Further contaminants are removed by binding the lysate to the TALON beads, as seen in the TALON flow-through lanes.

The band corresponding to Kif15 was excised from the gel, alkylated, reduced and digested using trypsin. To validate the purity of the protein sample used, the data obtained from the mass spectrometer was analysed using Mascot. This is a commonly used protein identification software (see chapter 3). To analyse the data, the *Spodoptera frugiperda* (SF9) database was searched as a background database to identify any other proteins expressed and purified with my protein. Also, the human database was used to identify the recombinantly expressed Kif15. The average protein coverage for Kif15 was ~ 75% (Figure 4.1Ci), with little contamination from keratin and ubiquitin in the samples (Figure 4.1Cii). This indicates the high purity of the Kif15 protein which will be used for subsequent cross-linking experiments. This is essential as contaminations in the sample can have a significant effect on the analysis of cross-linked peptide analysis.

Post-translational modifications of proteins can also have an effect on the conformation adopted by proteins. As such, it is important to identify any

modifications associated with the purified Kif15. A single phosphorylation site was identified (Figure 4.1D). This phosphorylation site is a previously described CDK1 phosphorylation site (Zhou et al., 2013). Multiple formylation sites have also been identified, in the motor domain of Kif15 and the neck region. Lysine formylation is a common feature of proteins involved in binding and regulating chromosome function (Wisniewski et al., 2008).

A

B

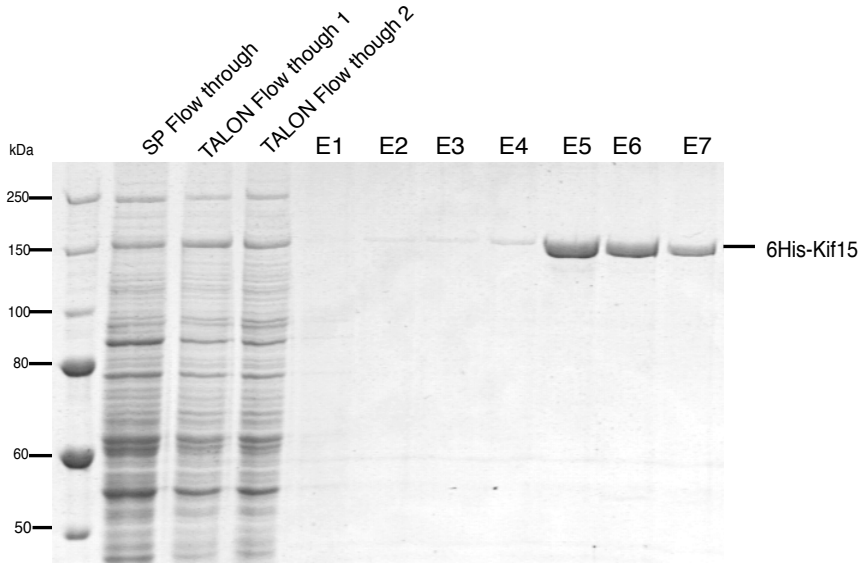

C

i

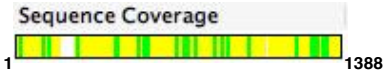

ii

Protein Identified	Peptide Count
Kif15	130
Keratin	4
Ubiquitin	2

D

Post-translational modification	Residues
Phosphorylation	Thr-399
Formylation	283, 319, 333, 366, 385, 438, 449, 451, 599

Figure 4.1: Purification and identification of Kif15. **A;** Schematic to illustrate the two step purification of 6His-Kif15. First the SF9 cells are lysed and the lysate containing the poly-histidine tagged Kif15 are bound to a SP column, which is an ion exchange column, then the sample is bound to TALON beads, a Cobalt metal affinity column. **B;** Coomassie gel to show the purification of 6His-Kif15. The flow-through samples from the SP and TALON columns show the impurities removed from the sample before Kif15 was eluted from the TALON column. Kif15 was eluted as 300 μl aliquots, which were used for subsequent cross-linking experiments. **Ci;** Identification of Kif15 using Mass Spectometry. Presented in this figure is the sequence coverage obtained for Kif15 (~80%), whereby the yellow regions are the unmodified peptides identified for Kif15 and the green regions are modifications associated with Kif15, such as methionine oxidation or cysteine alkylation which are introduced during the digeston protocol. **Cii;** Proteins identified from the extracted gel slice. As seen in this figure, Kif15 is the predominant protein identified, with a little contamination from Keratin and Ubiquitin**. D;** Post-translational modifications identified in Kif15.

To understand the structural assembly of Kif15 into a tetramer, the organisation of the protein into a monomer and a dimer must first be studied. To do this, the BS3 cross-linker was titrated against Kif15 to obtain a monomeric and dimeric Kif15 species. This was calculated as the molecular mass of the Kif15 protein expected as a monomeric (165 kDa) and dimeric species (330 kDa) (Figure 4.2B). Presented in figure 4.2A is a coomassie gel of the titration experiments done for Kif15. As seen on the SDS-PAGE gel, the titration of BS3 enables the formation of cross-linked monomeric Kif15 species, which migrates around 160 kDa. The fuzziness of the protein band indicates the presence of the BS3 cross-linker. As a control, untreated Kif15 protein was also run on the SDS-PAGE, which also runs at ~165 kDa as expected. Also, for a higher concentration of BS3, the monomeric species are converted into a dimer as indicated by the protein band which appears at ~330 kDa.

To analyse the monomeric cross-linked species, the band from lane 2 was excised, as this sample shows that the majority of the molecules are monomeric. The monomeric data is presented in chapter 3. To analyse the dimeric species, the band from lane 4 was excised as this represents a state where all the molecules are in a dimeric state. The untreated protein band from lane 1 was also excised and used as a control. After the gel bands were reduced and alkylated, the protein was digested using trypsin and analysed using mass spectrometry. The Stavrox software was used for the analysis of the cross-linked peptides. The software generated a list of theoretical cross-linked peptide candidates, based on an *in silico* digestion of Kif15, with lysine, serine and threonine residues as candidate reactive groups for BS3 cross-linking. Cysteine alkylation was set as a constant modification and methionine oxidation was set as a variable modification. The data was independently analysed for Kif15 monomer and the Kif15 dimer data.

A

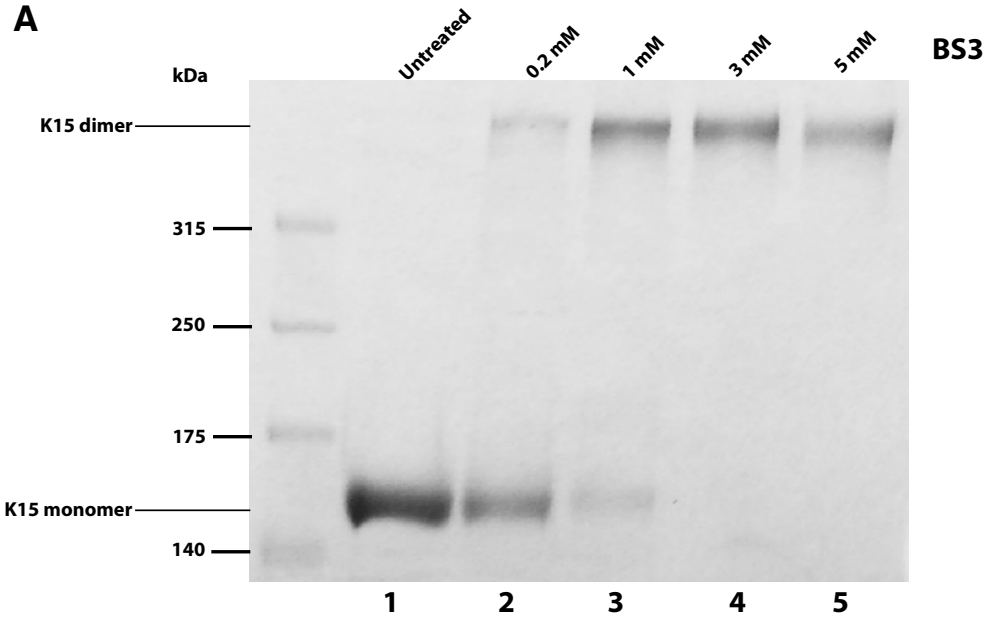

B

Kif15 Oligomerisation State	Predicted Mass	SDS Mass
	165 kDa	~160 kDa
	330 kDa	~330 kDa

Figure 4.2: Monomeric and dimeric cross-linking of Kif15. A; Coomassie gel showing titration experiments of BS3 cross-linker against Kif15, to obtain monomeric and dimeric species on the gel. **B;** Molecular masses associated with Kif15 monomer and dimer species.

Analysing the dimeric Kif15 species, lead to the identification of two types of cross-links; intra-molecular cross-links and inter-molecular cross-links. In figure 4.3A is a schematic to illustrate the cross-links identified for the dimeric Kif15. The dotted green lines indicate the intra-molecular cross-links identified for the dimer, which are 11 in total. As can be seen from table 4.2, many of these intra-molecular cross-links are long-distance cross-links, which indicate

the protein adopts a folded conformation as a dimer. For example, $K15_5$, cross-links Lys-549 in the peptide $_{547}LEK_{549}$ to Lys-1305 in the peptide $_{1301}AFQEK_{1305}$. This is an example of a long-distance cross-link from the unstructured region following the motor domain, to the leucine-zipper tail of Kif15, which indicates that the amino-terminal is folded and interacts with the carboxy-terminal end of the protein. Also, 4 inter-molecular dimeric cross-links were identified for Kif15, as indicated by the solid green lines between the two monomeric species (Figure 4.3A). These cross-links were mainly identified in the two middle coiled-coil regions of the protein (CC2 and CC3). With regards to the stagger of the inter-molecular cross-linked peptides identified for both the dimer and tetramer, there does not appear to be an obvious correlation to the length of the cross-linker. There is not a consistent number of amino acids difference between the cross-linked peptides. Similar conclusion was reached by Soares *et al.,* after experiments were conducted to study the dimeric and tetrameric organisation of the mitotic proteins NDE1 and NDEL1(Soares et al., 2012). The mass spectra for the dimeric inter-molecular cross-links are presented in figure 4.3B-E. As seen for all these spectra, good fragmentation for the cross-linked peptides is achieved, which helps to increase the confidence in these cross-linked peptides. Also, presented in table 4.1 is a summary of additional evidence gathered to increase the confidence of these cross-links.

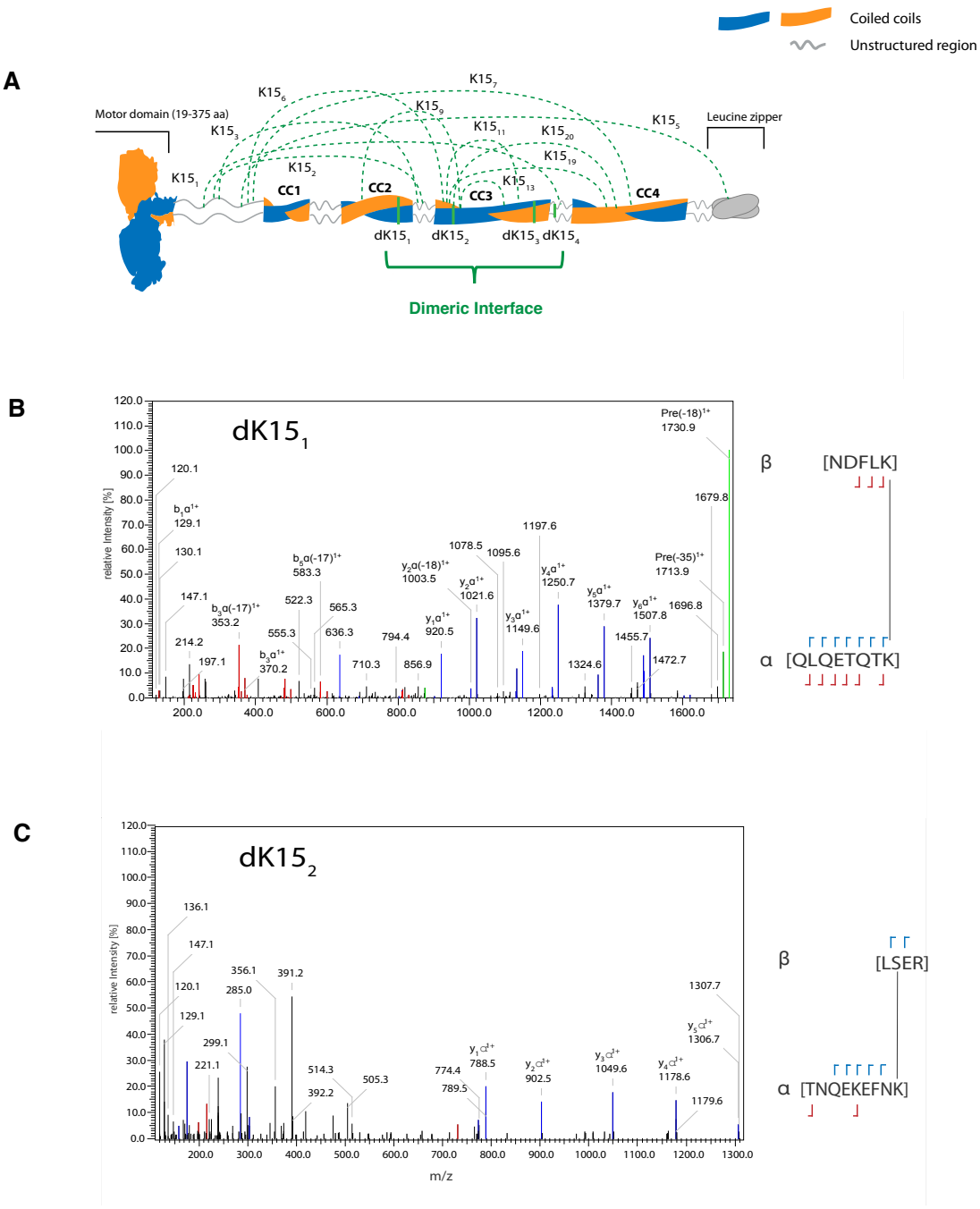

Figure 4.3: Dimeric organisation of Kif15. A; Structural organisation of Kif15, whereby the dotted green lines represent the intramolecular dimeric cross-links of Kif15, and the solid green lines are the inter-molecular dimeric cross-links seen for the dimeric Kif15 molecule. It is assumed that the intramolecular dimeric cross-links are specific for a single chain, whereas the inter-molecular dimer cross-links connects both chains. **B;** Cross-linking spectra for dimeric cross-link 1 ($dK15_1$). For the schematic fragmentation ions, the blue colour indicates the b-ions and the red indicates the y-ions. **C;** Cross-linking spectra for dimeric cross-link 1 (dK152). **D;** Cross-linking spectra for dimeric cross-link 1 ($dK15_3$). **E;** Cross-linking spectra for dimeric cross-link 1 ($dK15_2$). **F;** MaxQuant quantification of the precursor ion of inter-molecular dimeric cross-linked peptides.

D

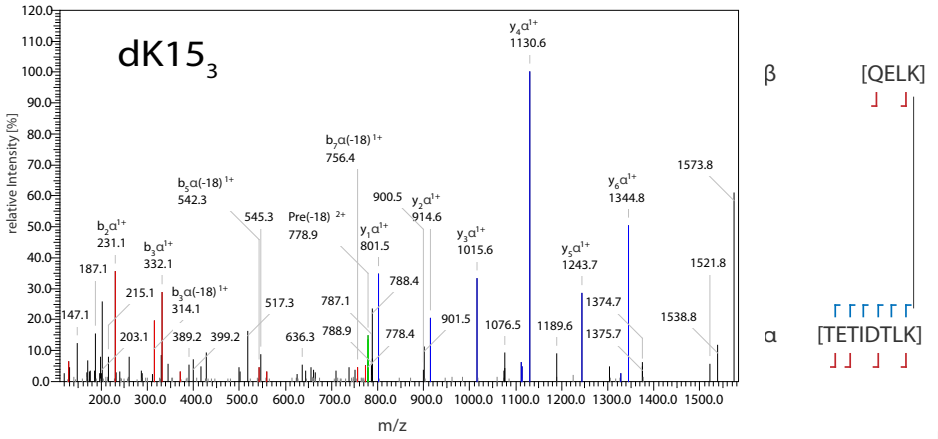
dK15 3
relative Intensity [%]
m/z
β [QELK]
α [TETIDTLK]

E

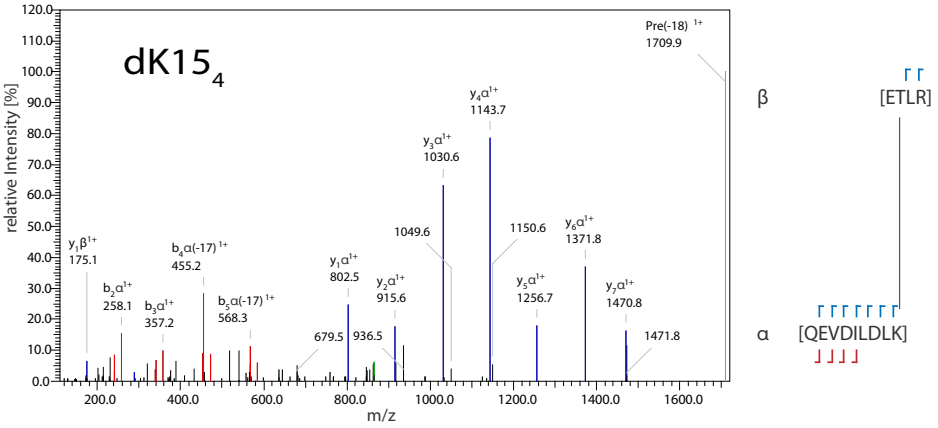
dK15 4
relative Intensity [%]
m/z
β [ETLR]
α [QEVDILDLK]

F

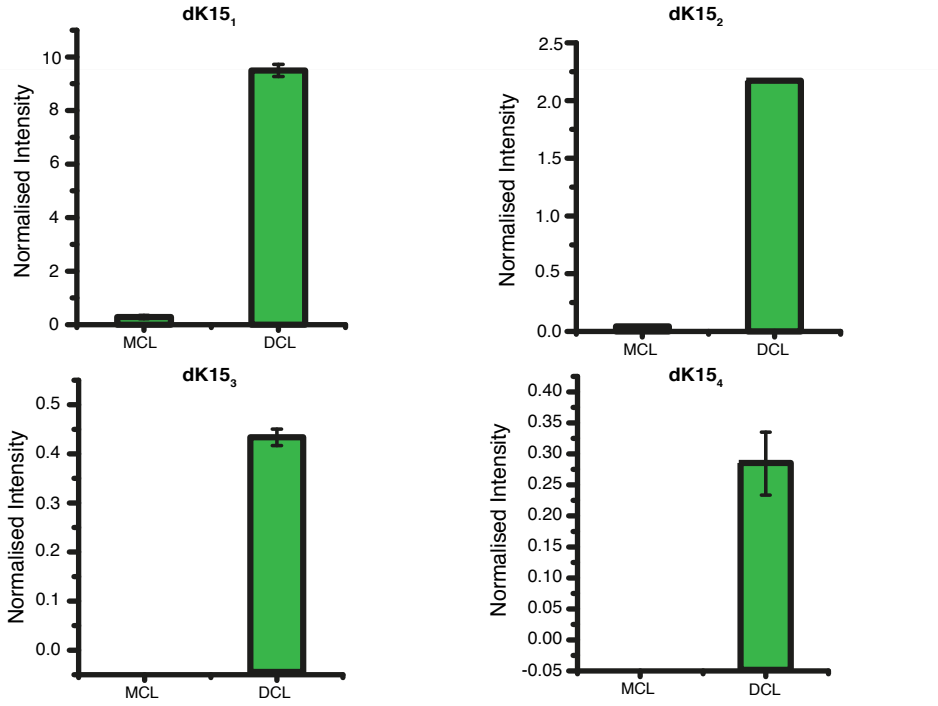
dK15 1
dK15 2
dK15 3
dK15 4
Normalised Intensity
MCL
DCL

To assess the structural organisation of Kif15, Stavrox was used to compare the presence and absence of cross-links between different oligomerization states. However, a more accurate and quantitative approach is required. To do this, the label-free quantitation (LFQ) module of MaxQuant was used. The LFQ module calculates the integrated peak area of the precursor ion and based on a retention time window and ppm error window, can compare different mass spectrometry output files to quantify the presence and absence of a precursor ion of interest (Cox et al., 2014). Peptide detection ("flyability") is dependent on chemical properties of the peptide, which affects its ionization, thus no direct comparison can be made between their ion intensities. However, the intensity of the same precursor ion can be compared across different samples. As seen in figure 4.3F, the four dimeric cross-links identified are quantified. As seen for all these dimeric cross-links, there is only a little background signal ($dK15_1$ and $dK15_2$) or none ($dK15_3$ and $dK15_4$) seen in the monomeric sample. The data was normalised to the top 3 unmodified peptides in each sample.

All of the intra-molecular cross-links for dimeric Kif15 were achieved using BS3 cross-linker. As this cross-linker has a spacer arm of 11.4 Å, any cross-links identified with BS3 can be used to provide information about the proximity of residues within the folded state of a protein. To examine shorter distance interactions we also used the cross-linker EDC; the EDC cross-linker does not add any atoms to the cross-linked species but instead directly attaches a carboxylic amino acid to a primary amine, through the formation of an intermediate ester group (Rivera-Santiago et al., 2015). This means that any cross-links formed using EDC are within a salt-bridge distance. All the inter-molecular cross-links identified with BS3 were also identified using EDC (table 4.1). This indicates that these inter-molecular dimeric cross-links are directly attached to one another. Interestingly, only the $K15_1$ intra-molecular dimeric cross-link was identified with EDC (table 4.1).

Cross-link Name	Peptide 1	Residue Number 1	Peptide 2	Residue Number2	BS3	Triplicates	EDC	BS3 isotope	Different Charge states	Different Cleavage States	Methionine Oxidation
K15 $_{1}$	DK($)K	409	KQEVDILDLK($)	1044	✔	✔	✔	✗	✔	✔	N/A
K15 $_{2}$	KS($)LIEK	438	VVLHSADKELSSVK($)	818	✔	✔	✗	✗	✔	✔	N/A
K15 $_{3}$	MIVK($)	461	VVLHSADK($)	812	✔	✔	✗	✗	✔	N/A	✔
K15 $_{5}$	LEK($)	549	AFQEK($)	1305	✔	✔	✗	✗	✔	N/A	N/A
K15 $_{6}$	SDK($)	562	TNQEKEFNK($)	834	✔	✔	✗	✗	✔	✗	N/A
K15 $_{7}$	AQK($)	573	EALIQELQHK($)	1106	✔	✔	✗	✗	✗	N/A	N/A
K15 $_{9}$	LQQHVDK($)	749	ACLQDSYDNLQEIMK($)	875	✔	✔	✗	✗	✔	N/A	✔
K15 $_{11}$	TNQEK($)	830	LEESLLATEK($)	968	✔	✔	✗	✗	✔	N/A	N/A
K15 $_{13}$	NLQNFKK($)	890	LSLQFEEDK($)	924	✔	✔	✗	✗	✔	✔	N/A
K15 $_{20}$	NEYNFK($)	1121	KENETLK($)	896	✔	✔	✗	✔ -d12	✔	N/A	N/A
K15 $_{21}$	MT($)DEVER	1288	ACLQDSYDNLQEIMK($)	875	✔	✔	✗	✗	✔	N/A	✔
dK15 $_{1}$	NDFLK($)	797	QLQETQTK($)	792	✔	✔	✔	✗	✔	✔	N/A
dK15 $_{2}$	LS($)ER	836	TNQEKEFNK($)	834	✔	✔	✔	✔ -d4	✗	✔	N/A
dK15 $_{3}$	QELK($)	1013	TETIDTLK($)	1019	✔	✔	✔	✗	✗	✔	N/A
dK15 $_{4}$	ET($)LR	1046	QEVDILDLK($)	1043	✔	✔	✔	✔ -d12	✔	✔	N/A
tK15 $_{1}$	DKK($)	410	S($)EQEK	428	✔	✔	✗	✔ -d12	✗	N/A	N/A
tK15 $_{2}$	LNEDREVK($)	1187	TSLEHLVT($)K	1178	✔	✔	✔	✔ -d12	✔	N/A	N/A

Table 4.1: Dimeric and terameric Kif15 cross-links.

4.2.3 Cross-linking/MS analysis for Tetrameric Kif15

As shown by several labs including the McAinsh lab, Kif15 assembles into a tetramer (Drechsler et al., 2014, Drechsler and McAinsh, 2016, Mann et al., 2017). To assess the structural organisation of tetrameric Kif15, cross-linking with BS3 and separation on SDS-PAGE gel was tried. However, due to the high molecular weight of a tetrameric complex (~760 kDa), it was unable to migrate into the gel. Therefore, a NativePAGE gel electrophoresis method was tried, whereby proteins of a larger molecular weight can be separated. Seen in figure 4.4A is the NativePAGE gel electrophoresis for the cross-linked tetrameric Kif15. The expected molecular mass for tetrameric Kif15 is ~760 kDa and by looking at the gel, a faint band is visible above the 720 kDa marker band, indicating there is a cross-linked tetramer present. This gel band was excised, reduced, alkylated and digested with trypsin. There appears to be a very faint band around the 1048 kDa marker. However, when untreated Kif15 is run on a Native-PAGE gel, we do not see higher oligomerisation states, suggesting this band may be indicative of an artificial oligomer introduced by the cross-linking.

Analysing the tetrameric Kif15 band revealed a few things. Firstly, Kif15 does indeed form a tetramer, as two distinct inter-molecular tetrameric cross-links were identified. As seen in figure 4.4C, the first tetrameric cross-link ($tK15_1$) occurs between Lys-410 of peptide $_{409}DKK_{410}$ and Ser-428 of peptide $_{428}SEQEK_{432}$ in the unstructured region adjacent to the motor domain of kif15. The second cross-link ($tK15_2$) identified is between Lys-1187 of peptide $_{1180}LNEDREVK_{1187}$ and Thr-1178 of peptide $_{1171}TSLEHLVTK_{1179}$ of the fourth coiled-coil region (CC4) (Figure 4.4D). This second cross-link was also identified using EDC cross-linker, indicating these residues are direct contact sites (Figure 4.4E). The positioning of these tetrameric cross-links also indicate that Kif15 can form a parallel tetramer. Also, the 11 intra-molecular cross-links identified for the dimeric Kif15 were also present for the tetramer. This seems to suggest that Kif15 assembles into a tetramer as a dimer of

dimers. Due to the diffusive appearance of the NativePAGE gel band, the cross-linking experiment was repeat in solution at low salt concentration, where the Kif15 protein exists as a tetramer. These experiments yielded similar results (data not presented).

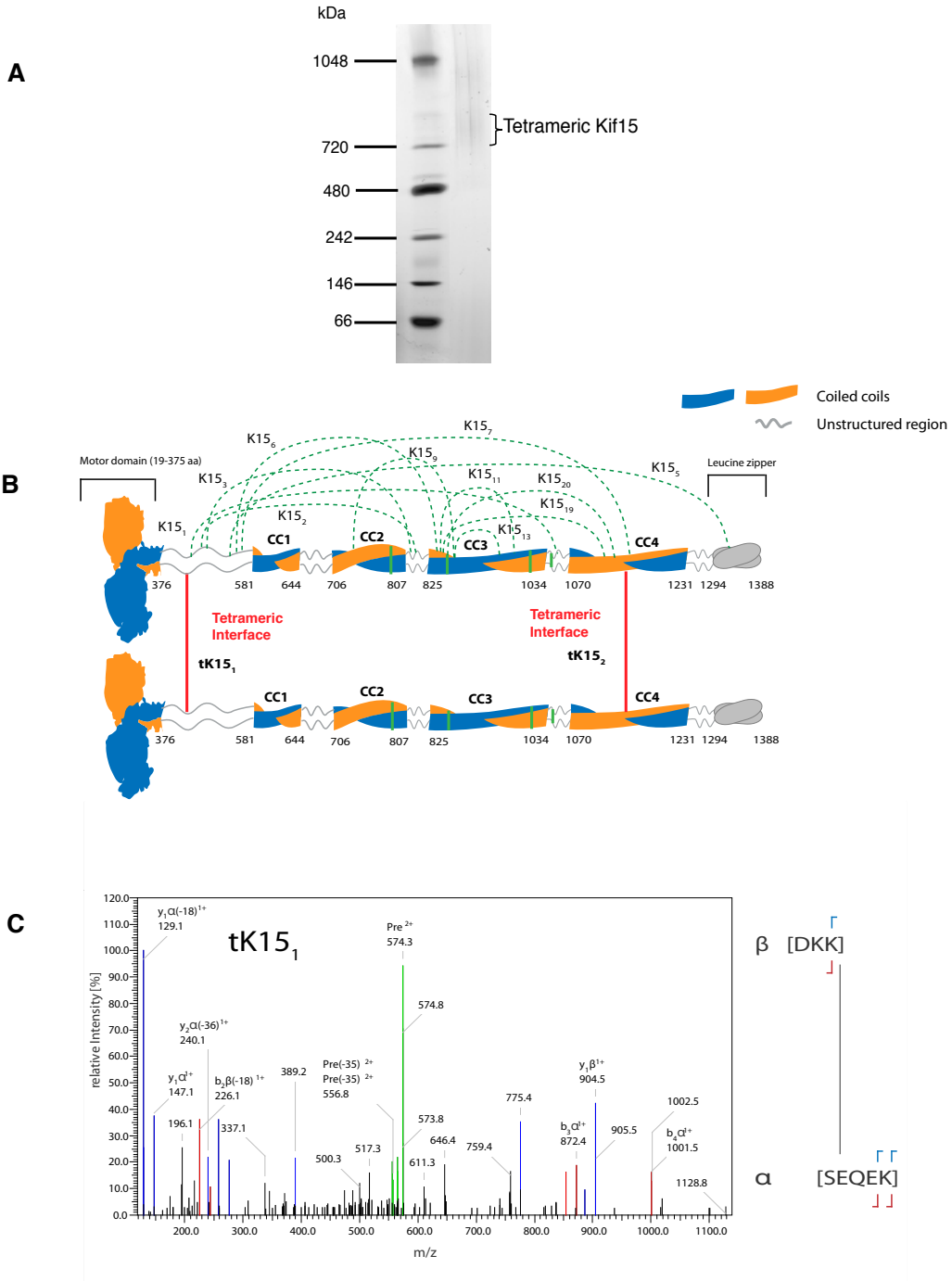

Figure 4.4: Tetrameric organisation of Kif15. A; Native-PAGE gel of cross-linked Kif15.**B;** Structural organisation of Kif15, whereby the dotted green lines represent the intramolecular dimeric cross-links of Kif15, and the solid green

lines are the inter-molecular dimeric cross-links seen for the dimeric Kif15 molecule. It is assumed that the intramolecular dimeric cross-links are specific for a single chain, whereas the inter-molecular dimer cross-links connects both chains The red lines represent the tetrameric cross-links identified **C;** Spectra for BS3 tetrameric cross-link 1 ($tK15_1$). For the schematic fragmentation ions, the blue colour indicates the b-ions and the red indicates the y-ions. D; Cross-linking spectra for BS3 tetrameric cross-link 2 ($tK15_2$). **E;** EDC spectra for tetrameric cross-link 2 ($tK15_2$). **F;** MaxQuant quantification of inter-molecular tetrameric cross-linked peptides.

D

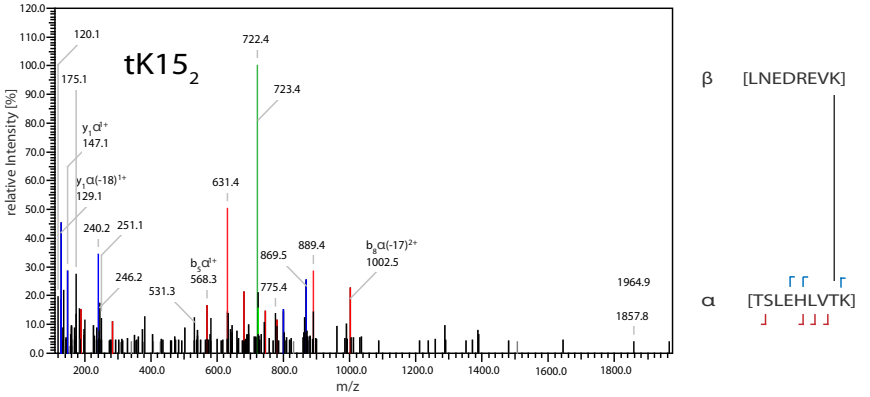
tK15$_2$
relative Intensity [%]
m/z
β [LNEDREVK]
α [TSLEHLVTK]

E

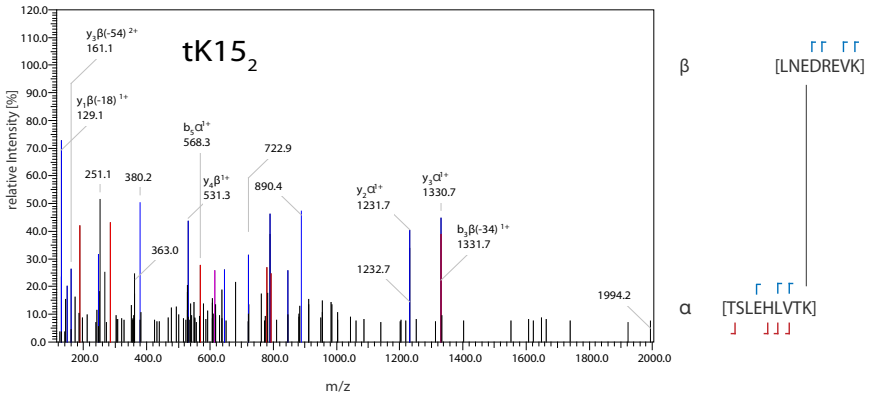
tK15$_2$
relative Intensity [%]
m/z
β [LNEDREVK]
α [TSLEHLVTK]

F

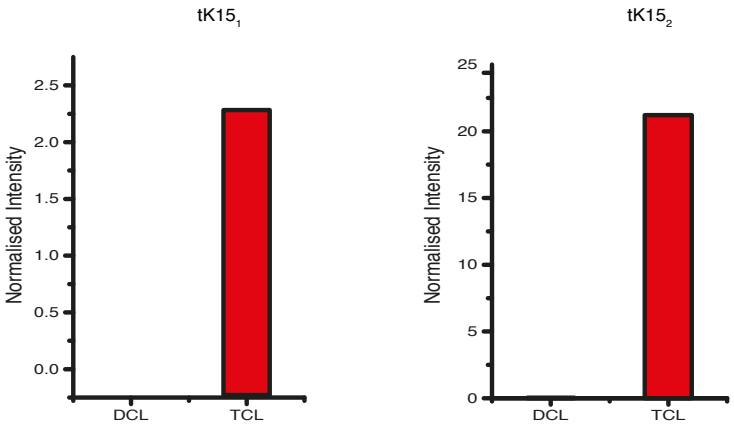
tK15$_1$
tK15$_2$
Normalised Intensity
DCL
TCL

4.2.4 Structural Predictions for Kif15 domain architecture

To further confirm the structural organisation of Kif15 into a tetramer, structural prediction analysis was done. The software used was LOGICOIL, a software that can predict the oligomeric organization of a protein, based on its protein sequence (Vincent et al., 2012). The software used the characteristic heptad repeat sequence for coiled –coils, to predict the organization of the protein. The heptad repeat, consists of the amino acids HPPHPPP, where the "H" refers to a hydrophobic residue and the "P" refers to a polar residue. The heptad repeat is a known structural motif in coiled –coils, whereby the amino acids are labelled from *a* to *g*, and the hydrophobic residues tend to occupy the *a* and *d* positions. The software assigns an oligo-coiled coil likelihood based on similarity to a training set of proteins (see table 4.2).

Training Set
1ECM
1EUMC
1GL2a
1GL2d
1X03
1YBZ
2B9Ba
2D8E
2FXM
2WPQa
2Z0V

Table 4.2: List of protein identifiers used as a training set for assigning oligo-coiled-coil likelihood.

Presented below in figure 4.5 is the structural predictions obtained from the LOGICOIL software. As expected, the most likely oligomerization state for Kif15 is a tetramer, with the first coiled-coil region being the most likely tetramerisation domain and a further 3 coiled-coil domains expected to form a parallel dimer. This is consistent with the data obtained from our cross-linking mass spectrometry results and the published results from the McAinsh and

Wadsworth labs. Also, the predicted conformation of the dimer is parallel, which suggest that Kif15 adopts a parallel tetramer conformation, which is also consistent with our cross-linking mass spectrometry results.

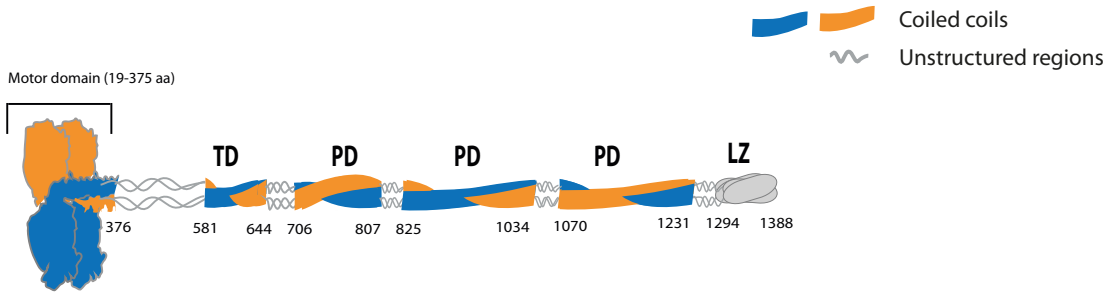

Figure 4.5: Predicted oligomerization state and domain architecture of Kif15. 4 coiled-coil domains are identified, with the first predicted to be involved in the tetramerisation of Kif15 and the other three involved in the formation of a parallel dimer. The final domain is the leucine zipper.

4.2.5 Preliminary EM Results

XL-MS provides a snapshot of real-time dynamic interactions of the molecules in solution, therefore the cross-links identified may be sampled from a large conformational space. As such, negative-stain EM would be important to confirm the data obtained with XL-MS. To provide further evidence for the tetrameric organisation of Kif15, preliminary experiments were carried out to assess the structural assembly of Kif15 using negative stain EM. Freshly purified Kif15 protein was buffer exchanged to 50 mM Sodium Phosphate, 20mM NaCl buffer to stabilize the tetrameric state of Kif15 in solution. The protein was stained with 0.7% and 0.2% Uranyl Acetate and visualized using JEOL 2011 with Gatan Ultrascan 4000 CCD used to image and collect data.

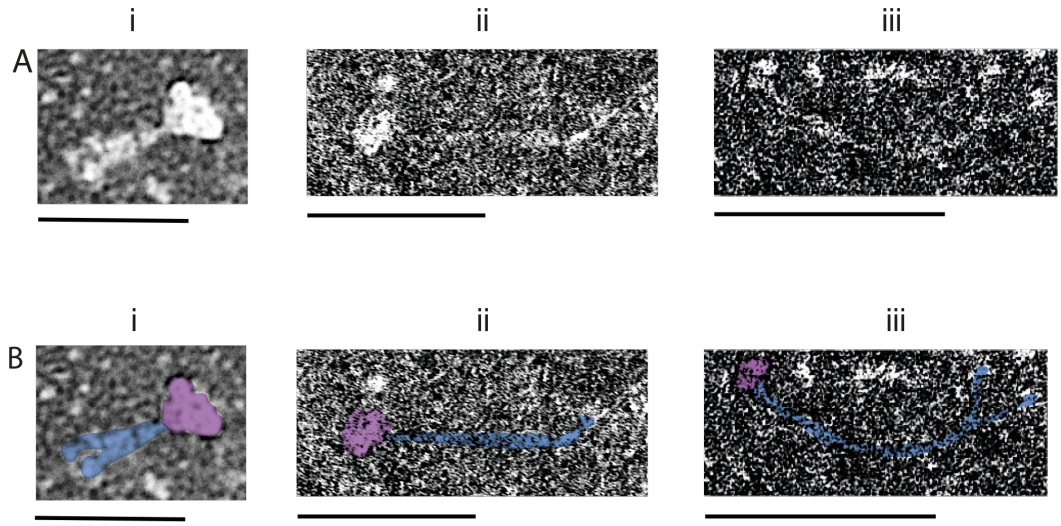

Figure 4.6: Preliminary Kif15 negative stain EM. The panels in B is the same as A, except for the addition of pseudo colours, whereby the motor domain is depicted in purple and the tail is blue. Scale bar is 100 nm.

As seen in figure 4.6 is the images acquired from the EM trials. Figure 4.6Ai, which looks slightly more compact than the other images, is acquired using 2 % uranyl acetate staining. 4.6Aii and 4.6Aiii was obtained using 0.7 % uranyl acetate. As is clear from the figures, Kif15 seems to form a parallel tetramer organisation. The motor domains appear as a large mass on one end, with an extended tail. It appears that for these images that Kif15 is adopting an extended conformation. Given that the extended Kif15 molecule is ~130 nm long, this is consistent with the data presented here. However, from the EM data collected, we also see globular folded conformations which is indicative of the auto-inhibited conformation of Kif15 (data not presented), but the staining protocol needs to be further optimised to make it easier to visualise. Nevertheless, these pilot data are consistent with the XL-MS data and the model that Kif15 forms a parallel tetramer.

4.3. Cross-linking/MS Analysis of Kif15 1-1293

4.3.1 Cross-linking/MS analysis for Kif15 1-1293

As with many other kinesins, Kif15 activity is modulated by auto-inhibition of its C-terminal tail, specifically by the leucine zipper of Kif15 (Sturgill et al., 2014; McHugh et al., 2017). From the previous data presented, the folded state of Kif15 was confirmed (Figure 4.3A and figure 4.4B) as many long range cross-links were identified.

One prediction of this auto-inhibited conformation would be that the deletion of the leucine-zipper would eliminate the long-distance cross-links identified for the Kif15 molecule. To confirm that these extended cross-links were specific to the full-length Kif15, the truncated protein lacking the last 93 amino acids was expressed and purified. The cross-linking experiments were carried out as previously described; the truncated protein was titrated against BS3 to form the monomeric species and dimeric species on a SDS-PAGE gel (figure 4.7B), which were excised, alkylated, reduced and digested with trypsin. For the tetrameric species, the cross-linking was done in-solution. To confirm that the cross-linked Kif15 protein is truncated, a basic mascot search was done to show the absence of the C-terminal end of Kif15, as seen in figure 4.7A. The sequence coverage shows that peptides have been identified for all the regions, except for the C-terminal end.

The cross-linked peptides for Kif15 1-1293 were analysed in the exact same way as the full-length protein. As seen in figure 4.7D, there is a striking difference in the conformation of the truncated Kif15, compared to the full-length protein. The Kif15 1-1293 protein adopts an elongated conformation, which does not seem to form any of the long-distance cross-links seen in the full-length molecule, such as $K15_1$, $K15_5$ and $K15_7$. An example quantification showing the absence of $K15_7$ in the truncated molecule is shown in figure 4.7F. This is consistent with the literature, as it has been shown that this Kif15

truncation is able to alleviate the auto-inhibited conformation of Kif15 and restore motility on microtubules (McHugh et al., 2017). Only 3 intra-molecular cross-linked peptides found in the full-length Kif15 molecule were identified in the truncated protein ($K15_{11,}$ $K15_{13}$ and $K15_{20}$). Instead, we see new intra-molecular cross-links appear, which are in much closer distance to each other. These new cross-links are identified in regions which are now accessible to cross-linking due to the unfolded state of the protein. However, the dimeric and tetrameric organization of Kif15 is still the same as the full-length protein, suggesting that the truncation does not interfere with the structural organization of Kif15 into a tetramer. An example quantification of an inter-molecular dimeric cross-link ($_dk15_1$) is presented in figure 4.7F to show the equal abundance of this cross-link between the truncated and the full-length Kif15 molecule. Cross-links identified for Kif15 1-1293 are summarised in table 4.3.

A

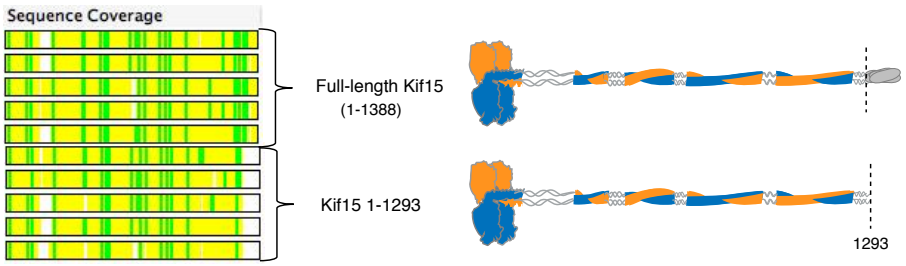

B

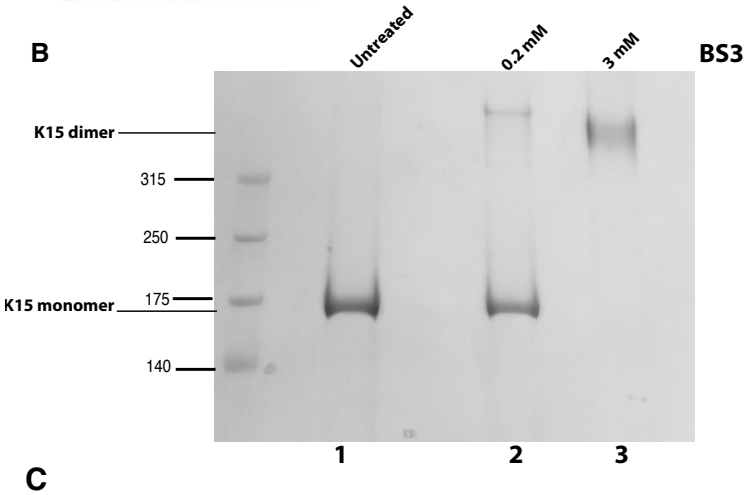

C

Kif15 1-1293 Oligomerisation State	Predicted Mass	SDS Mass
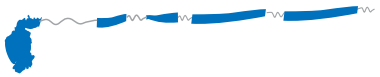	155 kDa	~160 kDa
	310 kDa	~320 kDa

Figure 4.7: Cross-linking of Kif15 1-293. A; Mass spectrometry analysis of full-length Kif15 and Kif15 1-1293 to confirm the truncation of the leucine zipper. **B;** Kif15 1-1293 cross-linking and separation of the monomeric and dimeric species on SDS-PAGE gel. **C;** Predicted and observed masses for Kif15 monomeric and dimeric masses separated on SDS-PAGE gel. **D;** Structural organisation of tetrameric Kif15 1-1293. Dotted green lines indicate the intra-molecular dimeric cross-links, and $_{mu}$K15 refers to the inter-molecular cross-links seen for the Kif15 1-1293 mutant. The solid green lines indicate the inter-molecular dimeric cross-links. The red lines indicate the tetrameric cross-links. **E;** MaxQuant quantification of intramolecular cross-link (K15$_7$) and inter-molecular dimeric ($_d$K151).

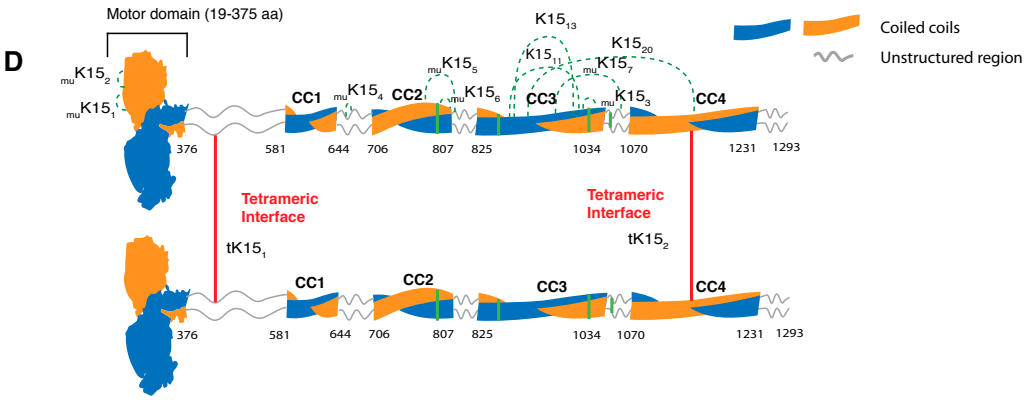
D
Motor domain (19-375 aa)
Coiled coils
Unstructured region
CC1
CC2
CC3
CC4
Tetrameric Interface
Tetrameric Interface
376
581
644
706
807
825
1034
1070
1231
1293

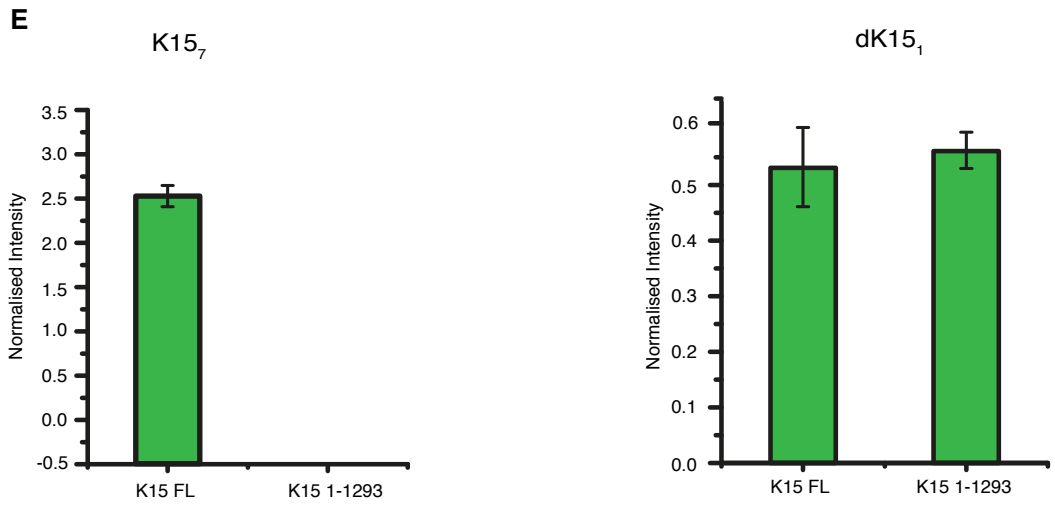
E
K15 FL
K15 1-1293
Normalised Intensity
dK15 FL
K15 1-1293
Normalised Intensity

Cross-link Name	Peptide 1	Residue Number 1	Peptide 2	Residue Number 2	BS3	Triplicates	BS3 isotope	Different Charge states	Different Cleavage States
K15 $_{11}$	TNQEK($)	830	LEESLLATEK($)	968	✔	✔	✗	✔	N/A
K15 $_{13}$	NLQNFKK($)	890	LSLQFEEDK($)	924	✔	✔	✗	✔	✔
K15 $_{20}$	NEYNFK($)	1121	KENETLK($)	896	✔	✔	✔ -d12	✔	N/A
$_{mu}$ K15 $_{1}$	AGAGK($)	168	S($)FLBK	173	✔	✔	✔ -d4	✗	N/A
$_{mu}$ K15 $_{2}$	DSLGGNAK($)	326	T($)AIIANVHPGSR	334	✔	✔	✔ -d12	✔	N/A
$_{mu}$ K15 $_{3}$	TSVBEK($)	1001	TETIDTLKQELK($)	1013	✔	✔	✔ -d12	✔	✔
$_{mu}$ K15 $_{4}$	IIT($)TPTK	660	IHAETLK($)	655	✔	✔	✔ -d4 and d12	✔	N/A
$_{mu}$ K15 $_{5}$	IDWTK($)	770	VVLHSADK($)	812	✔	✔	✔ -d4 and d12	✗	N/A
$_{mu}$ K15 $_{6}$	NDFLK($)	797	S($)EVHDLR	801	✔	✔	✔ -d12	✗	N/A
$_{mu}$ K15 $_{7}$	DSDKK($)	982	QEVDILDLK($)	1041	✔	✔	✔ -d12	✔	✔

Table 4.3: Intra-molecular dimeric cross-links identified for Kif15 1-1293.

4.4. Cross-linking/MS Analysis of Tpx2

4.4.1 Tpx2 oligomerisation state

Tpx2 is an important protein involved in microtubule nucleation and localisation of different proteins to the mitotic spindle (Groen et al., 2004). However, not much progress has been done to biochemically characterise the assembly of this protein into its oligomerisation state. Roostalu et al., 2016, reported that Tpx2 appears to be monomeric under the purification conditions they used, which was done under high ionic strength conditions (300 mM KCl). To study the oligomerisation state of this protein, 6His-Tpx2 was expressed and purified as specified in Drechsler et al., 2014. The protein was eluted in a buffer at physiological ionic strength (75 mM NaCl) and the purified protein, which runs as expected at ~100 kDa, is presented in figure 4.8A.

To characterise the oligomerisation state of Tpx2, several experiments were carried out. Firstly, a NativePAGE gel electrophoresis was performed. As seen in figure 4.8B, the Tpx2 bands appears around the 242 kDa marker band, which indicates that the protein is dimeric under physiological ionic conditions. Also, using an mKate2 tagged construct of Tpx2, TIRF microscopy photo bleaching experiments were carried out. The intensity steps are indicative of the photo bleaching of single fluorophores and as such, a two-step change in intensity indicates the protein is dimeric (figure 4.8C). Structural prediction analysis using the software LOGICOIL confirmed that a parallel dimer was the likeliest structural conformation adopted by Tpx2 (figure 4.8D).

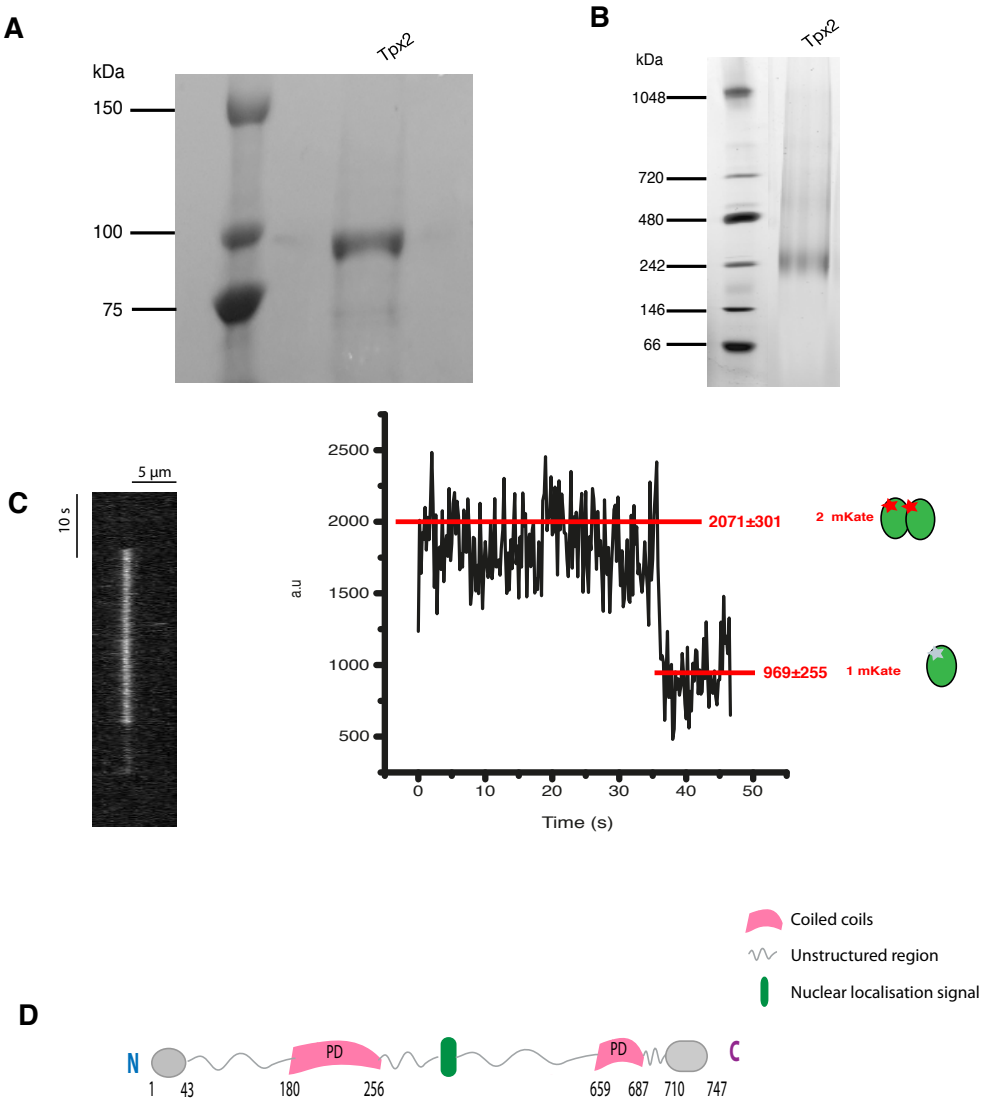

Figure 4.8: Tpx2 oligomerisation state. A; Coomassie gel of purified 6His-Tpx2. **B;** Native-PAGE gel of purified Tpx2. **C;** Photo bleaching steps for mKate fluorophores on Tpx2 molecule. **D;** Structural prediction for Tpx2 oligomerisaion state. The pink regions indicate the coiled-coil domains which are predicted to form a parallel dimer.

4.4.2 Cross-linking/MS analysis for Monomeric and Dimeric Tpx2

To analyse the organisation of Tpx2 into a dimer, cross-linking mass spectrometry experiments were carried out. The BS3 cross-linker concentration was titrated against Tpx2 to optimise the concentration for the formation of monomeric Tpx2 cross-linked species. For the monomeric cross-linked species, the sample was loaded on a standard SDS-PAGE gel (figure 4.9A). The dimeric cross-linked Tpx2 species was run on a Native-PAGE gel (figure 4.9D). For the monomer, the band from lane 3 was excised, alkylated, reduced and digested with trypsin. The data was analysed as previously described in section 4.2.1.

The monomeric cross-links for Tpx2 are shown in Figure 4.9B. In total, 4 cross-links have been identified, whereby 2 are long distance cross-links and 2 are closer to each other. The first long distance cross-link ($Tpx2_1$) is between Lys-701 of peptide $_{701}KEELAR_{706}$ and G-501 of peptide $_{488}EDEEEDEPVVIK_{501}$. The second extended cross-link ($Tpx2_4$) is between Lys-128 of peptide$_{124}LSAQK_{128}$ and Lys-443 of peptide $_{438}IQERESK_{443}$. In figure 4.7C is the $Tpx2_4$ cross-linked spectra identified using EDC.

To analyse the dimeric Tpx2 cross-links, the cross-linked sample was isolated using NativePAGE gel electrophoresis to maintain the dimeric nature of the protein (figure 4.9D). Presented in figure 4.9E is the cross-linked peptides identified for the dimeric Tpx2 molecule. As is clear from this diagram, the carboxy-terminal end of Tpx2, including the second coiled-coil domain (CC2) are important for stabilising the dimeric state of Tpx2 as all of the dimeric cross-links are identified in this region. Also, intra-molecular cross-links $Tpx2_1$, $Tpx2_3$ and $Tpx2_4$ from the monomer are also seen for the dimer.

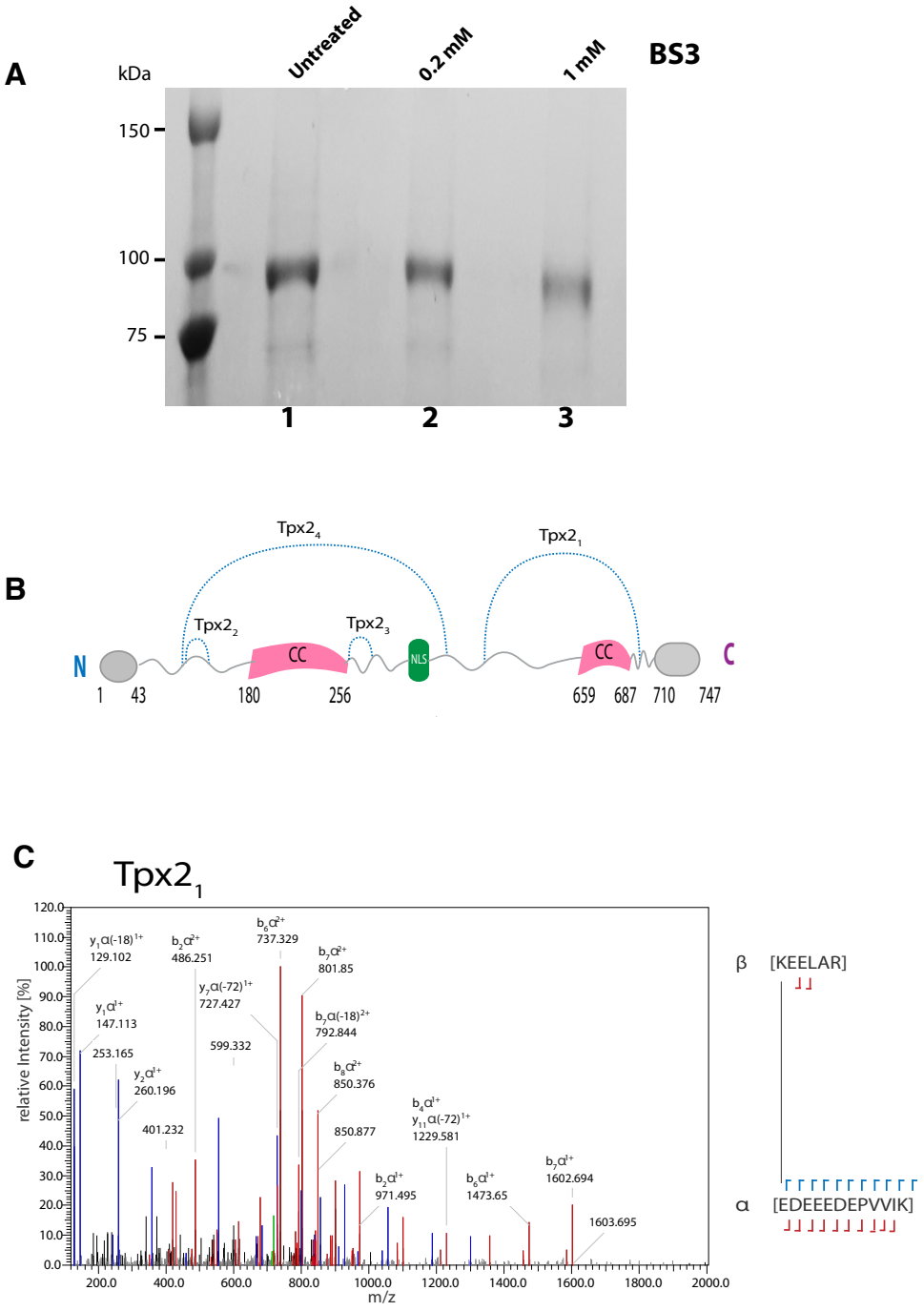

Figure 4.9: Monomeric and dimeric cross-linking for Tpx2. A; Coomassie gel of BS3 titration experiments to optimise monomeric cross-linking of Tpx2. **B;** Monomeric cross-links identified for Tpx2. **C;** Mass spectra of the Tpx2$_1$ cross-link using EDC. **D;** Native-PAGE gel for dimeric cross-linked Tpx2. **E;** intra-molecular and inter-molecular dimeric cross-links identified for Tpx2. **F;** Mass spectra for $_d$Tpx2$_3$.

D

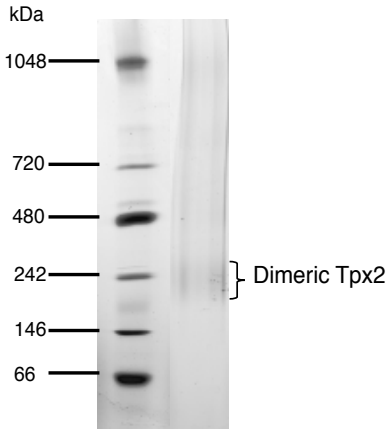
kDa
1048
720
480
242
146
66
Dimeric Tpx2

E

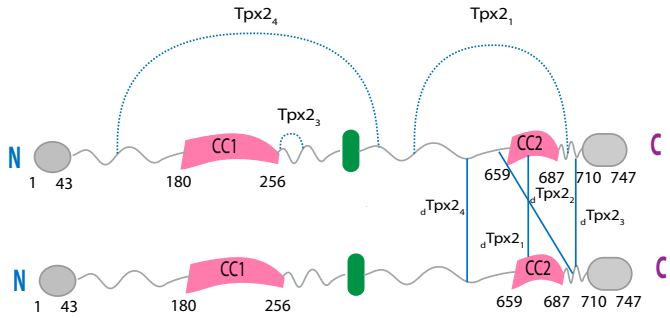
Tpx2$_4$
Tpx2$_1$
Tpx2$_3$
N
CC1
CC2
C
1 43 180 256
659 687 710 747
$_d$Tpx2$_4$
$_d$Tpx2$_2$
$_d$Tpx2$_3$
$_d$Tpx2$_1$

F

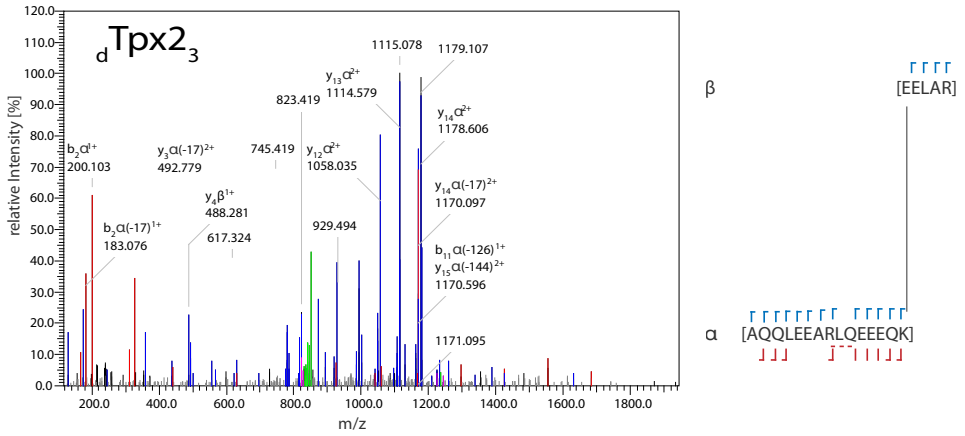
$_d$Tpx2$_3$
relative Intensity [%]
m/z
1115.078
1179.107
$y_{13}\alpha^{2+}$ 1114.579
823.419
$y_{14}\alpha^{2+}$ 1178.606
$b_2\alpha^{1+}$ 200.103
$y_3\alpha(-17)^{2+}$ 492.779
745.419
$y_{12}\alpha^{2+}$ 1058.035
$y_{14}\alpha(-17)^{2+}$ 1170.097
$y_4\beta^{1+}$ 488.281
$b_2\alpha(-17)^{1+}$ 183.076
617.324
929.494
$b_{11}\alpha(-126)^{1+}$
$y_{15}\alpha(-144)^{2+}$ 1170.596
1171.095
β [EELAR]
α [AQQLEEARLQEEEQK]

Cross-link	Peptide 1	Residue Number 1	Peptide 2	Residue Number 2	Cross-link Type	Triplicates	EDC
Tpx2 $_{1}$	K($)EELAR	701	E($)DEEEDEPVVIK	501	MCL/$_{intra}$ DCL	✔	✔
Tpx2 $_{2}$	E($)KHHVK	134	LSAQK($)DLEQK	128	MCL/$_{intra}$ DCL	✔	✔
Tpx2 $_{3}$	K($)HPSSPAR	289	NQE($)EYKEVNFTSELR	276	MCL	✔	✔
Tpx2 $_{4}$	LSAQK($)	128	IQE($)RESK	443	MCL/$_{intra}$ DCL	✔	✔
$_{d}$Tpx2 $_{1}$	KE($)K	664	PNTVISQEPFVPK($)	674	$_{inter}$ DCL	✔	✔
$_{d}$Tpx2 $_{2}$	K($)EK	643	LQE($)EEQKK	696	$_{inter}$ DCL	✔	✔
$_{d}$Tpx2 $_{3}$	EELAR	703	AQQLE EARLQEEEQK	700	$_{inter}$ DCL	✔	✔
$_{d}$Tpx2 $_{4}$	QQK($)EAABFK	620	AQTWKHQLEEE($)LR	615	$_{inter}$ DCL	✔	✔

Table 4.4: monomeric and dimeric Tpx2 cross-links identified.

4.5. Cross-linking/MS Analysis of Kif15/Tpx2 Complex

4.5.1 Cross-linking/MS analysis for Kif15/Tpx2 complex

It is known that Tpx2 and Kif15 can directly bind to each other and Tpx2 is required to localise Kif15 to the mitotic spindle. Work from the Wadsworth lab has identified the C-terminal end of Tpx2 as important in regulating Kif15 localisation and function (Mann et al., 2017).

To assess the direct binding between Tpx2 and Kif15, cross-linking mass spectrometry experiments were carried out. As previously described, 30-fold excess of Tpx2 is required to enable complex formation with Kif15 (Drechsler et al., 2017). The cross-linking experiments were done for Kif15 and Tpx2 using EDC cross-linker in-solution, followed by an in-solution tryptic digest. Presented in figure 4.10A is a diagram showing the cross-linking sites identified between Kif15 and Tpx2. In total, 3 cross-links were identified between Kif15 and Tpx2 (KT_1, KT_2 and KT_3). All of these cross-links localise to the fourth coiled-coil domain (CC4) and not the leucine zipper of Kif15. It is known that Kif15 binding to Tpx2 in the absence of microtubules is a low affinity binding and this binding to the fourth coiled-coil domain may be indicative of this. The Tpx2 binding site is mainly the middle region of the protein, with one cross-link identified near the N-terminal end. Interestingly, the intra-molecular cross-links seen for Kif15 dimer and tetramer are also identified in the presence of Tpx2 (green lines). This suggests that Tpx2 is able to stabilise the folded conformation of Kif15. Presented in figure 4.10B is the spectra for the cross-link KT_2.

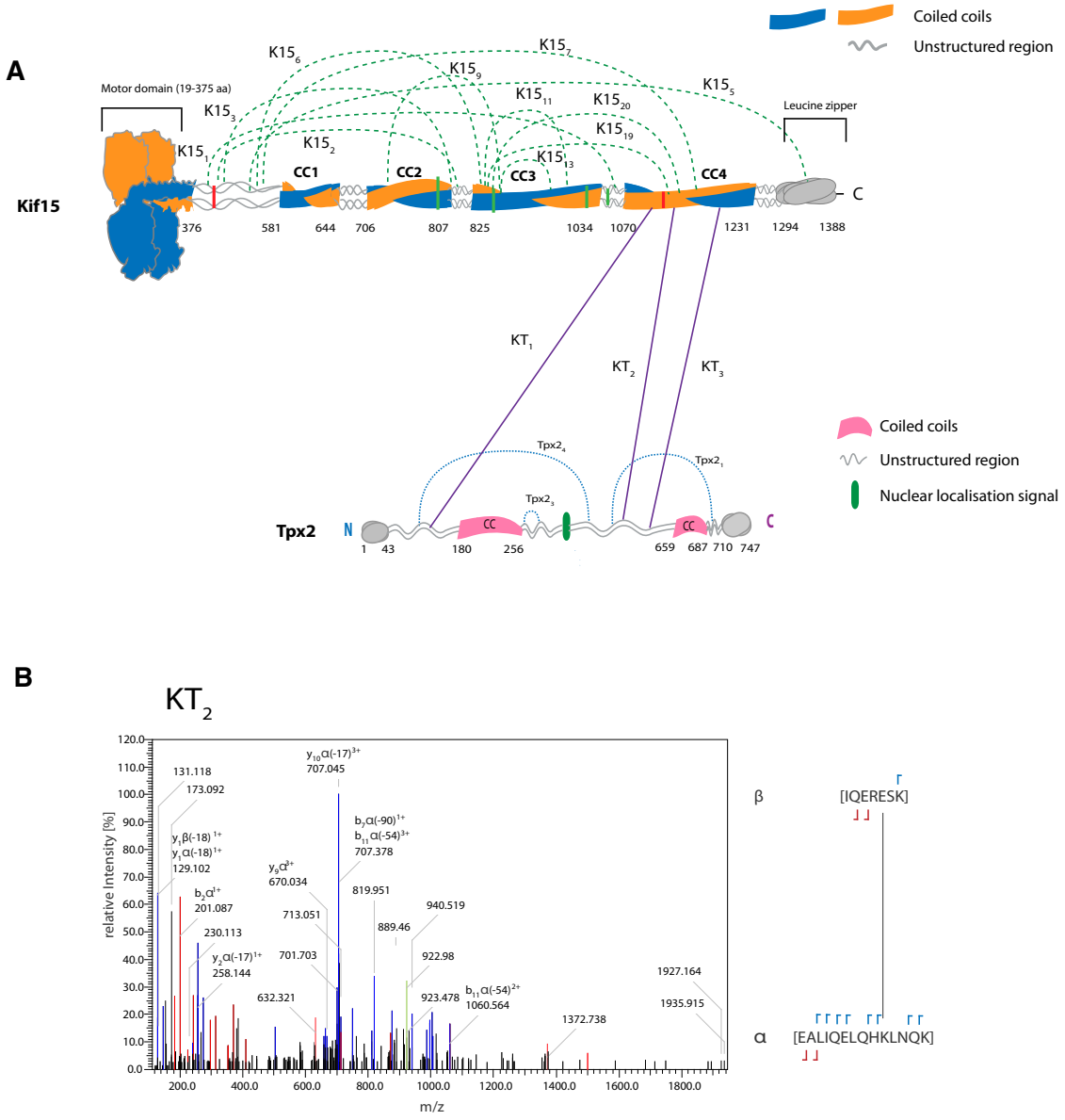

Figure 4.10: Cross-linking of Kif15 and TPX2 in the absence of microtubules. A; Cross-links identified between Kif15 and Tpx2 (KT_1, KT_2, KT_3). **B;** Mass spectra for the KT_2 cross-link identified between Kif15 and Tpx2.

4.5.1 Cross-linking/MS analysis for Kif15/Tpx2/MT complex

As the binding between Tpx2 and Kif15 is enhanced by the presence of microtubules, the next experiment was to probe the interaction between Kif15 and Tpx2 in the presence of microtubules. Tpx2 and Kif15 were incubated for 10 minutes with GMP-CPP stabilized microtubules in the presence of AMP-PNP to enable the kinesin to lock onto the microtubules. The sample was then spun at high-speed to remove unbound kinesin and Tpx2 and free tubulin subunits. The sample was then cross-linked with EDC for 1 hour and quenched for 30 minutes. A standard in-solution digest protocol was then followed.

In the presence of microtubules, Kif15 binding to Tpx2 adopts a different conformation (figure 4.11A). The leucine zipper of Kif15 forms 3 cross-links with the middle region of Tpx2 ($_{MT}KT_1$, $_{MT}KT_2$ and $_{MT}KT_3$). There is one cross-link from the fourth coiled-coil domain of Kif15 that interacts with Tpx2. This shows a significant conformational shift in the binding between tpx2 and Kif15 between the presence and the absence of microtubules. In the absence of the microtubules, the binding is exclusively localized to the fourth coiled-coiled (CC4) domain of Kif15, whereas in the presence of microtubules, the binding is mainly in the leucine zipper of Kif15. In both cases, Kif15 adopts a folded conformation as many long-distance cross-links for Kif15 are found. This suggests that Tpx2 binding to Kif15 stabilises the kinesin in its auto-inhibited conformation.

A single cross-link between Tpx2 and α-tubulin was identified. This cross-link mapped to residue K-336 of the α-tubulin monomer in helix-10, which sits at the inter-dimer interface of the microtubule (Nogales et al., 1998). No cross-links were identified between Kif15 and the microtubules.

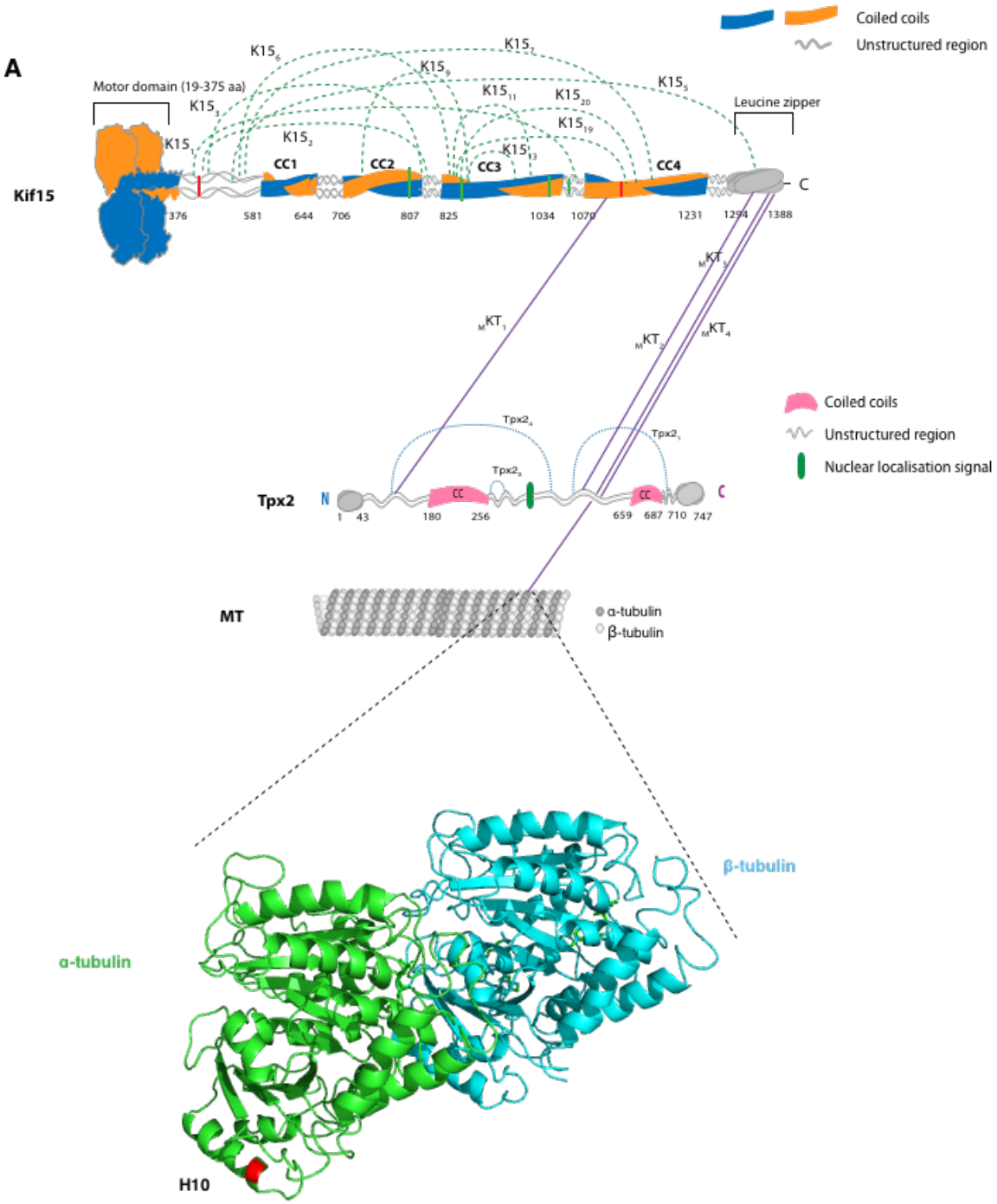

Figure 4.11: Cross-linking of Kif15 and TPX2 in the presence of microtubules. A; Cross-links identified between Kif15 and Tpx2 in the presence of microtubules ($_{MT}KT_1$, $_{MT}KT_2$, $_{MT}KT_3$). Highlighted in red in the crystal structure of the tubulin heterodimer is the K-336, which forms a cross-link with Tpx2. In green is the α-tubulin and in cyan is the β-tubulin. Structure adapted from Nogales et al., 1998. **B;** Mass spectra for the KT_2 cross-link identified between Kif15 and Tpx2.

B

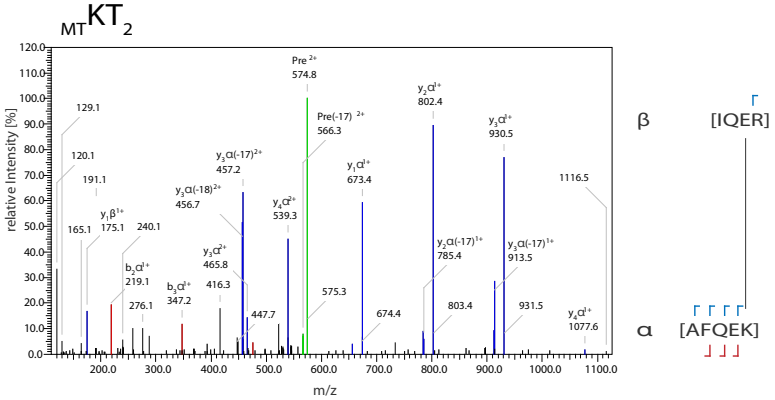
MTKT2
relative Intensity [%]
m/z
Pre 2+ 574.8
Pre(-17) 2+ 566.3
129.1
120.1
191.1
165.1
175.1
240.1
219.1
276.1
347.2
416.3
447.7
457.2
456.7
465.8
539.3
575.3
673.4
674.4
785.4
802.4
803.4
913.5
930.5
931.5
1077.6
1116.5
β [IQER]
α [AFQEK]

Cross-link Name	Peptide 1	Residue Number 1	Peptide 2	Residue Number 2	Triplicates	EDC
KT_1	DLEQK($)EK (Tpx2)	133	KNE($)YNFK (Kif15)	1120	✔	✔
KT_2	IQERE($)SK (TPX2)	445	EALIQELQHK($)LNQK (Kif15)	1106	✔	✔
KT_3	GEVPK($)FK (Tpx2)	565	EMENLRLE($)SQQLIEK (Kif15)	1207	✔	✔
$_{MT}KT_1$	LSAQK($) (Tpx2)	128	KEE($)VEQK (Kif15)	1113	✔	✔
$_{MT}KT_2$	ARPNTVISQEPFVPK($) (Tpx2)	641	E($)KK (Kif15)	1382	✔	✔
$_{MT}KT_3$	E($)LQKGEVPKFK (Tpx2)	556	LK($)K (Kif15)	1360	✔	✔
$_{MT}KT_4$	IQE($)R (Tpx2)	443	AFQEK($) Kif15	1305	✔	✔
TMT_1	E($)KK (Tpx2)	643	DVNAAIATIK($) (TBA1A_Pig -alpha tubulin)	336	✔	✔

Table 4.5: Kif15, Tpx2 and MT cross-links identified.

4.6 Conclusion

Presented in this chapter is the cross-linking mass spectrometry data to show the structural organization of Kif15 from a monomeric state, to a dimer and finally a tetramer. Kif15 forms a folded conformation, where long distance cross-links are found which extend from the N-terminal end to the C-terminal tail (such as $K15_5$ and $K15_7$). Kif15 also forms distinct inter-molecular dimeric cross-links ($dK15_1$, $dK15_2$, $dK15_3$ and $dK15_4$) which are mainly localized in the second (CC2) and third coiled-coil (CC3) domains, which are predicted to stabilize a parallel dimer structure. Two distinct tetrameric cross-links ($tK15_1$ and $tK15_2$) were identified, which appears to suggest Kif15 organises into a parallel tetramer conformation. One tetrameric interface is near the predicted tetramerisation domain and the second cross-link is found in the fourth coiled-coil (CC4) domain.

This data confirming that Kif15 forms a tetramer is of great importance as it helps to clear up a controversial issue in the field regarding the structural organization of Kif15 (Hancock et al., 2014). The McAinsh lab and Wadsworth lab have both confirmed that Kif15 assembles into a tetrameric conformation under physiological conditions, and can fall apart into a dimer at high salt concentrations. However, the Ohi lab suggest that Kif15 functions as a dimer, under their experimental conditions (HEPES buffer with 300 mM NaCl), which has previously been confirmed to destabilize the tetrameric state of Kif15 into a dimer (Drechsler et al., 2014).

Also, presented in this chapter is the structural organization of Kif15 1-1293, which lacks the C-terminal domain (last 93 amino acids) that is important for stabilizing the auto-inhibited conformation of Kif15. As expected, this mutant lacks the long-distance cross-links (such as $K15_5$ and $K15_7$) present in the full-length protein and therefore adopts a more open conformation. The unfolded conformation adopted by Kif15 1-1293 also reveals new cross-links identified (such as $_{MU}K15_4$, $_{MU}K15_5$ and $_{MU}K15_6$). The dimeric and tetrameric cross-links

are still present, which suggests that the mutant does not interfere with its ability to form a tetramer.

Also seen in this chapter is the cross-linking mass spectrometry analysis to study the structural organisation of Tpx2 into a dimer. The Surrey lab have previously presented data to suggest that Tpx2 is a dimer, under high ionic salt concentrations (300 mM KCl). However, from our experiments, it was found that Tpx2 organises into a dimer at physiological ionic conditions (75 mM NaCl).

Tpx2 is a known binding partner of Kif15 which inhibits the motors motility on microtubules *in-vitro*. However, in the absence of microtubules, this binding is low affinity. To study the interaction between Tpx2 and Kif15, the cross-linking experiments were done in the presence and absence of microtubules. There is a striking conformational shift between these experiments; in the absence of microtubules, Tpx2 mainly interacts with the fourth coiled-coil domain of Kif15 (KT_1, KT_2 and KT_3), whereas in the presence of microtubules, the main interaction site is the leucine zipper of Kif15 ($_{MT}K15_2$, $_{MT}K15_3$, $_{MT}K15_4$).

Interestingly, Kif15 adopts the same folded conformation in the presence of Tpx2, regardless of the presence or absence of microtubules. This may suggest that the mechanism by which Tpx2 inhibits Kif15 motility is through the stabilisation of the auto-inhibited conformation of Kif15.

Chapter 5: Towards *in-vivo* analysis of Kif15 structure and function

5.1 Introduction

Based on the data presented in the previous chapter, we now have an improved model of how Kif15 motors are organised into a tetramer *in-vitro* and which interaction sites are important in stabilising the Kif15-Tpx2 complex. However, the majority of work to characterise Kif15 function is based on *in-vitro* motility assays, therefore, more *in-vivo* work will be needed to further understand how the structural organisation of Kif15 contributes to the function of the motor in cells. It is therefore crucial to establish a system to remove endogenous Kif15 from cells and then introduce transgenes harbouring specific mutations that alter the structural organisation of the KIF15 motor and/or its capacity to interact with binding partners (*i.e.* Tpx2). Previous work using genome editing has reported that Kif15 is non-essential in HeLa cells (Sturgill et al., 2016) and so we set out to build such a cell line in human retinal pigment epithelial cells (hTERT-RPE1). These cells are immortalised with telomerase, but have a stable diploid karyotype and are a powerful system to dissect the function of Kif15, specifically the mechanism by which it is able to drive Eg5-independent bipolar spindle assembly. Presented in this chapter is the initial characterisation of the phenotypes observed for RPE1 Kif15 knock-out clones.

Similarly, all the XL-MS data presented in this thesis was generated by cross-linking purified proteins and multi-protein complexes *in vitro*. One caveat of this approach is that these interactions are not always indicative of how the protein folds or functions in cells. To gain insight into how this protein is folded in cells and which protein complexes it can form, a second cross-linker was tested. This cleavable, disuccinimidyl sulfoxide (DSSO) cross-linker has been optimised for cross-linking proteins on beads after an affinity pull-down approach. DSSO cross-linking can not only reveal the structural organisation of Kif15 *in-vivo*, but also show what proteins Kif15 interacts with and their

precise interaction sites. Before this cross-linker can be tested on Kif15 complexes isolated from human cells, initial experiments were carried out on purified Kif15 to test the fragmentation chemistry of DSSO. Using this approach, the broader protein-protein interaction networks formed by Kif15 *in vivo* will be tractable.

5.2 CRISPR knock-out cell lines for Kif15

To provide further understanding of the role of Kif15 *in-vivo*, genome editing using CRISPR-Cas9 system was used to generate Kif15 knock-out cell lines in RPE1 cells that stably express mCherry-alpha-tubulin. Small guide (sg) RNAs were designed that targeted the first exon of KIF15; the aim being to generate INDELs that would result in premature stop codons and a loss of protein expression. Following transformation with a plasmid expressing both the sgRNA and GFP-Cas9, I isolated a population of GFP positive cells. Next, by diluting and plating the cells I generated 40 single cell clones and choose 20 for further analysis by quantitative immunofluorescence. Both Parental RPE1 cells and isolated clones were stained with antibodies that recognise the carboxy-terminus of the Kif15 protein (Figure 5.1). As expected Kif15 was localised to the mitotic spindle microtubules in the parental cells co-localising with the mCherry-alpha-Tubulin signal (Fig 5.1A). It is not clear from these images that Kif15 is localised at the kinetochores; further staining using kinetochore markers such as CREST will be needed to validate this. This analysis revealed two distinct localisation phenotypes for the CRISPR clones: In the first (1/20 clones screened), we found that Kif15 protein was undetectable on the mitotic spindle. This clone is named MC174 and is shown in Figure 5.1B. Because our antibodies recognise the carboxy-terminus of the protein it is likely that this clone has lost both KIF15 alleles – although this will need confirmation by western blotting and genome sequencing. The second phenotype named MC175, which was found in 8 of 20 clones also displays a loss of Kif15 from the mitotic spindle, however surprisingly the motor is now localised at the kinetochores (Fig. 5.1C). These experiments demonstrate how we can target the KIF15 locus with the Cas9 system and opens up important

new research possibilities to analyse the *in-vivo* function of Kif15 (See discussion for details).

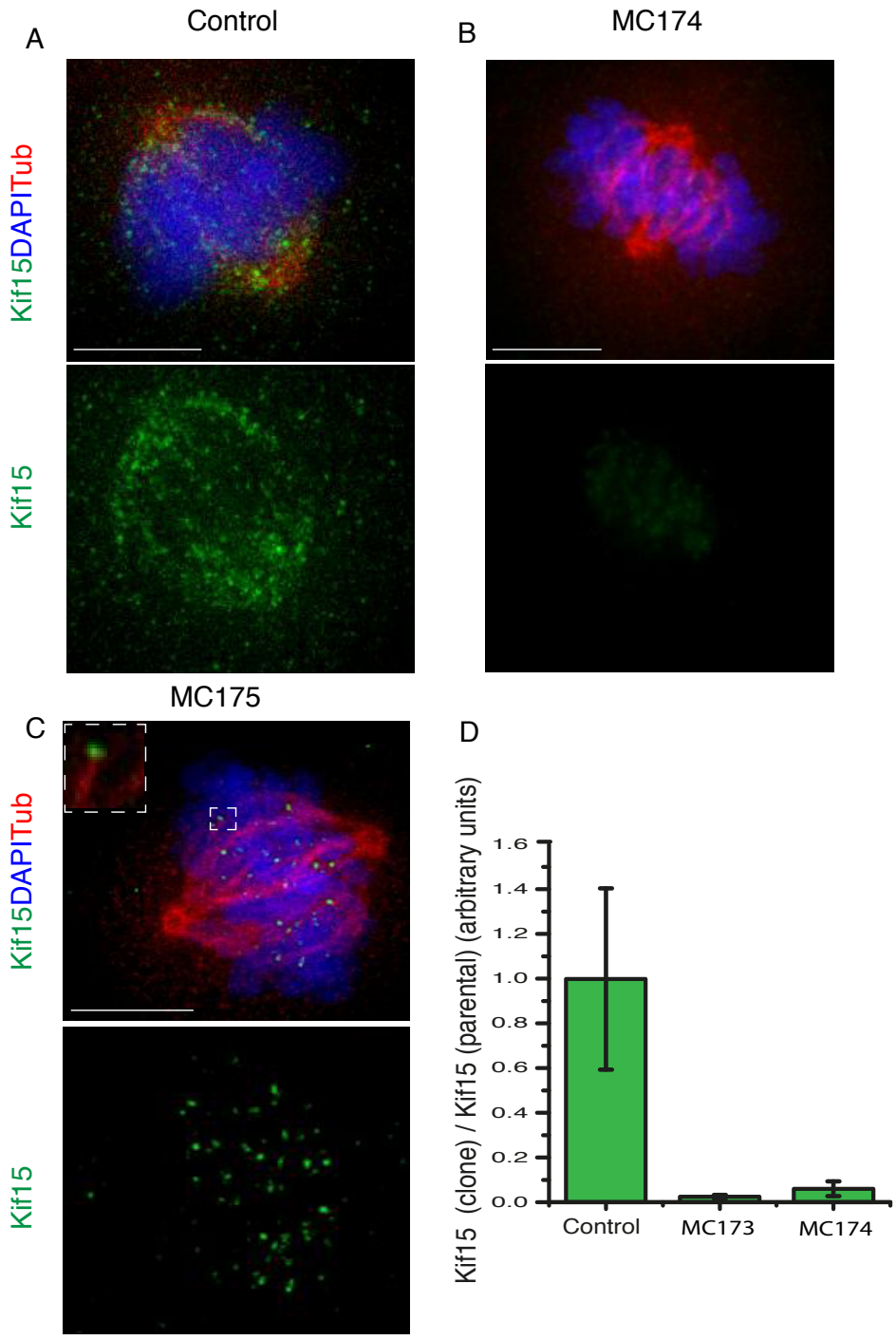

Figure 5.1: Generation of Kif15 knock-out cell lines. A; Parental RPE-mCherry-tubulin cell arrested at metaphase and stained for Kif15 (green) and DAPI (blue) **B;** Clone MC174 arrested at metaphase and stained for Kif15 and DAPI and imaged for α-tubulin (red). **C;** Clone MC175 arrested at metaphase and stained for Kif15 (green) and DAPI (blue) and imaged for α-tubulin (red). Scale bar is 10 μm. **D;** Quantified spindle microtubule localisation of Kif15. Quantification of the intensity of the signal at the mitotic spindle was

background subtracted and normalised relative to the parental spindle intensity.

5.2 DSSO cross-linking

In recent years, a cleavable disuccinimidyl sulfoxide (DSSO) has been developed to provide unambiguous identification of cross-linked peptides. DSSO has also been used to study protein-protein interactions *in-vivo* by carrying out the cross-linking on beads. The cross-linker is able to be cleaved at two distinct sites by Collision-Induced Dissociation (CID), which produces reporter ions which can easily be identified. This fragmentation occurs prior to peptide backbone fragmentation, thus can be used as a condition to allow fragmentation only after the reporter ions have been identified.

Before testing the DSSO cross-linker on affinity purified protein complexes, we first tested this cross-linker on our purified full length Kif15 protein from insect cells. In a first experiment, 2 μM Kif15 was cross-linked with 1 mM DSSO and digested following the in-solution digest protocol. Presented in figure 5.2 is an example of a cross-linked peptide, $_{1258}$SK($)IVEEMLK$_{1265}$ and $_{1244}$NEQEESIK($)ER$_{1251}$, identified using DSSO. In figure 5.2A is the structure of the DSSO cross-linker. As is clear from the diagram, fragmentation can occur on either side of the sulfoxide group. Figure 5.2B is the CID fragmentation of the DSSO cross-linker backbone. CID fragmentation is used to produce enough energy to fragment the cross-linker backbone but not fragment the cross-linked peptides. The fragmentation on either side of the C-S bond generates a pair of peptide fragments for each of the cross-linked peptide (α-β). The annotation α_A/β_s indicates that the fragmentation of the DSSO cross-linker has resulted in the α peptide being modified with the alkene group, whereas the β peptide is modified with the sulfenic acid group. In total, there are four reporter ions associated with DSSO cross-linker fragmentation; α_A, α_s, β_A, β_s. The mass difference between the α_A/β_A and α_s/β_s fragments is 32 Da, which is the mass difference between the thiol and alkene groups

(Figure 5.2B). Presented in figure 5.2C is the EThcD fragmentation of the cross-linked peptides. The Orbitrap fusion instrument allows a combination fragmentation using ETD and HCD (EThcD), which has been shown to provide the best fragmentation coverage for DSSO cross-linked peptides. The next step now would be to affinity purify Kif15 and do the cross-linking on beads to identify any protein complexes Kif15 forms *in-vivo*.

A

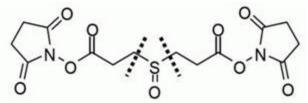

B

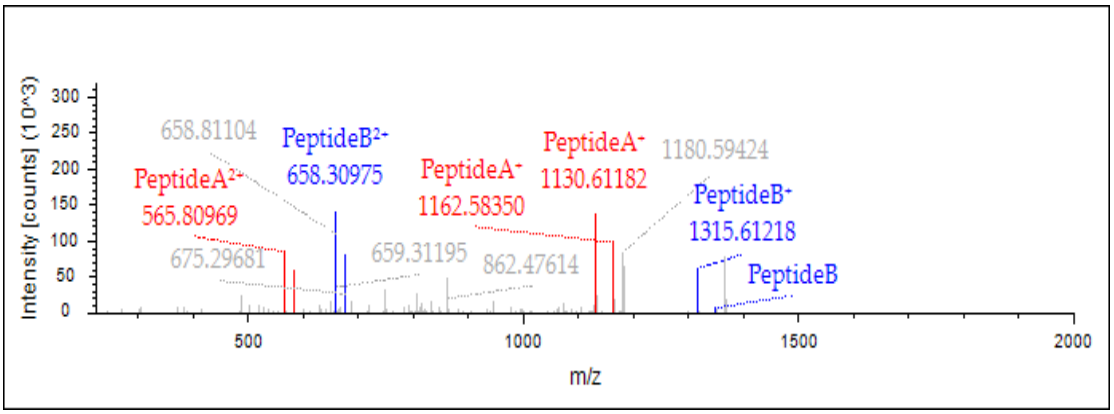

C

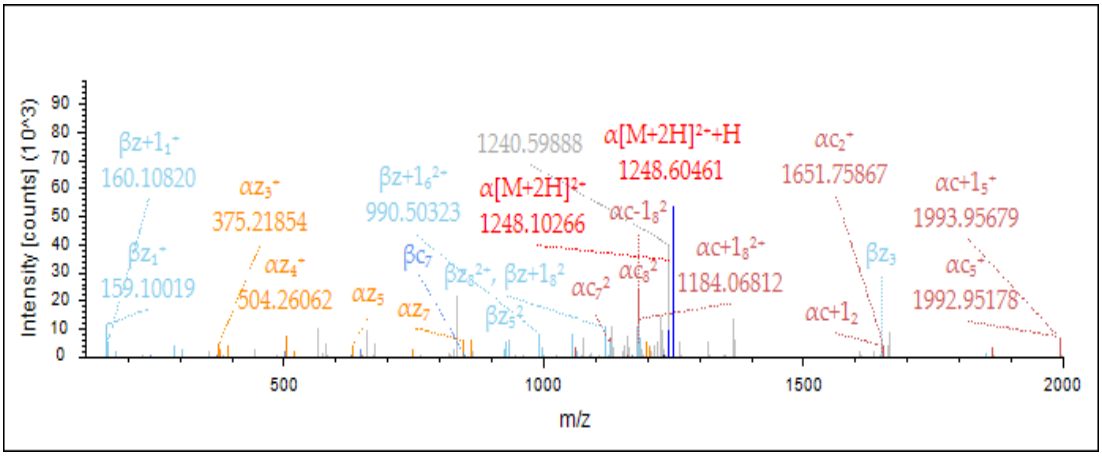

Figure 5.2: DSSO cross-linking of Kif15. A; Structure of DSSO cross-linker. **B;** MS2 fragmentation of DSSO backbone using CID. **C;** MS2 fragmentation of cross-linked peptides using EThcD.

5.3 Conclusion

In this chapter we have established and developed two key new tools that are essential for future work. Firstly, the putative CRISPR Kif15 knock-out cell lines provide an exciting opportunity to characterise the role of Kif15 *in-vivo*. However, the clones first need to be sequenced to verify the exact mutation which is causing the striking phenotype difference between the CRISPR clones. These cell lines can then be used to characterise Kif15 cross-linking mutants *in-vivo*, to study their effects on motor localisation and function. Secondly, now that preliminary experiments have confirmed the fragmentation chemistry of the DSSO cross-linker, it can now be tested on affinity-purified Kif15 to confirm the structural organization of kif15 tetramers *in-vivo* to confirm our structural model and identify any Kif15 protein interaction networks.

Chapter 6: Discussion

6.1 Discussion

Overall, in this thesis we have successfully been able to develop a cross-linking mass spectrometry and analysis workflow to study protein topology and protein-protein interactions. XL-MS has become a widely popular tool to study protein structure in their native state and has been integrated into the workflow of other high-resolution structural techniques (Schmidt and Urlaub, 2017). The highlight of this work using XL-MS, is that we have been able to elucidate for the first time the tetrameric structural assembly of Kif15 and how it interacts with its binding partner and regulatory subunit, Tpx2.

It is important however, to note and discuss a number of caveats regarding the use of XL-MS. Firstly, the abundance of cross-linked peptides is much lower than linear peptides and mono-linked peptides. This makes the data analysis more complicated and protein concentrations for cross-linking should be balanced to optimise the abundance of cross-linked peptides on one hand but also to prevent protein aggregation in the event of excess protein concentration. Also, because the cross-linking provides a snapshot of the real-time dynamic interactions of a protein, cross-links identified may be sampled from a large conformational space, thus this needs to be taken into consideration when the data is being analysed. i.e. one cannot assume that all cross-linking events are associated with a single molecular species. Finally, the BS3 cross-linker has been widely used as the cross-linker of choice in this field, however given its functional distance of 11.4 Å, cross-linked residues identified using this reagent may not indicate direct contact sites, but rather provide an idea of residue proximity.

6.1.1 Kif15 organises into a parallel tetramer conformation

To fully understand the function of Kif15 at a cellular level, it is important to understand its oligomeric state, which will affect its ability to generate the microtubule-based forces required for the establishment and the maintenance of the bipolar spindle during mitosis. The dominant motor involved in bipolar spindle assembly and maintenance is the Kinesin-5, Eg5. Eg5 has been established as a bipolar tetrameric kinesin (Acar et al., 2013, Scholey et al., 2014), whereby the two sets of motor heads enable the motor to attached to anti-parallel microtubules and drive extensile sliding (Kapitein et al., 2005). Unlike many other dimeric Kinesins, the rigidity of the coiled-coil domains of Eg5 tail, prevents the two sets of motor heads from binding to the same microtubule (Scholey et al., 2014). Despite, Kif15 playing a compensatory role for Eg5 in the assembly and maintenance of the bipolar spindle, these two motors have some significantly different localisations and modes of action. For example, Kif15 localisation is enhanced on k-fibres, where the microtubules are parallel bundles instead of anti-parallel microtubules (Sturgill et al., 2014). Also, Kif15 generates forces, which antagonise those produced by Eg5 (Sturgill and Ohi, 2013, Vladimirou et al., 2013). Due to the markedly different mechanisms of action of these motors, it is crucial to undertake a detailed biochemical characterisation of the Kif15 motor and how its quaternary state contributes to mitotic spindle function.

There are conflicting views regarding the structural organisation of Kif15 motors. The first Kif15 protein discovered was the *Xenopus* homologue, Xklp2, which was shown to be homodimeric using hydrodynamic analysis methods of the full-length protein (Wittmann et al., 1998). However, the initial biochemical analysis of full-length human Kif15 (*h*KiF15) revealed a homotetrameric configuration at physiological ionic strength (~150mM NaCl), which was confirmed using a combination of techniques, including Native-PAGE gel, size-exclusion chromatography combined with multi-angle light scattering (SEC-MALS) and photo-bleaching experiments of single-molecules

using total internal reflection microscopy (TIRF) (Drechsler et al., 2014). However, data published by Ohi and colleagues (Sturgill et al., 2014, Reinemann et al., 2017), reported contradictory results; a truncated form of *h*Kif15 (lacking amino acids 8-21) appeared as a dimer as evidenced by photobleaching experiments and size–exclusion chromatography (Sturgill et al., 2014). It is important to note that these experiments were all carried out in the presence of 300 mM KCL, which is unanimously agreed to promote the formation of a dimeric population. Indeed, Drechsler et al., directly showed how increasing salt to 300 mM NaCl converted the protein from monodispersed molecule with a sedimentation coefficient ~12S at physiological ionic strength (0-150 mM NaCl), into a species that runs at ~8S. This is consistent with the SEC-MALS experiments which showed that at physiological ionic strength, the majority of Kif15 molecules have a molecular weight of 744.4 ± 14.1 kDa which corresponds to the tetramer, with a minor dimeric population also detectable (360.1 ± 6.5 kDa). Interestingly, the Xklp2 purification experiments were originally carried out in the presence of HEPES buffer, which has also been shown by Drechsler et al., to stabilise the dimeric conformation of the motor. The data in the field are therefore self-consistent when salt-dependence is taken into account. These experiments do not of course address whether the motor is a dimer or tetramer *in vivo*. To assess the oligomerisation state of *h*Kif15 *in-vivo*, endogenous Kif15 from human mitotic and interphase cell extracts were shown to be largely tetrameric with a smaller dimeric population (Drechsler and McAinsh, 2016, Mann et al., 2017). Dreschler et al., confirmed these results using the same sedimentation experiments used for the recombinant Kif15, and once again, the endogenous Kif15 was also shown to be a tetramer with a sedimentation coefficient ~12S at physiological ionic strength. Mann et al., went a step further and purified endogenous GFP-Kif15 from both interphase and mitotic cell extracts and used single molecule imaging to show how Kif15 motors bleached in three steps consistent with a tetrameric organisation. These data support a model in which *h*Kif15 is likely to be a dimer-of-dimers with assembly into a tetramer being salt-sensitive. It is unlikely that Kif15 can further polymerise into higher-

order oligomers. It has been shown that the Kif15 motor is a highly acrobatic motor that can navigate complex microtubule intersections through track-switching during processive runs (Drechsler et al., 2014). It is plausible to imagine that a Kif15 polymer would be inherently less flexible to undergo such acrobatic switches. Also, for some functions, such as regulating catastrophe events on the microtubule plus-end, Kif15 motors can cooperate in teams consisting up to 11 tetramers (Drechsler and McAinsh, 2016).

Our work provides direct support for this model. First, XL-MS data for the dimeric population of Kif15 can be mapped onto predicted structural elements in the molecule: There are three predicted coiled-coils (CC2-4) that have a preference for a parallel organisation (Figure 4.5). The inter-molecular dimeric cross-links for Kif15 were identified in CC3, CC4 and the unstructured region connecting these coiled-coils. We suggest that these regions form the structural core of the dimeric Kif15. Second, from our XL-MS data, we identified two key sites in the molecule that are in close proximity in the tetrameric state ($_{T}K15_{1}$ and $_{T}K15_{2}$). The first is positioned in unstructured region adjacent to the motor domain while the second is within the fourth coiled coil (CC4). We thus envisage that Kif15 organises into a tetramer as a dimer-of-dimers, whereby at least at least one of the tetrameric cross-links identified are stabilised through electrostatic interactions. To understand the organisation of the α-helices where these cross-linked residues lie, a helical wheel diagram was drawn. As seen from the helical wheel diagram for the second tetrameric Kif15 cross-link ($_{T}K15_{2}$), the two cross-link residues are present on opposite α-helices, which display an almost perfect charge reversal in the amino acids present in these helices. One α-helix is NPPPPN, whereby the “N” indicates a non-polar side chain and “P” indicates a polar side chain. The opposite strand is PNNPNP. This seems to indicate that the tetrameric Kif15 is stabilised through ionic interactions, which can dissociate into a dimer in a salt-dependent manner. This is consistent with the data previously discussed, showing that tetrameric conformation of Kif15 is indeed ionic strength dependent, as physiological ionic strength stabilises the tetrameric

conformation of the motor, whereas non-physiological salt concentrations dissociates the motor into a dimer (Drechsler and McAinsh, 2016). This mode of interaction also suggests that Kif15 tetramers do not form a BASS domain like structure as found for the Eg5 tetramer.

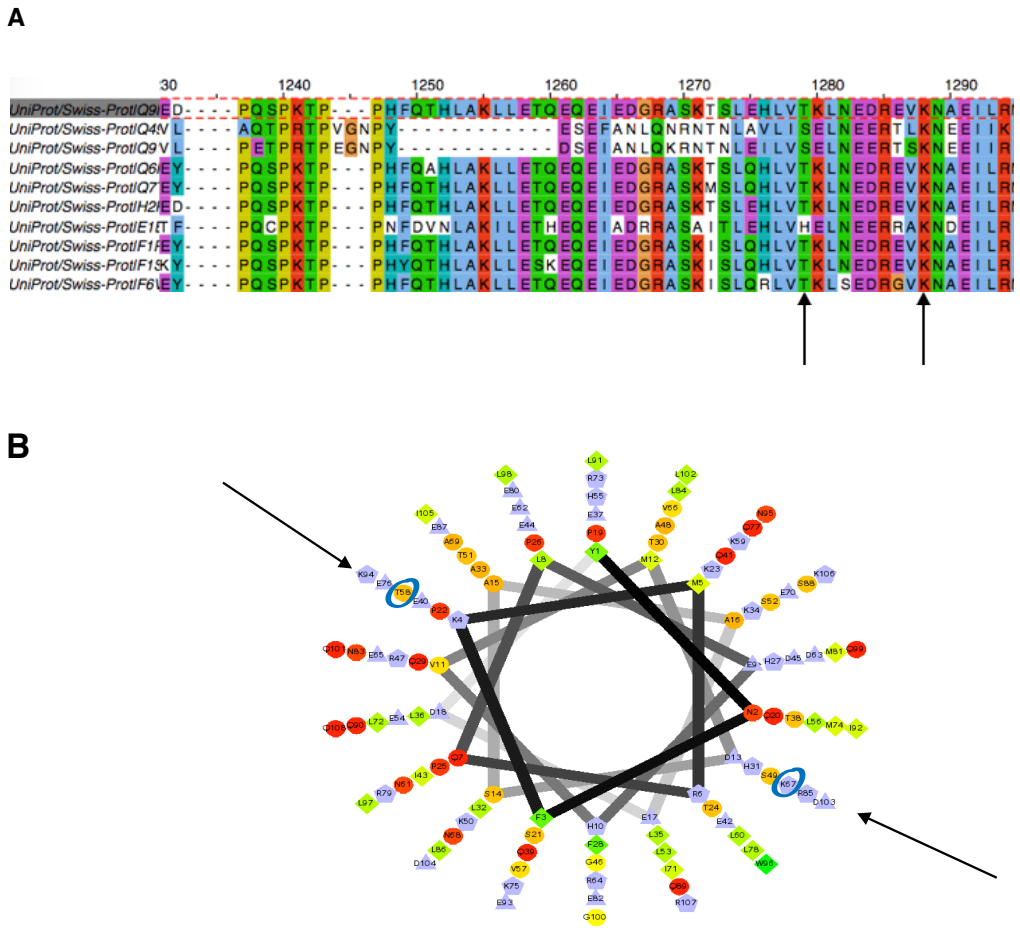

Figure 6.1: Sequence alignment and helical wheel analysis of the second tetrameric cross-link identified ($_{T}K15_{2}$). A; Sequence alignment of the cross-linked residues Thr-1178 and Lys-1187 in $_{T}K15_{2}$. B; Helical wheel diagram of cross-link $_{T}K15_{2}$. The wheel diagram allows the representation of α-helices, specifically the ability to look down the helical axis to see the residues which are interacting together.

Also, the location of the tetrameric cross-links identified support a model in which Kif15 adopts a parallel tetrameric conformation, which is also supported by our preliminary EM data. Our data helps to further explain recent experiments showing that a change in the microtubule geometry affects the

velocity differential between Kif15 motor domain pairs required for microtubule transport (Drechsler and McAinsh, 2016). The best explanation for why a change in microtubule geometry would induce a conformational change which selectively impairs the stepping of one motor domain pair would be a parallel tetramer conformation; this would enable the coiled-coil tail to provide asymmetric structure so that any torsion may affect only one set of motor domain pair. This is consistent with data from the symmetric anti-parallel tetramer Eg5, which does not show any velocity differential induced by a change in microtubule geometry (Kapitein et al., 2005).

6.1.2 Kif15 Leucine Zipper is required to stabilise its auto-inhibited state

Kif15 is thought to regulate its activity through auto-inhibition of its C-terminal coil 2 (residues 961–1388) with the motor domain (Sturgill et al., 2014). Furthermore, the leucine-zipper (residues 1294-1388), which also is known to bind to Tpx2, has been shown to promote the auto-inhibited conformation of Kif15, which is a strongly-bound state unlike the autoinhibited conformation of Kinesin-1, which is a weakly-bound state (McHugh et al., 2017). To assess the molecular mechanism of this auto-inhibited conformation of Kif15, we compared the structural assembly of the full-length Kif15 molecule with Kif15 1-1293. Given that the Kif15 tail ($Kif15_{1149–1388}$) on its own cannot bind microtubules, this suggests that the mechanism of auto-inhibition is regulated through the back-folding of the motor, which results in blocking the Kif15 motor domain (Klejnot et al., 2014). This is consistent with the cross-linking for the full-length Kif15 protein, as many long distance cross-links were found, which indicates the folded nature of the molecule (figure 6.2). Of particular interest was the long-distance cross-link extending from the leucine zipper to the N-terminal end of the molecule ($K15_5$). Interestingly, no cross-links extending from the motor domain were identified. This may be due to a limitation of the cross-linker not being very amenable to folded globular domains. Consistent with this back-folding model and experiments from McHugh et al, depletion of the LZ (Kif15 1-1293 molecule) resulted in loss of the long distance cross-links

identified in the full-length protein, indicating that it adopts a more extended conformation. This extended conformation also reveals regions which are now accessible to the cross-linker and forms new short-distance cross-links, such as the motor domain, CC3 and CC4. Thus, Kif15 can exist in at least two distinct conformational states, one that is inhibitory to motor function. We term these as Kif15^{on} and Kif15^{off}.

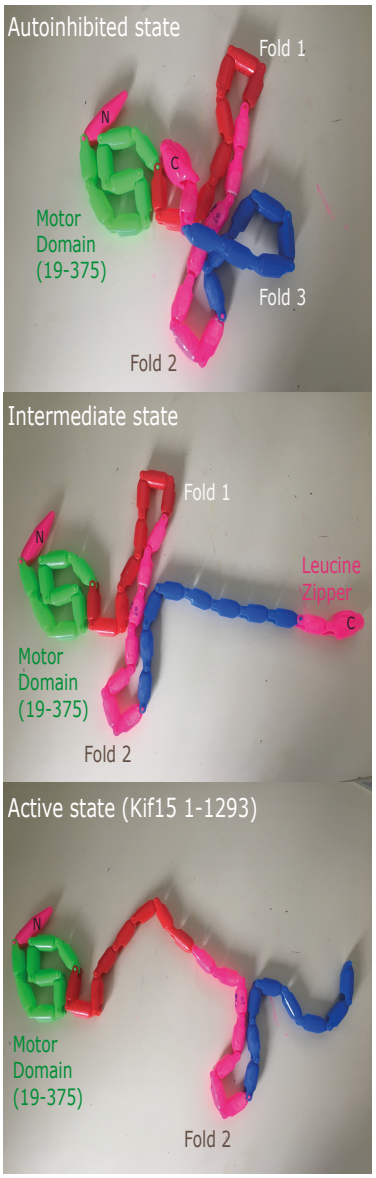

Figure 6.2: Potential structural organisation of Kif15 in active and autoinhibited conformations. Each segment is ~40 amino acids. According to the XL-MS data for Kif15 full-length, it appears that Kif15 has three main folds, consisting of fold 1 (amino acids ~500-800), fold 2 (amino acids ~800-1100) and fold 3 (amino acids ~1100-tail to 500).

Of interest would be to further explore the mechanism by which this auto-inhibitory is relieved thus promoting the switch from Kif15^{off} to Kif15^{on}. As seen with many other Kinesins, such as CENP-E, such auto-inhibition is relieved by phosphorylation (Espeut et al., 2008). Aurora A phosphorylation of Kif15 at serine 1169 has been shown to be important for the mitotic spindle localisation of the motor (van Heesbeen et al., 2017). One hypothesis would be that this phosphorylation is required to spatially regulate Kif15 within the mitotic spindle, so that it is activated as required (Figure 6.3). During interphase, the motor activity is limited, thus it is mainly in an auto-inhibited conformation. Aurora A phosphorylation localises the motor to the mitotic spindle, where its activity is required for bipolar spindle maintenance, thus it adopts an active conformation. Interestingly, the S-1169 (S49) residue is adjacent to the circled K67 residue involved in stabilising the tetrameric structure of the helical wheel diagram (Figure 6.1B). It may be that the stabilisation of Kif15 tetramer through cross-link $_{T}K15_{2}$ (circled residues in helical wheel) induces a conformation which exposes S-1169 for Aurora A phosphorylation and subsequent localisation of the motor to the spindle. This would explain why majority of the Kif15 motors on the spindle display a tetrameric conformation (Mann et al., 2017). However, Aurora A is not the only protein shown to be required to localise the motor to the spindle, as binding to Tpx2 also re-locates Kif15 to the mitotic spindle. It is not clear whether Tpx2 is directly required for targeting Kif15 to the mitotic spindle or whether this MAP plays an indirect role through activation of the Aurora A kinase. (for further discussion see *6.1.3 Tpx2 stabilises the Auto-inhibited conformation of Kif15).*

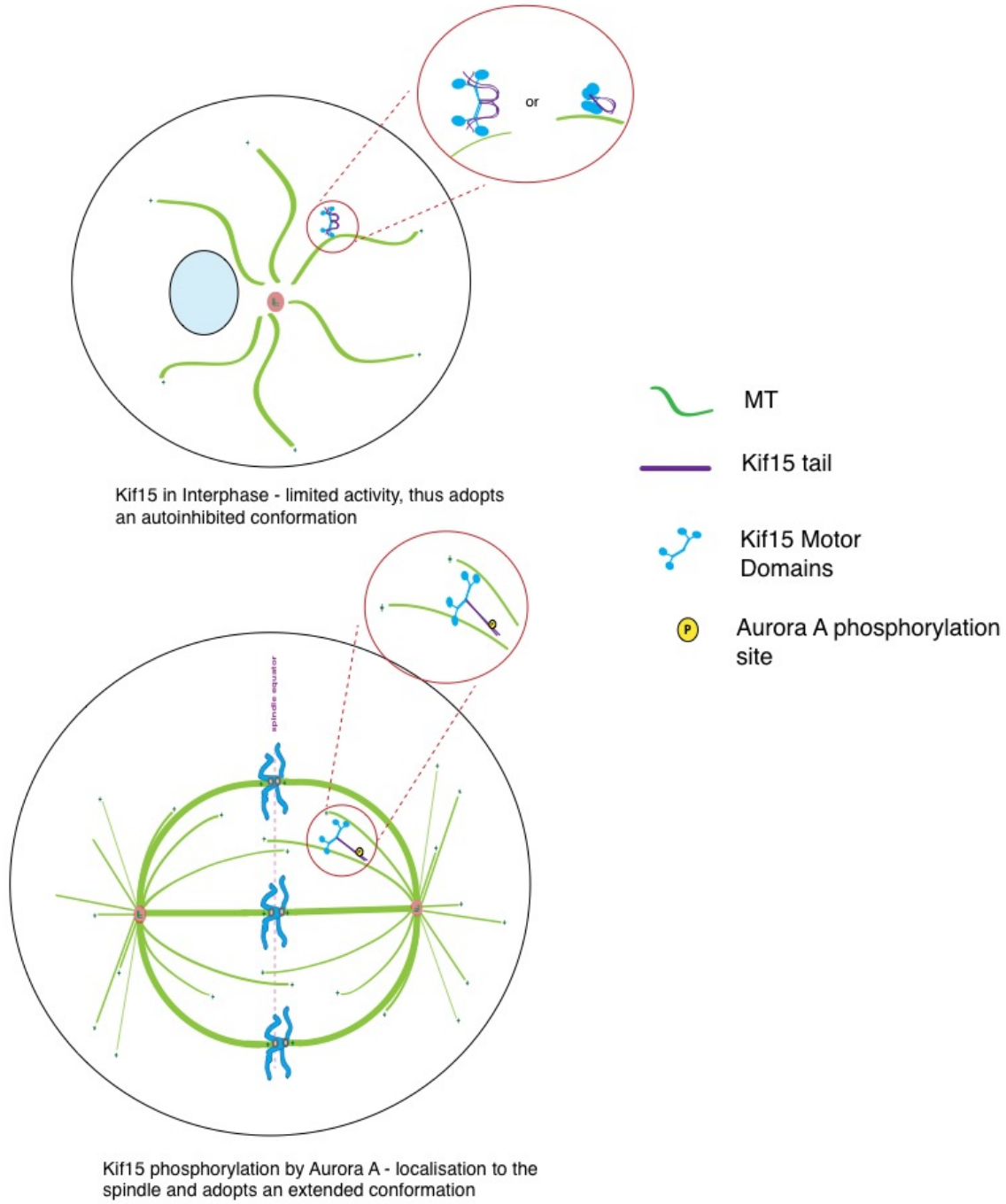

Figure 6.3: Possible model for Kif15 autoinhibition regulation. In interphase cells, where Kif15 activity is limited, the motor is mostly in its autoinhibited conformation. Phosphorylation by Aurora A relocates the motor to the mitotic spindle, where it unfolds and resumes full motility.

Of particular interest is the conformational shift in the binding between Tpx2 and Kif15 in the presence and absence of microtubules. In the absence of microtubules, Tpx2 exclusively binds to/near the fourth coiled-coil (CC4) region of Kif15. However, in the presence of microtubules, Tpx2 mainly contacts the leucine zipper of Kif15, with one cross-link found to CC4 of Kif15. The conformational shift in binding region between Tpx2 and Kif15 is likely affinity-driven as in the absence of microtubules, these proteins do not bind tightly to one another (Drechsler et al., 2014). It has also been shown that Tpx2 is able to inhibit Kif15 in a leucine zipper-independent manner (McHugh et al. 2017). This is consistent with the data presented here as in the presence of microtubules, in addition to the cross-links to the leucine zipper of Kif15, we also identified a cross-link binding to CC4 of Kif15.

Tpx2 also inhibits Eg5 motility through binding to its C-terminal tail. For Kif15, the presence of Tpx2 generates a static (higher load-bearing) cross-link between the motor and the microtubules (Drechsler et al., 2014). This might be useful in stabilising and further bundling the parallel microtubules found in the k-fibre. It has been shown that Tpx2 also inhibits Eg5 motility through binding to its C-terminal tail (Balchand et al., 2015). It is probable that that the presence of Tpx2 also stabilises the antiparallel microtubules, which are required for Eg5 motility. Despite the role of Tpx2 in aiding Kif15 binding to the microtubules, none of the experiments carried out were able to reveal any direct cross-links between the microtubules and Kif15. The reason for this is unclear, however the conformation of the microtubule-Kif15 binding sites, may not make it amenable for cross-linking.

Our cross-linking data only revealed a single cross-link between Tpx2 and MT. The cross-link observed was between Tpx2 (E-643) and the MT (K-336). The K-336 residue of α-tubulin is localized on helix-10, which has been shown to be in the inter-dimer interface (Nogales et al., 1998). Similar conclusion was reached by Zhang et al., where they determined the cryo-EM structure of Tpx2 bound to the microtubule surface (Zhang et al., 2017).

Tpx2 interaction with the longitudinal and lateral tubulin interface occurs through two flexible regions termed “ridge” and “wedge”. The wedge region consists of the short helix-10 and binds in-between adjacent protofilaments. This mode of interaction with the MT suggests that Tpx2 stabilizes the microtubules through promoting interaction between the tubulin subunits.

Studies by Sturgill *et al.,* suggest that Tpx2 does not play an explicit role in Kif15 targeting to the mitotic spindle (Sturgill et al., 2014). Rather, Tpx2-Kif15 binding is an indirect consequence of the role of Tpx2 in MT bundling and k-fibre formation. However, to support this idea, no interaction between Kif15 and Tpx2 in the absence of microtubules would be detected. From our XL-MS data, we see that Tpx2 is able to bind Kif15 in the absence of microtubules, although this interaction has been reported to be of low affinity (Drechsler et al., 2014). Mutation experiments of these Kif15-Tpx2 interaction sites would be required to fully understand the role Tpx2 plays in Kif15 spindle targeting.

6.1.4 Tpx2 adopts a dimeric conformation

Tpx2 is an important regulator of microtubules, including MT nucleation (Petry et al., 2013). The C-terminal half of *Xenopus* Tpx2 has recently been characterised as consisting of distinct α-helical domains (α3-α7) (Alfaro-Aco et al., 2017). Despite these individual domains do not bind to the microtubules independently, but rather, the more of these individual domains are joined together, the higher their affinity to the microtubules. This would suggest that Tpx2 dimerization enhances its microtubule binding affinity. However, Roostalu *et al.,* report that Tpx2 purified under high-ionic strength conditions (300 mM KCl), exists as a monomer (Roostalu et al., 2015). From our own data, we see that under physiological strength (75 mM), Tpx2 exists as a dimer. This may be another case whereby protein oligomerisation is regulated through ionic interactions. It would be interesting to test whether the

oligomerisation state of Tpx2 enhances the affinity of the protein to bind the microtubules.

6.1.5 Kif15 Knock-out CRISPR cell lines

As presented in chapter 5, we have been able to obtain two types of Kif15 RPE1-mCherry-tubulin CRISPR clones with distinct phenotypes. The CRISPR gRNA used targets exon 1 of Kif15 and the clones were screened using immunofluorescence. One clone is depleted of Kif15, whereas the second Kif15 clone is depleted from the spindle, but exclusively localises to the kinetochores. Further work, including sequencing of the clones will need to be carried out to identify the INDELS in the genome sequences. Sturgill *et al.,* have also generated a Kif15 HeLa cell line largely lacking Kif15 using the CRISPR-Cas9 system (Sturgill et al., 2016). However, they used a sgRNA targeting exon 20 of Kif15, suggesting some endogenous Kif15 (up to amino acid ~800) is still present in the cells. The Kif15 knock-out cell line generated can be used to provide a greater understanding of the role Kif15 plays in bipolar spindle assembly; mutations in Kif15 can be tested in these cells lacking endogenous Kif15 to study the effect of Kif15 tetramerization, Tpx2 binding and phosphorylation on Kif15 function and localisation.

It is known that the N-terminal residues of kinesins are required for force generation, thus any construct lacking these amino acids, such as the one used by Reineman *et al.,* may affect the mechanochemical properties of a motor (Khalil et al., 2008). Our preliminary CRISPR data where the cut site is localized to the N-terminal residues of the Kif15 motor has also shown an interesting phenotype in clone MC174, where the motor is localized to the microtubule plus-end or the kinetochore. Preliminary work on Kif15 has shown that the motor does not co-localise with the kinetochores (Vanneste et al., 2009), however more recent work has shown Kif15 to co-localise with Hec-1 at the kinetochores (Sturgill and Ohi, 2013). From our data, it is not

clear whether Kif15 is accumulated on the plus-ends as seen in *in-vitro* reconstitution experiments (Drechsler and McAinsh, 2016) or localised on the kinetochores. However, given that the Cas9 enzyme cuts between the 5th and 6th nucleotide of Kif15 exon 1, this could generate a hyperactive mutation in the cover strand of the motor, which shows Kif15 motors at the microtubule plus-ends or the kinetochores. This is consistent with data from Kinesin-1, whereby mutations in the N-terminal cover-strand residues promoted increased processivity of the motor (Khalil et al., 2008).

6.1.6 XL-MS of Kif1C

Our optimised XL-MS method and analysis workflow has also been adopted to study the organisation of Kinesin-3 Kif1C, in collaboration with N. Siddiqui, Straube lab. This data revealed that Kif1C adopts an auto-inhibited conformation, whereby two of the back-folding cross-links identified makes contact with the same lysine residue in the motor domain. This lysine residue has been shown to make contacts with the microtubule surface, thus it is likely that autoinhibition using the tail prevents motor head binding to the microtubules. This is another example of how XL-MS was used to study structural organisation of Kinesin.

6.2 Conclusion and future directions

In conclusion, work presented in this thesis has progressed our understanding of the Kif15 molecular motor at a structural level. We confirmed that Kif15 is indeed a tetramer, which most likely adopts a parallel dimer-of-dimers conformation. We also revealed how Tpx2 inhibits Kif15 through the stabilisation of its autoinhibited conformation. There are several key experiments which would further advance our understanding of how Kif15 is regulated. Firstly, confirming the parallel tetramer organisation of Kif15 by

optimising EM experiments is essential and potentially using cryo-EM to provide high resolution structural information. Also, *in-vitro* Aurora A phosphorylation assays of Kif15, followed by XL-MS, would aid the understanding of what conformational effects this kinase phosphorylation has on the structure of Kif15 and its interaction with Tpx2. Single-molecule assays could also be used to study the effects of Aurora A phosphorylation on Kif15 motility. Point mutations of the tetrameric cross-links and interaction sites for Tpx2 should be explored *in-vivo* using the generated CRISPR Kif15 knock-out cell lines, to study what effect they have on Kif15 localisation and function. Also, further understanding of Kif15 function in cells can be achieved; with Cas9 cutting at N-terminus we can now make GFP knock-in cell lines and purify endogenous motor complexes to look for binding partners, do the *in-vivo* cross-linking on beads and investigate post-translational modifications of this motor. More broadly, these tools should also enable the non-mitotic functions of Kif15 to be investigated.

Chapter 7: Bibliography

ACAR, S., CARLSON, D. B., BUDAMAGUNTA, M. S., YAROV-YAROVOY, V., CORREIA, J. J., NINONUEVO, M. R., JIA, W., TAO, L., LEARY, J. A., VOSS, J. C., EVANS, J. E. & SCHOLEY, J. M. 2013. The bipolar assembly domain of the mitotic motor kinesin-5. *Nat Commun,* 4**,** 1343.

AKHMANOVA, A. & STEINMETZ, M. O. 2008. Tracking the ends: a dynamic protein network controls the fate of microtubule tips. *Nat Rev Mol Cell Biol,* 9**,** 309-22.

ALFARO-ACO, R., THAWANI, A. & PETRY, S. 2017. Structural analysis of the role of TPX2 in branching microtubule nucleation. *J Cell Biol,* 216**,** 983-997.

ALVAREZ-FERNANDEZ, M. & MEDEMA, R. H. 2013. Novel functions of FoxM1: from molecular mechanisms to cancer therapy. *Front Oncol,* 3**,** 30.

ANDREASSON, J. O., MILIC, B., CHEN, G. Y., GUYDOSH, N. R., HANCOCK, W. O. & BLOCK, S. M. 2015. Examining kinesin processivity within a general gating framework. *Elife,* 4.

ARMOND, J. W., VLADIMIROU, E., ERENT, M., MCAINSH, A. D. & BURROUGHS, N. J. 2015. Probing microtubule polymerisation state at single kinetochores during metaphase chromosome motion. *J Cell Sci,* 128**,** 1991-2001.

ASBURY, C. L., FEHR, A. N. & BLOCK, S. M. 2003. Kinesin moves by an asymmetric hand-over-hand mechanism. *Science,* 302**,** 2130-4.

BAKHOUM, S. F., THOMPSON, S. L., MANNING, A. L. & COMPTON, D. A. 2009. Genome stability is ensured by temporal control of kinetochore-microtubule dynamics. *Nat Cell Biol,* 11**,** 27-35.

BALCHAND, S. K., MANN, B. J., TITUS, J., ROSS, J. L. & WADSWORTH, P. 2015. TPX2 Inhibits Eg5 by Interactions with Both Motor and Microtubule. *J Biol Chem,* 290**,** 17367-79.

BAYLISS, R., SARDON, T., VERNOS, I. & CONTI, E. 2003. Structural basis of Aurora-A activation by TPX2 at the mitotic spindle. *Mol Cell,* 12**,** 851-62.

BECHSTEDT, S., WIECZOREK, M., NOUJAIM, M. & BROUHARD, G. J. 2011. Variations on the single-molecule assay for microtubule-associated proteins and kinesins. *Methods Mol Biol,* 777**,** 167-76.

BENOIT, M., ASENJO, A. B. & SOSA, H. 2018. Cryo-EM reveals the structural basis of microtubule depolymerization by kinesin-13s. *Nat Commun,* 9**,** 1662.

BLANGY, A., LANE, H. A., D'HERIN, P., HARPER, M., KRESS, M. & NIGG, E. A. 1995. Phosphorylation by p34cdc2 regulates spindle association of human Eg5, a kinesin-related motor essential for bipolar spindle formation in vivo. *Cell,* 83**,** 1159-69.

BLOCK, S. M., GOLDSTEIN, L. S. & SCHNAPP, B. J. 1990. Bead movement by single kinesin molecules studied with optical tweezers. *Nature,* 348**,** 348-52.

BOLETI, H., KARSENTI, E. & VERNOS, I. 1996. Xklp2, a novel Xenopus centrosomal kinesin-like protein required for centrosome separation during mitosis. *Cell,* 84**,** 49-59.

BROUWERS, N., MALLOL MARTINEZ, N. & VERNOS, I. 2017. Role of Kif15 and its novel mitotic partner KBP in K-fiber dynamics and chromosome alignment. *PLoS One,* 12**,** e0174819.

CAI, D., HOPPE, A. D., SWANSON, J. A. & VERHEY, K. J. 2007. Kinesin-1 structural organization and conformational changes revealed by FRET stoichiometry in live cells. *J Cell Biol,* 176**,** 51-63.

CAO, L., WANG, W., JIANG, Q., WANG, C., KNOSSOW, M. & GIGANT, B. 2014. The structure of apo-kinesin bound to tubulin links the nucleotide cycle to movement. *Nat Commun,* 5**,** 5364.

CARLETON, M., MAO, M., BIERY, M., WARRENER, P., KIM, S., BUSER, C., MARSHALL, C. G., FERNANDES, C., ANNIS, J. & LINSLEY, P. S. 2006. RNA interference-mediated silencing of mitotic kinesin KIF14 disrupts cell cycle progression and induces cytokinesis failure. *Mol Cell Biol,* 26**,** 3853-63.

CARLIER, M. F. & PANTALONI, D. 2007. Control of actin assembly dynamics in cell motility. *J Biol Chem,* 282**,** 23005-9.

CARTER, N. J. & CROSS, R. A. 2005. Mechanics of the kinesin step. *Nature,* 435**,** 308-12.

CARTER, N. J. & CROSS, R. A. 2006. Kinesin's moonwalk. *Curr Opin Cell Biol,* 18**,** 61-7.

CASE, R. B., PIERCE, D. W., HOM-BOOHER, N., HART, C. L. & VALE, R. D. 1997. The directional preference of kinesin motors is specified by an element outside of the motor catalytic domain. *Cell,* 90**,** 959-66.

CHALKLEY, R. J., MEDZIHRADSZKY, K. F., LYNN, A. J., BAKER, P. R. & BURLINGAME, A. L. 2010. Statistical analysis of Peptide electron transfer dissociation fragmentation mass spectrometry. *Anal Chem,* 82**,** 579-84.

CHEN, W. S., CHEN, Y. J., HUANG, Y. A., HSIEH, B. Y., CHIU, H. C., KAO, P. Y., CHAO, C. Y. & HWANG, E. 2017. Ran-dependent TPX2 activation promotes acentrosomal microtubule nucleation in neurons. *Sci Rep,* 7**,** 42297.

CHU, X., CHEN, X., WAN, Q., ZHENG, Z. & DU, Q. 2016. Nuclear Mitotic Apparatus (NuMA) Interacts with and Regulates Astrin at the Mitotic Spindle. *J Biol Chem,* 291**,** 20055-67.

COCHRAN, J. C., GATIAL, J. E., 3RD, KAPOOR, T. M. & GILBERT, S. P. 2005. Monastrol inhibition of the mitotic kinesin Eg5. *J Biol Chem,* 280**,** 12658-67.

COX, J., HEIN, M. Y., LUBER, C. A., PARON, I., NAGARAJ, N. & MANN, M. 2014. Accurate proteome-wide label-free quantification by delayed normalization and maximal peptide ratio extraction, termed MaxLFQ. *Mol Cell Proteomics,* 13**,** 2513-26.

COX, J. & MANN, M. 2008. MaxQuant enables high peptide identification rates, individualized p.p.b.-range mass accuracies and proteome-wide protein quantification. *Nat Biotechnol,* 26**,** 1367-72.

COY, D. L., HANCOCK, W. O., WAGENBACH, M. & HOWARD, J. 1999. Kinesin's tail domain is an inhibitory regulator of the motor domain. *Nat Cell Biol,* 1**,** 288-92.

CREVEL, I. M., ALONSO, M. C. & CROSS, R. A. 2004. Monastrol stabilises an attached low-friction mode of Eg5. *Curr Biol,* 14**,** R411-2.

CROSS, R. A. 1995. On the hand-over-hand footsteps of kinesin heads. *J Muscle Res Cell Motil,* 16**,** 91-4.

CROSS, R. A. 2004. The kinetic mechanism of kinesin. *Trends Biochem Sci,* 29**,** 301-9.

DECHAT, T., PFLEGHAAR, K., SENGUPTA, K., SHIMI, T., SHUMAKER, D. K., SOLIMANDO, L. & GOLDMAN, R. D. 2008. Nuclear lamins: major factors in

the structural organization and function of the nucleus and chromatin. *Genes Dev,* 22**,** 832-53.
DRECHSLER, H. & MCAINSH, A. D. 2016. Kinesin-12 motors cooperate to suppress microtubule catastrophes and drive the formation of parallel microtubule bundles. *Proc Natl Acad Sci U S A,* 113**,** E1635-44.
DRECHSLER, H., MCHUGH, T., SINGLETON, M. R., CARTER, N. J. & MCAINSH, A. D. 2014. The Kinesin-12 Kif15 is a processive track-switching tetramer. *Elife,* 3**,** e01724.
EDAMATSU, M. 2014. Bidirectional motility of the fission yeast kinesin-5, Cut7. *Biochem Biophys Res Commun,* 446**,** 231-4.
EMS-MCCLUNG, S. C. & WALCZAK, C. E. 2010. Kinesin-13s in mitosis: Key players in the spatial and temporal organization of spindle microtubules. *Semin Cell Dev Biol,* 21**,** 276-82.
ENDRES, N. F., YOSHIOKA, C., MILLIGAN, R. A. & VALE, R. D. 2006. A lever-arm rotation drives motility of the minus-end-directed kinesin Ncd. *Nature,* 439**,** 875-8.
ESPEUT, J., GAUSSEN, A., BIELING, P., MORIN, V., PRIETO, S., FESQUET, D., SURREY, T. & ABRIEU, A. 2008. Phosphorylation relieves autoinhibition of the kinetochore motor Cenp-E. *Mol Cell,* 29**,** 637-43.
ETIENNE-MANNEVILLE, S. 2010. From signaling pathways to microtubule dynamics: the key players. *Curr Opin Cell Biol,* 22**,** 104-11.
EVANS, L., MITCHISON, T. & KIRSCHNER, M. 1985. Influence of the centrosome on the structure of nucleated microtubules. *J Cell Biol,* 100**,** 1185-91.
FENG, J., HU, Z., CHEN, H., HUA, J., WU, R., DONG, Z., QIANG, L., LIU, Y., BAAS, P. W. & LIU, M. 2016. Depletion of kinesin-12, a myosin-IIB-interacting protein, promotes migration of cortical astrocytes. *J Cell Sci,* 129**,** 2438-47.
FISCHER, L., CHEN, Z. A. & RAPPSILBER, J. 2013. Quantitative cross-linking/mass spectrometry using isotope-labelled cross-linkers. *J Proteomics,* 88**,** 120-8.
FLETCHER, D. A. & MULLINS, R. D. 2010. Cell mechanics and the cytoskeleton. *Nature,* 463**,** 485-92.
FUNABIKI, H. & MURRAY, A. W. 2000. The Xenopus chromokinesin Xkid is essential for metaphase chromosome alignment and must be degraded to allow anaphase chromosome movement. *Cell,* 102**,** 411-24.
GANEM, N. J. & COMPTON, D. A. 2004. The KinI kinesin Kif2a is required for bipolar spindle assembly through a functional relationship with MCAK. *J Cell Biol,* 166**,** 473-8.
GAYEK, A. S. & OHI, R. 2014. Kinetochore-microtubule stability governs the metaphase requirement for Eg5. *Mol Biol Cell,* 25**,** 2051-60.
GENNERICH, A. & VALE, R. D. 2009. Walking the walk: how kinesin and dynein coordinate their steps. *Curr Opin Cell Biol,* 21**,** 59-67.
GOODWIN, S. S. & VALE, R. D. 2010. Patronin regulates the microtubule network by protecting microtubule minus ends. *Cell,* 143**,** 263-74.
GOSHIMA, G. & VALE, R. D. 2003. The roles of microtubule-based motor proteins in mitosis: comprehensive RNAi analysis in the Drosophila S2 cell line. *J Cell Biol,* 162**,** 1003-16.
GOTZE, M., PETTELKAU, J., SCHAKS, S., BOSSE, K., IHLING, C. H., KRAUTH, F., FRITZSCHE, R., KUHN, U. & SINZ, A. 2012. StavroX--a software for analyzing

crosslinked products in protein interaction studies. *J Am Soc Mass Spectrom,* 23**,** 76-87.
GRIFFITH, L. M. & POLLARD, T. D. 1982. The interaction of actin filaments with microtubules and microtubule-associated proteins. *J Biol Chem,* 257**,** 9143-51.
GRILL, S. W., GONCZY, P., STELZER, E. H. & HYMAN, A. A. 2001. Polarity controls forces governing asymmetric spindle positioning in the Caenorhabditis elegans embryo. *Nature,* 409**,** 630-3.
GRILL, S. W., HOWARD, J., SCHAFFER, E., STELZER, E. H. & HYMAN, A. A. 2003. The distribution of active force generators controls mitotic spindle position. *Science,* 301**,** 518-21.
HACKNEY, D. D. 1994. Evidence for alternating head catalysis by kinesin during microtubule-stimulated ATP hydrolysis. *Proc Natl Acad Sci U S A,* 91**,** 6865-9.
HACKNEY, D. D., BAEK, N. & SNYDER, A. C. 2009. Half-site inhibition of dimeric kinesin head domains by monomeric tail domains. *Biochemistry,* 48**,** 3448-56.
HACKNEY, D. D., LEVITT, J. D. & SUHAN, J. 1992. Kinesin undergoes a 9 S to 6 S conformational transition. *J Biol Chem,* 267**,** 8696-701.
HAFNER, J., MAYR, M. I., MOCKEL, M. M. & MAYER, T. U. 2014. Pre-anaphase chromosome oscillations are regulated by the antagonistic activities of Cdk1 and PP1 on Kif18A. *Nat Commun,* 5**,** 4397.
HANCOCK, W. O. 2014. Mitotic kinesins: a reason to delve into kinesin-12. *Curr Biol,* 24**,** R968-70.
HARIHARAN, V. & HANCOCK, W. O. 2009. Insights into the Mechanical Properties of the Kinesin Neck Linker Domain from Sequence Analysis and Molecular Dynamics Simulations. *Cell Mol Bioeng,* 2**,** 177-189.
HELMKE, B. P., GOLDMAN, R. D. & DAVIES, P. F. 2000. Rapid displacement of vimentin intermediate filaments in living endothelial cells exposed to flow. *Circ Res,* 86**,** 745-52.
HENDERSHOTT, M. C. & VALE, R. D. 2014. Regulation of microtubule minus-end dynamics by CAMSAPs and Patronin. *Proc Natl Acad Sci U S A,* 111**,** 5860-5.
HENNINGSEN, U. & SCHLIWA, M. 1997. Reversal in the direction of movement of a molecular motor. *Nature,* 389**,** 93-6.
HERRMANN, H., BAR, H., KREPLAK, L., STRELKOV, S. V. & AEBI, U. 2007. Intermediate filaments: from cell architecture to nanomechanics. *Nat Rev Mol Cell Biol,* 8**,** 562-73.
HIROKAWA, N. 1998. Kinesin and dynein superfamily proteins and the mechanism of organelle transport. *Science,* 279**,** 519-26.
HIROKAWA, N., PFISTER, K. K., YORIFUJI, H., WAGNER, M. C., BRADY, S. T. & BLOOM, G. S. 1989. Submolecular domains of bovine brain kinesin identified by electron microscopy and monoclonal antibody decoration. *Cell,* 56**,** 867-78.
HONNAPPA, S., GOUVEIA, S. M., WEISBRICH, A., DAMBERGER, F. F., BHAVESH, N. S., JAWHARI, H., GRIGORIEV, I., VAN RIJSSEL, F. J., BUEY, R. M., LAWERA, A., JELESAROV, I., WINKLER, F. K., WUTHRICH, K., AKHMANOVA, A. & STEINMETZ, M. O. 2009. An EB1-binding motif acts as a microtubule tip localization signal. *Cell,* 138**,** 366-76.

HOWARD, J., HUDSPETH, A. J. & VALE, R. D. 1989. Movement of microtubules by single kinesin molecules. *Nature,* 342**,** 154-8.

JEDRYCHOWSKI, M. P., HUTTLIN, E. L., HAAS, W., SOWA, M. E., RAD, R. & GYGI, S. P. 2011. Evaluation of HCD- and CID-type fragmentation within their respective detection platforms for murine phosphoproteomics. *Mol Cell Proteomics,* 10**,** M111.009910.

JIANG, K., HUA, S., MOHAN, R., GRIGORIEV, I., YAU, K. W., LIU, Q., KATRUKHA, E. A., ALTELAAR, A. F., HECK, A. J., HOOGENRAAD, C. C. & AKHMANOVA, A. 2014. Microtubule minus-end stabilization by polymerization-driven CAMSAP deposition. *Dev Cell,* 28**,** 295-309.

KAAN, H. Y., HACKNEY, D. D. & KOZIELSKI, F. 2011. The structure of the kinesin-1 motor-tail complex reveals the mechanism of autoinhibition. *Science,* 333**,** 883-5.

KALKHOF, S. & SINZ, A. 2008. Chances and pitfalls of chemical cross-linking with amine-reactive N-hydroxysuccinimide esters. *Anal Bioanal Chem,* 392**,** 305-12.

KAPITEIN, L. C., KWOK, B. H., WEINGER, J. S., SCHMIDT, C. F., KAPOOR, T. M. & PETERMAN, E. J. 2008. Microtubule cross-linking triggers the directional motility of kinesin-5. *J Cell Biol,* 182**,** 421-8.

KAPITEIN, L. C., PETERMAN, E. J., KWOK, B. H., KIM, J. H., KAPOOR, T. M. & SCHMIDT, C. F. 2005. The bipolar mitotic kinesin Eg5 moves on both microtubules that it crosslinks. *Nature,* 435**,** 114-8.

KEVENAAR, J. T., BIANCHI, S., VAN SPRONSEN, M., OLIERIC, N., LIPKA, J., FRIAS, C. P., MIKHAYLOVA, M., HARTERINK, M., KEIJZER, N., WULF, P. S., HILBERT, M., KAPITEIN, L. C., DE GRAAFF, E., AHKMANOVA, A., STEINMETZ, M. O. & HOOGENRAAD, C. C. 2016. Kinesin-Binding Protein Controls Microtubule Dynamics and Cargo Trafficking by Regulating Kinesin Motor Activity. *Curr Biol,* 26**,** 849-61.

KHALIL, A. S., APPLEYARD, D. C., LABNO, A. K., GEORGES, A., KARPLUS, M., BELCHER, A. M., HWANG, W. & LANG, M. J. 2008. Kinesin's cover-neck bundle folds forward to generate force. *Proc Natl Acad Sci U S A,* 105**,** 19247-52.

KHODJAKOV, A., COLE, R. W., OAKLEY, B. R. & RIEDER, C. L. 2000. Centrosome-independent mitotic spindle formation in vertebrates. *Curr Biol,* 10**,** 59-67.

KIKKAWA, M., SABLIN, E. P., OKADA, Y., YAJIMA, H., FLETTERICK, R. J. & HIROKAWA, N. 2001. Switch-based mechanism of kinesin motors. *Nature,* 411**,** 439-45.

KIM, Y., HEUSER, J. E., WATERMAN, C. M. & CLEVELAND, D. W. 2008. CENP-E combines a slow, processive motor and a flexible coiled coil to produce an essential motile kinetochore tether. *J Cell Biol,* 181**,** 411-9.

KLEJNOT, M., FALNIKAR, A., ULAGANATHAN, V., CROSS, R. A., BAAS, P. W. & KOZIELSKI, F. 2014. The crystal structure and biochemical characterization of Kif15: a bifunctional molecular motor involved in bipolar spindle formation and neuronal development. *Acta Crystallogr D Biol Crystallogr,* 70**,** 123-33.

KLINE-SMITH, S. L., KHODJAKOV, A., HERGERT, P. & WALCZAK, C. E. 2004. Depletion of centromeric MCAK leads to chromosome congression and segregation defects due to improper kinetochore attachments. *Mol Biol Cell,* 15**,** 1146-59.

KUFER, T. A., SILLJE, H. H., KORNER, R., GRUSS, O. J., MERALDI, P. & NIGG, E. A. 2002. Human TPX2 is required for targeting Aurora-A kinase to the spindle. *J Cell Biol,* 158**,** 617-23.

KULL, F. J., SABLIN, E. P., LAU, R., FLETTERICK, R. J. & VALE, R. D. 1996. Crystal structure of the kinesin motor domain reveals a structural similarity to myosin. *Nature,* 380**,** 550-5.

KULL, F. J., VALE, R. D. & FLETTERICK, R. J. 1998. The case for a common ancestor: kinesin and myosin motor proteins and G proteins. *J Muscle Res Cell Motil,* 19**,** 877-86.

LAWRENCE, C. J., DAWE, R. K., CHRISTIE, K. R., CLEVELAND, D. W., DAWSON, S. C., ENDOW, S. A., GOLDSTEIN, L. S., GOODSON, H. V., HIROKAWA, N., HOWARD, J., MALMBERG, R. L., MCINTOSH, J. R., MIKI, H., MITCHISON, T. J., OKADA, Y., REDDY, A. S., SAXTON, W. M., SCHLIWA, M., SCHOLEY, J. M., VALE, R. D., WALCZAK, C. E. & WORDEMAN, L. 2004. A standardized kinesin nomenclature. *J Cell Biol,* 167**,** 19-22.

LEE, Y. R., LI, Y. & LIU, B. 2007. Two Arabidopsis phragmoplast-associated kinesins play a critical role in cytokinesis during male gametogenesis. *Plant Cell,* 19**,** 2595-605.

LEITNER, A., WALZTHOENI, T., KAHRAMAN, A., HERZOG, F., RINNER, O., BECK, M. & AEBERSOLD, R. 2010. Probing native protein structures by chemical cross-linking, mass spectrometry, and bioinformatics. *Mol Cell Proteomics,* 9**,** 1634-49.

LIU, D., LIU, X., SHANG, Z. & SINDELAR, C. V. 2017. Structural basis of cooperativity in kinesin revealed by 3D reconstruction of a two-head-bound state on microtubules. *Elife,* 6.

LIU, M., NADAR, V. C., KOZIELSKI, F., KOZLOWSKA, M., YU, W. & BAAS, P. W. 2010. Kinesin-12, a mitotic microtubule-associated motor protein, impacts axonal growth, navigation, and branching. *J Neurosci,* 30**,** 14896-906.

MA, H. T., ERDAL, S., HUANG, S. & POON, R. Y. 2014. Synergism between inhibitors of Aurora A and KIF11 overcomes KIF15-dependent drug resistance. *Mol Oncol,* 8**,** 1404-18.

MA, N., TITUS, J., GABLE, A., ROSS, J. L. & WADSWORTH, P. 2011. TPX2 regulates the localization and activity of Eg5 in the mammalian mitotic spindle. *J Cell Biol,* 195**,** 87-98.

MADLER, S., BICH, C., TOUBOUL, D. & ZENOBI, R. 2009. Chemical cross-linking with NHS esters: a systematic study on amino acid reactivities. *J Mass Spectrom,* 44**,** 694-706.

MAKAROV, A. 2000. Electrostatic axially harmonic orbital trapping: a high-performance technique of mass analysis. *Anal Chem,* 72**,** 1156-62.

MANEY, T., HUNTER, A. W., WAGENBACH, M. & WORDEMAN, L. 1998. Mitotic centromere-associated kinesin is important for anaphase chromosome segregation. *J Cell Biol,* 142**,** 787-801.

MANN, B. J., BALCHAND, S. K. & WADSWORTH, P. 2017. Regulation of Kif15 localization and motility by the C-terminus of TPX2 and microtubule dynamics. *Mol Biol Cell,* 28**,** 65-75.

MAYR, M. I., HUMMER, S., BORMANN, J., GRUNER, T., ADIO, S., WOEHLKE, G. & MAYER, T. U. 2007. The human kinesin Kif18A is a motile microtubule depolymerase essential for chromosome congression. *Curr Biol,* 17**,** 488-98.

MCEWEN, B. F., HEAGLE, A. B., CASSELS, G. O., BUTTLE, K. F. & RIEDER, C. L. 1997. Kinetochore fiber maturation in PtK1 cells and its implications for the mechanisms of chromosome congression and anaphase onset. *J Cell Biol,* 137**,** 1567-80.

MCHUGH, T., DRECHSLER, H., MCAINSH, A. D., CARTER, N. J. & CROSS, R. A. 2018. Kif15 functions as an active mechanical ratchet. *Mol Biol Cell***,** mbcE18030151.

MERKLEY, E. D., CORT, J. R. & ADKINS, J. N. 2013. Cross-linking and mass spectrometry methodologies to facilitate structural biology: finding a path through the maze. *J Struct Funct Genomics,* 14**,** 77-90.

MIKESH, L. M., UEBERHEIDE, B., CHI, A., COON, J. J., SYKA, J. E., SHABANOWITZ, J. & HUNT, D. F. 2006. The utility of ETD mass spectrometry in proteomic analysis. *Biochim Biophys Acta,* 1764**,** 1811-22.

MIKI, H., OKADA, Y. & HIROKAWA, N. 2005. Analysis of the kinesin superfamily: insights into structure and function. *Trends Cell Biol,* 15**,** 467-76.

MILIC, B., CHAKRABORTY, A., HAN, K., BASSIK, M. C. & BLOCK, S. M. 2018. KIF15 nanomechanics and kinesin inhibitors, with implications for cancer chemotherapeutics. *Proc Natl Acad Sci U S A,* 115**,** E4613-e4622.

MITCHISON, T. & KIRSCHNER, M. 1984. Dynamic instability of microtubule growth. *Nature,* 312**,** 237-42.

MOORES, C. A., YU, M., GUO, J., BERAUD, C., SAKOWICZ, R. & MILLIGAN, R. A. 2002. A mechanism for microtubule depolymerization by KinI kinesins. *Mol Cell,* 9**,** 903-9.

MORI, T., VALE, R. D. & TOMISHIGE, M. 2007. How kinesin waits between steps. *Nature,* 450**,** 750-4.

MOUNTAIN, V., SIMERLY, C., HOWARD, L., ANDO, A., SCHATTEN, G. & COMPTON, D. A. 1999. The kinesin-related protein, HSET, opposes the activity of Eg5 and cross-links microtubules in the mammalian mitotic spindle. *J Cell Biol,* 147**,** 351-66.

MURETTA, J. M., REDDY, B. J. N., SCARABELLI, G., THOMPSON, A. F., JARIWALA, S., MAJOR, J., VENERE, M., RICH, J. N., WILLARD, B., THOMAS, D. D., STUMPFF, J., GRANT, B. J., GROSS, S. P. & ROSENFELD, S. S. 2018. A posttranslational modification of the mitotic kinesin Eg5 that enhances its mechanochemical coupling and alters its mitotic function. *Proc Natl Acad Sci U S A,* 115**,** E1779-e1788.

NOGALES, E., WOLF, S. G. & DOWNING, K. H. 1998. Structure of the alpha beta tubulin dimer by electron crystallography. *Nature,* 391**,** 199-203.

PETRY, S., GROEN, A. C., ISHIHARA, K., MITCHISON, T. J. & VALE, R. D. 2013. Branching microtubule nucleation in Xenopus egg extracts mediated by augmin and TPX2. *Cell,* 152**,** 768-77.

RAPPSILBER, J. 2011. The beginning of a beautiful friendship: cross-linking/mass spectrometry and modelling of proteins and multi-protein complexes. *J Struct Biol,* 173**,** 530-40.

RAPPSILBER, J., MANN, M. & ISHIHAMA, Y. 2007. Protocol for micro-purification, enrichment, pre-fractionation and storage of peptides for proteomics using StageTips. *Nat Protoc,* 2**,** 1896-906.

REINEMANN, D. N., STURGILL, E. G., DAS, D. K., DEGEN, M. S., VOROS, Z., HWANG, W., OHI, R. & LANG, M. J. 2017. Collective Force Regulation in Anti-parallel Microtubule Gliding by Dimeric Kif15 Kinesin Motors. *Curr Biol,* 27**,** 2810-2820.e6.

RICE, S., LIN, A. W., SAFER, D., HART, C. L., NABER, N., CARRAGHER, B. O., CAIN, S. M., PECHATNIKOVA, E., WILSON-KUBALEK, E. M., WHITTAKER, M., PATE, E., COOKE, R., TAYLOR, E. W., MILLIGAN, R. A. & VALE, R. D. 1999. A structural change in the kinesin motor protein that drives motility. *Nature,* 402**,** 778-84.

RIDLEY, A. J. & HALL, A. 1992. The small GTP-binding protein rho regulates the assembly of focal adhesions and actin stress fibers in response to growth factors. *Cell,* 70**,** 389-99.

RIEDER, C. L. 1981. The structure of the cold-stable kinetochore fiber in metaphase PtK1 cells. *Chromosoma,* 84**,** 145-58.

RIVERA-SANTIAGO, R. F., SRISWASDI, S., HARPER, S. L. & SPEICHER, D. W. 2015. Probing structures of large protein complexes using zero-length cross-linking. *Methods,* 89**,** 99-111.

ROGERS, G. C., CHUI, K. K., LEE, E. W., WEDAMAN, K. P., SHARP, D. J., HOLLAND, G., MORRIS, R. L. & SCHOLEY, J. M. 2000. A kinesin-related protein, KRP(180), positions prometaphase spindle poles during early sea urchin embryonic cell division. *J Cell Biol,* 150**,** 499-512.

ROOSTALU, J., CADE, N. I. & SURREY, T. 2015. Complementary activities of TPX2 and chTOG constitute an efficient importin-regulated microtubule nucleation module. *Nat Cell Biol,* 17**,** 1422-34.

ROOSTALU, J., HENTRICH, C., BIELING, P., TELLEY, I. A., SCHIEBEL, E. & SURREY, T. 2011. Directional switching of the kinesin Cin8 through motor coupling. *Science,* 332**,** 94-9.

ROSENBLATT, J. 2005. Spindle assembly: asters part their separate ways. *Nat Cell Biol,* 7**,** 219-22.

SABLIN, E. P., KULL, F. J., COOKE, R., VALE, R. D. & FLETTERICK, R. J. 1996. Crystal structure of the motor domain of the kinesin-related motor ncd. *Nature,* 380**,** 555-9.

SANDU, P., CREPIN, V. F., DRECHSLER, H., MCAINSH, A. D., FRANKEL, G. & BERGER, C. N. 2017. The Enterohemorrhagic Escherichia coli Effector EspW Triggers Actin Remodeling in a Rac1-Dependent Manner. *Infect Immun,* 85.

SAVITSKI, M. M., NIELSEN, M. L. & ZUBAREV, R. A. 2006. ModifiComb, a new proteomic tool for mapping substoichiometric post-translational modifications, finding novel types of modifications, and fingerprinting complex protein mixtures. *Mol Cell Proteomics,* 5**,** 935-48.

SAWIN, K. E., LEGUELLEC, K., PHILIPPE, M. & MITCHISON, T. J. 1992. Mitotic spindle organization by a plus-end-directed microtubule motor. *Nature,* 359**,** 540-3.

SAWIN, K. E. & MITCHISON, T. J. 1995. Mutations in the kinesin-like protein Eg5 disrupting localization to the mitotic spindle. *Proc Natl Acad Sci U S A,* 92**,** 4289-93.

SCHAAR, B. T., CHAN, G. K., MADDOX, P., SALMON, E. D. & YEN, T. J. 1997. CENP-E function at kinetochores is essential for chromosome alignment. *J Cell Biol,* 139**,** 1373-82.
SCHMIDT, C. & ROBINSON, C. V. 2014. A comparative cross-linking strategy to probe conformational changes in protein complexes. *Nat Protoc,* 9**,** 2224-36.
SCHMIDT, C. & URLAUB, H. 2017. Combining cryo-electron microscopy (cryo-EM) and cross-linking mass spectrometry (CX-MS) for structural elucidation of large protein assemblies. *Curr Opin Struct Biol,* 46**,** 157-168.
SCHNITZER, M. J. & BLOCK, S. M. 1997. Kinesin hydrolyses one ATP per 8-nm step. *Nature,* 388**,** 386-90.
SCHOLEY, J. E., NITHIANANTHAM, S., SCHOLEY, J. M. & AL-BASSAM, J. 2014. Structural basis for the assembly of the mitotic motor Kinesin-5 into bipolar tetramers. *Elife,* 3**,** e02217.
SCHUYLER, S. C. & PELLMAN, D. 2001. Microtubule "plus-end-tracking proteins": The end is just the beginning. *Cell,* 105**,** 421-4.
SEEGER, M. A., ZHANG, Y. & RICE, S. E. 2012. Kinesin tail domains are intrinsically disordered. *Proteins,* 80**,** 2437-46.
SEGBERT, C., BARKUS, R., POWERS, J., STROME, S., SAXTON, W. M. & BOSSINGER, O. 2003. KLP-18, a Klp2 kinesin, is required for assembly of acentrosomal meiotic spindles in Caenorhabditis elegans. *Mol Biol Cell,* 14**,** 4458-69.
SELLERS, J. R. 2000. Myosins: a diverse superfamily. *Biochim Biophys Acta,* 1496**,** 3-22.
SHANG, Z., ZHOU, K., XU, C., CSENCSITS, R., COCHRAN, J. C. & SINDELAR, C. V. 2014. High-resolution structures of kinesin on microtubules provide a basis for nucleotide-gated force-generation. *Elife,* 3**,** e04686.
SHAO, C., ZHANG, Y. & SUN, W. 2014. Statistical characterization of HCD fragmentation patterns of tryptic peptides on an LTQ Orbitrap Velos mass spectrometer. *J Proteomics,* 109**,** 26-37.
SHARP, D. J., ROGERS, G. C. & SCHOLEY, J. M. 2000. Microtubule motors in mitosis. *Nature,* 407**,** 41-7.
SINDELAR, C. V. & DOWNING, K. H. 2007. The beginning of kinesin's force-generating cycle visualized at 9-A resolution. *J Cell Biol,* 177**,** 377-85.
SINZ, A. 2006. Chemical cross-linking and mass spectrometry to map three-dimensional protein structures and protein-protein interactions. *Mass Spectrom Rev,* 25**,** 663-82.
SIVARAMAKRISHNAN, S., DEGIULIO, J. V., LORAND, L., GOLDMAN, R. D. & RIDGE, K. M. 2008. Micromechanical properties of keratin intermediate filament networks. *Proc Natl Acad Sci U S A,* 105**,** 889-94.
SOARES, D. C., BRADSHAW, N. J., ZOU, J., KENNAWAY, C. K., HAMILTON, R. S., CHEN, Z. A., WEAR, M. A., BLACKBURN, E. A., BRAMHAM, J., BOTTCHER, B., MILLAR, J. K., BARLOW, P. N., WALKINSHAW, M. D., RAPPSILBER, J. & PORTEOUS, D. J. 2012. The mitosis and neurodevelopment proteins NDE1 and NDEL1 form dimers, tetramers, and polymers with a folded back structure in solution. *J Biol Chem,* 287**,** 32381-93.
STOUT, J. R., YOUNT, A. L., POWERS, J. A., LEBLANC, C., EMS-MCCLUNG, S. C. & WALCZAK, C. E. 2011. Kif18B interacts with EB1 and controls astral microtubule length during mitosis. *Mol Biol Cell,* 22**,** 3070-80.

STURGILL, E. G., DAS, D. K., TAKIZAWA, Y., SHIN, Y., COLLIER, S. E., OHI, M. D., HWANG, W., LANG, M. J. & OHI, R. 2014. Kinesin-12 Kif15 targets kinetochore fibers through an intrinsic two-step mechanism. *Curr Biol,* 24**,** 2307-13.

STURGILL, E. G., NORRIS, S. R., GUO, Y. & OHI, R. 2016. Kinesin-5 inhibitor resistance is driven by kinesin-12. *J Cell Biol,* 213**,** 213-27.

STURGILL, E. G. & OHI, R. 2013. Kinesin-12 differentially affects spindle assembly depending on its microtubule substrate. *Curr Biol,* 23**,** 1280-90.

TANENBAUM, M. E., MACUREK, L., GALJART, N. & MEDEMA, R. H. 2008. Dynein, Lis1 and CLIP-170 counteract Eg5-dependent centrosome separation during bipolar spindle assembly. *Embo j,* 27**,** 3235-45.

TANENBAUM, M. E., MACUREK, L., JANSSEN, A., GEERS, E. F., ALVAREZ-FERNANDEZ, M. & MEDEMA, R. H. 2009. Kif15 cooperates with eg5 to promote bipolar spindle assembly. *Curr Biol,* 19**,** 1703-11.

TANENBAUM, M. E., MACUREK, L., VAN DER VAART, B., GALLI, M., AKHMANOVA, A. & MEDEMA, R. H. 2011. A complex of Kif18b and MCAK promotes microtubule depolymerization and is negatively regulated by Aurora kinases. *Curr Biol,* 21**,** 1356-65.

TAO, L., MOGILNER, A., CIVELEKOGLU-SCHOLEY, G., WOLLMAN, R., EVANS, J., STAHLBERG, H. & SCHOLEY, J. M. 2006. A homotetrameric kinesin-5, KLP61F, bundles microtubules and antagonizes Ncd in motility assays. *Curr Biol,* 16**,** 2293-302.

TSAI, M. Y., WANG, S., HEIDINGER, J. M., SHUMAKER, D. K., ADAM, S. A., GOLDMAN, R. D. & ZHENG, Y. 2006. A mitotic lamin B matrix induced by RanGTP required for spindle assembly. *Science,* 311**,** 1887-93.

VAN HEESBEEN, R., RAAIJMAKERS, J. A., TANENBAUM, M. E., HALIM, V. A., LELIEVELD, D., LIEFTINK, C., HECK, A. J. R., EGAN, D. A. & MEDEMA, R. H. 2017. Aurora A, MCAK, and Kif18b promote Eg5-independent spindle formation. *Chromosoma,* 126**,** 473-486.

VAN HEESBEEN, R. G., TANENBAUM, M. E. & MEDEMA, R. H. 2014. Balanced activity of three mitotic motors is required for bipolar spindle assembly and chromosome segregation. *Cell Rep,* 8**,** 948-56.

VANNESTE, D., FERREIRA, V. & VERNOS, I. 2011. Chromokinesins: localization-dependent functions and regulation during cell division. *Biochem Soc Trans,* 39**,** 1154-60.

VANNESTE, D., TAKAGI, M., IMAMOTO, N. & VERNOS, I. 2009. The role of Hklp2 in the stabilization and maintenance of spindle bipolarity. *Curr Biol,* 19**,** 1712-7.

VARGA, V., HELENIUS, J., TANAKA, K., HYMAN, A. A., TANAKA, T. U. & HOWARD, J. 2006. Yeast kinesin-8 depolymerizes microtubules in a length-dependent manner. *Nat Cell Biol,* 8**,** 957-62.

VERHEY, K. J., LIZOTTE, D. L., ABRAMSON, T., BARENBOIM, L., SCHNAPP, B. J. & RAPOPORT, T. A. 1998. Light chain-dependent regulation of Kinesin's interaction with microtubules. *J Cell Biol,* 143**,** 1053-66.

VLADIMIROU, E., MCHEDLISHVILI, N., GASIC, I., ARMOND, J. W., SAMORA, C. P., MERALDI, P. & MCAINSH, A. D. 2013. Nonautonomous movement of chromosomes in mitosis. *Dev Cell,* 27**,** 60-71.

WANG, W., CANTOS-FERNANDES, S., LV, Y., KUERBAN, H., AHMAD, S., WANG, C. & GIGANT, B. 2017. Insight into microtubule disassembly by kinesin-13s from the structure of Kif2C bound to tubulin. *Nat Commun,* 8**,** 70.

WEINGER, J. S., QIU, M., YANG, G. & KAPOOR, T. M. 2011. A nonmotor microtubule binding site in kinesin-5 is required for filament crosslinking and sliding. *Curr Biol,* 21**,** 154-60.

WICHE, G. 1998. Role of plectin in cytoskeleton organization and dynamics. *J Cell Sci,* 111 (Pt 17)**,** 2477-86.

WICKSTEAD, B. & GULL, K. 2006. A "holistic" kinesin phylogeny reveals new kinesin families and predicts protein functions. *Mol Biol Cell,* 17**,** 1734-43.

WILHELM, T. & JONES, A. M. 2014. Identification of related peptides through the analysis of fragment ion mass shifts. *J Proteome Res,* 13**,** 4002-11.

WISNIEWSKI, J. R., ZOUGMAN, A. & MANN, M. 2008. Nepsilon-formylation of lysine is a widespread post-translational modification of nuclear proteins occurring at residues involved in regulation of chromatin function. *Nucleic Acids Res,* 36**,** 570-7.

WITTMANN, T., BOLETI, H., ANTONY, C., KARSENTI, E. & VERNOS, I. 1998. Localization of the kinesin-like protein Xklp2 to spindle poles requires a leucine zipper, a microtubule-associated protein, and dynein. *J Cell Biol,* 143**,** 673-85.

WOOD, K. W., SAKOWICZ, R., GOLDSTEIN, L. S. & CLEVELAND, D. W. 1997. CENP-E is a plus end-directed kinetochore motor required for metaphase chromosome alignment. *Cell,* 91**,** 357-66.

WORDEMAN, L. 2010. How kinesin motor proteins drive mitotic spindle function: Lessons from molecular assays. *Semin Cell Dev Biol,* 21**,** 260-8.

WORDEMAN, L. & MITCHISON, T. J. 1995. Identification and partial characterization of mitotic centromere-associated kinesin, a kinesin-related protein that associates with centromeres during mitosis. *J Cell Biol,* 128**,** 95-104.

YANG, J. T., LAYMON, R. A. & GOLDSTEIN, L. S. 1989. A three-domain structure of kinesin heavy chain revealed by DNA sequence and microtubule binding analyses. *Cell,* 56**,** 879-89.

YEN, T. J., COMPTON, D. A., WISE, D., ZINKOWSKI, R. P., BRINKLEY, B. R., EARNSHAW, W. C. & CLEVELAND, D. W. 1991. CENP-E, a novel human centromere-associated protein required for progression from metaphase to anaphase. *Embo j,* 10**,** 1245-54.

ZHAI, Y., KRONEBUSCH, P. J. & BORISY, G. G. 1995. Kinetochore microtubule dynamics and the metaphase-anaphase transition. *J Cell Biol,* 131**,** 721-34.

ZHANG, R., ROOSTALU, J., SURREY, T. & NOGALES, E. 2017. Structural insight into TPX2-stimulated microtubule assembly. *Elife,* 6.

ZHOU, H., DI PALMA, S., PREISINGER, C., PENG, M., POLAT, A. N., HECK, A. J. & MOHAMMED, S. 2013. Toward a comprehensive characterization of a human cancer cell phosphoproteome. *J Proteome Res,* 12**,** 260-71.

ZHU, C. & JIANG, W. 2005. Cell cycle-dependent translocation of PRC1 on the spindle by Kif4 is essential for midzone formation and cytokinesis. *Proc Natl Acad Sci U S A,* 102**,** 343-8.

ZHU, C., ZHAO, J., BIBIKOVA, M., LEVERSON, J. D., BOSSY-WETZEL, E., FAN, J. B., ABRAHAM, R. T. & JIANG, W. 2005. Functional analysis of human

microtubule-based motor proteins, the kinesins and dyneins, in mitosis/cytokinesis using RNA interference. *Mol Biol Cell,* 16**,** 3187-99.